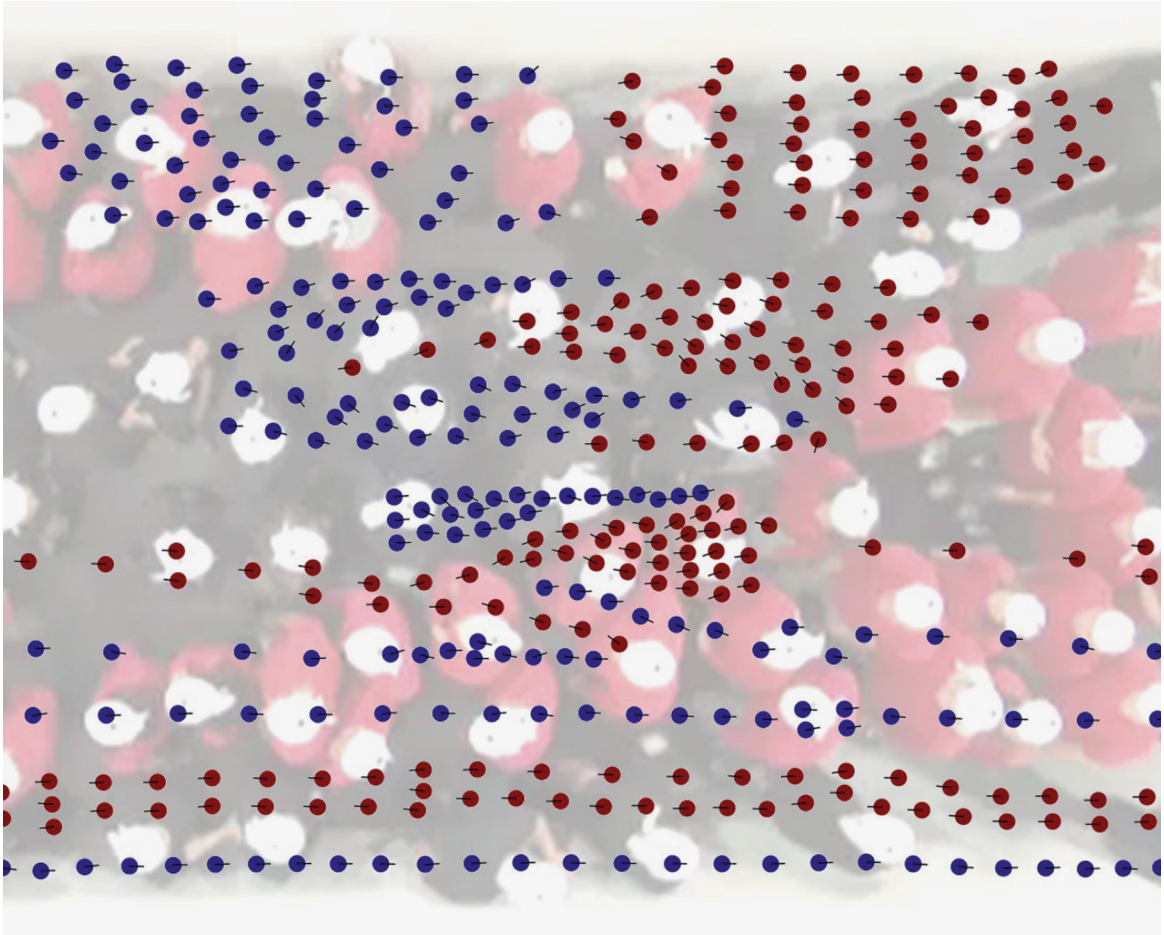

Operational Navigation of Agents and Self-organization Phenomena in Velocity-based Models for Pedestrian Dynamics

Qiancheng Xu

IAS Series
Band / Volume 49
ISBN 978-3-95806-620-5

Mitglied der Helmholtz-Gemeinschaft

JÜLICH
Forschungszentrum

Schriften des Forschungszentrums Jülich
IAS Series Band / Volume 49

Forschungszentrum Jülich GmbH
Institute for Advanced Simulation (IAS)
Civil Safety Research (IAS-7)

Operational Navigation of Agents and Self-organization Phenomena in Velocity-based Models for Pedestrian Dynamics

Qiancheng Xu

Schriften des Forschungszentrums Jülich
IAS Series

Band / Volume 49

ISSN 1868-8489

ISBN 978-3-95806-620-5

Bibliografische Information der Deutschen Nationalbibliothek.
Die Deutsche Nationalbibliothek verzeichnet diese Publikation in der
Deutschen Nationalbibliografie; detaillierte Bibliografische Daten
sind im Internet über http://dnb.d-nb.de abrufbar.

Herausgeber und Vertrieb:	Forschungszentrum Jülich GmbH Zentralbibliothek, Verlag 52425 Jülich Tel.: +49 2461 61-5368 Fax: +49 2461 61-6103 zb-publikation@fz-juelich.de www.fz-juelich.de/zb
Umschlaggestaltung:	Grafische Medien, Forschungszentrum Jülich GmbH
Druck:	Grafische Medien, Forschungszentrum Jülich GmbH
Copyright:	Forschungszentrum Jülich 2022

Schriften des Forschungszentrums Jülich
IAS Series, Band / Volume 49

D 468 (Diss. Wuppertal, Univ., 2022)

ISSN 1868-8489
ISBN 978-3-95806-620-5

Vollständig frei verfügbar über das Publikationsportal des Forschungszentrums Jülich (JuSER)
unter www.fz-juelich.de/zb/openaccess.

Acknowledgements

During my doctoral study, I received help from many people. First, I would like to express my great thanks to Prof. Dr. Armin Seyfried. He taught me how to do research and write papers scientifically. He is always very patient in answering my questions and discussing with me enthusiastically, which has benefited me a lot. I would also like to thank Dr. Mohcine Chraibi, a good teacher and a good friend of mine. I got a lot of experience from him in both work and life. His guidance and encouragement progress me.

All the colleagues in the Forschungszentrum Jülich and the Bergische Universität Wuppertal helped me a lot in the last four years. I would like to thank all of them here. In particular: Jette Schumann gave me a lot of experience on my doctoral dissertation and defense; My office mate Ghadeer Derbas always encourages me and gives advice when I am in trouble; Rudina Subaih had many meaningful discussions with me.

Moreover, I would like to thank Prof. Dr. Antoine Tordeux for his guidance in developing the model for pedestrian dynamics. I would also like to thank Prof. Dr. Andreas Schadschneider, Prof. Dr. Bert Leerkamp, and Prof. Dr. Fabian Brännström for their willingness to be members of my examination committee.

Finally, I would like to thank my wife Jingjing especially. She has been by my side from undergraduate to doctoral. We have overcome one difficulty after another and made progress together. Without her support and company, I could not have completed my doctoral study. And I would like to thank the support from my parents and my wife's parents, the accompanying from my friends and basketball teammates, and the funding from China Scholarship Council.

Abstract

While moving in space, pedestrians often adjust their direction of movement and/or their speed to avoid collisions with others and obstacles. This steering process is influenced by physical factors from the environment, as well as psychological factors of pedestrians such as motivation. Therefore, when modeling the movement of pedestrians especially for reproducing self-organization phenomena, it is important to consider these factors.

This cumulative dissertation includes four publications related to velocity-based models for pedestrian dynamics. Three of them study the navigation of pedestrians and related self-organization phenomena, and the remaining one is an applied study related to the control measures adopted by German supermarkets during the COVID-19 pandemic. Velocity-based models consider pedestrians as particles also called agents and describe their movement at the operational level, by means of first-order differential equations. Velocity-based models, contrary to cellular automata, are continuous in space. Moreover, the new position of pedestrians is determined directly by a velocity function instead of an integrating of acceleration in force-based models.

In publication I, a velocity-based model that considers several basic behaviors of pedestrians is proposed and validated with the fundamental diagram of unidirectional pedestrian flow. Besides, the effect of agents' shape on the overall dynamics is studied. Although this basic model is able to guarantee the volume exclusion and reproduce the fundamental diagram of unidirectional pedestrian flow, it does not perform well in complex scenarios, where self-organization phenomena occur. Therefore, in publication II and III, the previously developed basic model is used to quantitatively study clogging in bottleneck scenarios and lane-formation in bidirectional flow scenarios, respectively. In addition, in publication III, an anticipation mechanism is introduced into the basic model to describe lane-formation in bidirectional flow scenarios more realistically. Based

on the analysis in publications II and III, a new structure of the model for pedestrian dynamics is proposed in the outlook chapter of this dissertation. Finally, in publication IV, the velocity-based model is used to evaluate the effectiveness of control measures adopted by German supermarkets during the COVID-19 pandemic in 2020.

Zusammenfassung

Wenn sich Fußgänger in Menschenmengen bewegen, passen sie oft ihre Bewegungsrichtung und/oder ihre Geschwindigkeit an, um Kollisionen mit anderen Personen und Hindernissen zu vermeiden. Beeinflusst wird dieser Lenkvorgang durch physikalische Faktoren aus der Umgebung, aber auch durch psychologische Faktoren des Fußgängers wie die Motivation. Daher ist es bei der Modellierung der Bewegung von Fußgängern insbesondere zur Reproduktion von Selbstorganisationsphänomenen wichtig, diese Faktoren zu berücksichtigen.

Diese kumulative Dissertation umfasst vier Veröffentlichungen zu geschwindigkeitsbasierten Modellen für die Fußgängerdynamik. Drei dieser Veröffentlichungen untersuchen die Navigation von Fußgängern und damit verbundene Selbstorganisationsphänomene, während die vierte eine angewandte Studie zu den Kontrollmaßnahmen deutscher Supermärkte während der COVID-19-Pandemie. Geschwindigkeitsbasierte Modelle betrachten Fußgänger als Teilchen, auch die Agenten genannt werden, und beschreiben ihre Bewegung auf operativer Ebene mit Hilfe von Differentialgleichungen erster Ordnung. Geschwindigkeitsbasierte Modelle sind im Gegensatz zu zellulären Automaten im Raum kontinuierlich. Außerdem wird die neue Position von Fußgängern direkt durch eine Geschwindigkeitsfunktion bestimmt, anstatt die Beschleunigung in kraftbasierte Modelle zu integrieren.

In der Publikation I wird ein geschwindigkeitsbasiertes Modell, das grundlegende Verhaltensweisen von Fußgängern berücksichtigt, vorgestellt und mit dem Fundamentaldiagramm des unidirektionalen Fußgängerflusses validiert. Außerdem wird der Einfluss der Agentenform auf die Gesamtdynamik untersucht. Dieses vereinfachte Modell ist in der Lage, den Volumenausschluss zu gewährleisten und das Fundamentaldiagramm des unidirektionalen Personenstrom zu reproduzieren, stößt jedoch in komplexen Szenarien, in denen Selbstorganisationsphänomene auftreten,

an seine Grenzen. Daher wird in den Publikationen II und III das zuvor entwickelte Modell verwendet, um die Verstopfung in Engpassszenarien bzw. die Spurbildung in bidirektionalen Strömungsszenarien quantitativ zu untersuchen. Darüber hinaus wird in der Publikation III ein Antizipationsmechanismus in das Modell eingeführt, um die Spurbildung in bidirektionalen Strömungsszenarien realistischer zu beschreiben. Basierend auf der Analyse in den Publikationen II und III wird im Ausblick dieser Dissertation eine neue Struktur des Modells für die Fußgängerdynamik vorgeschlagen. Schließlich wird in der Publikation IV das geschwindigkeitsbasierte Modell verwendet, um die Wirksamkeit der Kontrollmaßnahmen deutscher Supermärkte während der COVID-19-Pandemie im Jahr 2020 zu bewerten.

Abbreviations

AVM	Anticipation velocity model
CA	Cellular automaton
CSM	Collision-free speed model
FD	Fundamental diagram
GCVM	Generalized collision-free velocity model

List of publications

Publication I

Xu Q, Chraibi M, Tordeux A, Zhang J. Generalized collision-free velocity model for pedestrian dynamics. Physica A: Statistical Mechanics and its Applications, 2019, 535: 122521.

Publication II

Xu Q, Chraibi M, Seyfried A. Prolonged clogs in bottleneck simulations for pedestrian dynamics. Physica A: Statistical Mechanics and its Applications, 2021, 573: 125934.

Publication III

Xu Q, Chraibi M, Seyfried A. Anticipation in a velocity-based model for pedestrian dynamics. Transportation research part C: emerging technologies, 2021, 133: 103464.

Publication IV

Xu Q, Chraibi M. On the effectiveness of the measures in supermarkets for reducing contact among customers during COVID-19 period. Sustainability, 2020, 12(22): 9385.

Author's contribution

Publication I
Conceptualization: Qiancheng Xu, Mohcine Chraibi, Antoine Tordeux
Software: Qiancheng Xu
Formal Analysis: Qiancheng Xu
Investigation: Qiancheng Xu
Methodology: Qiancheng Xu, Mohcine Chraibi, Antoine Tordeux
Visualization: Qiancheng Xu
Writing – Original Draft Preparation: Qiancheng Xu
Writing – Review & Editing: Qiancheng Xu, Mohcine Chraibi, Antoine Tordeux, Jun Zhang

Publication II
Conceptualization: Qiancheng Xu, Mohcine Chraibi, Armin Seyfried
Software: Qiancheng Xu
Formal Analysis: Qiancheng Xu
Investigation: Qiancheng Xu
Methodology: Qiancheng Xu, Mohcine Chraibi, Armin Seyfried
Visualization: Qiancheng Xu
Writing – Original Draft Preparation: Qiancheng Xu
Writing – Review & Editing: Qiancheng Xu, Mohcine Chraibi, Armin Seyfried

Publication III
Conceptualization: Qiancheng Xu, Mohcine Chraibi, Armin Seyfried
Software: Qiancheng Xu
Formal Analysis: Qiancheng Xu
Investigation: Qiancheng Xu
Methodology: Qiancheng Xu, Mohcine Chraibi, Armin Seyfried
Visualization: Qiancheng Xu
Writing – Original Draft Preparation: Qiancheng Xu

Writing – Review & Editing: Qiancheng Xu, Mohcine Chraibi, Armin Seyfried

Publication IV

Conceptualization: Qiancheng Xu, Mohcine Chraibi
Software: Qiancheng Xu
Formal Analysis: Qiancheng Xu
Investigation: Qiancheng Xu
Methodology: Qiancheng Xu, Mohcine Chraibi
Visualization: Qiancheng Xu
Writing – Original Draft Preparation: Qiancheng Xu
Writing – Review & Editing: Qiancheng Xu, Mohcine Chraibi

Contents

Chapter 1

Introduction

1.1 Motivation

1.1.1 Crowd disasters

Nowadays, with the increase of the world's population and the convenience of transportation, the scale of events in which numerous persons gather in specific locations is getting bigger. The safety of the crowd in these events is an important issue for both participants themselves and the organizers. Although most of these events are carefully planned before they are held, accidents may still be unavoidable, even in some small-scale events, when high densities of people are in combination with unfavorable geometrical constructs such as bottlenecks. For example, the Hillsborough disaster in Sheffield, England, on 15 April 1989, led to 96 deaths and 766 injuries [1]. The Love Parade disaster in Duisburg, Germany, on 24 July 2010, caused 21 deaths and at least 500 injuries [2]. The crowd crush in Shanghai, China on 31 December 2014, resulted in 36 deaths and 49 injuries [3]. Recently, on April 30, the crowd crush occurred in Meron, Israel, in which 45 people were dead and 150 were injured [4].

To avoid these disasters, events of the crowd must be cautiously planned by using handbooks or simulations that are validated with the result of experiments or field studies. Among these methods, simulations offer an efficient tool for testing different scenarios, beforehand. Besides, simulations can be easily evaluated and interpreted through appropriate visualization. By studying the movement of pedestrians and the phenomena observed in crowds, pedestrian dynamics can be described in simulations by mathematical models. After verification and validation, these models are efficient tools to examine the safety of large events and explore the efficiency and safety of different organizational measures.

1.1.2 Building designs

As the urban population increases, the buildings in big cities become much larger and more complex, which makes a safe evacuation of people in emergency situations a serious task. For instance, when a fire or a natural disaster such as an earthquake occurs, people in a building need to evacuate in a short time. The efficiency of the evacuation process is mainly affected by the structure of the building, e.g., the layout and shape of rooms, the length and width of corridors, the location and height of staircases, and the location and width of exits. Usually, changing the structure of an already constructed building is costly. Therefore, it is important to evaluate the building with respect to safety, comfort, and efficient design before construction and during the planning phase.

The guidance for designing the structure of buildings can be divided into two categories, which are prescriptive and performance-based methods [5]. The prescriptive method is mainly based on experience and according to the type of buildings, provides the minimal or maximal number of some features, e.g., the minimal width of exit and the maximal number of occupants. This method can be easily followed by choosing satisfactory parameters of facilities but is insufficient for buildings with complex structures. Therefore, the performance-based method is developed, which focus on designing buildings based on users' requirements [6]. One of the main steps in the performance-based method is using evaluation tools to assess whether the proposed solution meets the performance requirements, e.g., required safe egress time should be larger than available safe egress time. Knowing how people move in different scenarios is important for this evaluation. However, up to now, there is no general valid description of the pedestrian movement, because it depends on multiple factors like the environment, culture, region, and characteristics of pedestrians.

In spite of this, handbooks and simulations can be used for the evaluation process. Handbooks provide the information of pedestrian dynamics as a reference for facility design, which includes the mean dimension and the free-flow walking speed of pedestrians at different ages, the relation between pedestrian flow and density at different scenarios, etc. [7, 8, 9]. However, handbooks regard the crowd as homogeneous and are unable to consider the heterogeneity of individuals. This insufficiency can be well made up by numerical simulations through assign individual parameters to the agent in microscopic models.

1.1.3 Evaluating control measures for pandemics

The spread of COVID-19 has caused a huge impact on humans' life worldwide. The virus that causes COVID-19 spreads mainly when an infected person is in close contact with other people for a certain period of time [10]. Therefore, many control measures are adopted to reduce close contact among people. For example, stores in Germany take measures including limiting the number of customers and asking customers to keep social distance (a minimum of 1.5 m). However, the effectiveness of these measures is unknown and is hard to measure as it is (ethically) not possible to conduct experiments with humans under these special conditions. With the simulation of customers' movement in confined stores, these measures can be evaluated by using suitable indexes to reflect the degree of contact among customers. Moreover, the model for pedestrian dynamics can be extended to an epidemiology model by combining the knowledge and data about the transmission of viruses.

1.2 State-of-the-art models of pedestrian dynamics

The behaviors and actions of pedestrians are usually classified into three different levels [11]. The strategic level is the highest one, which defines the activities pedestrians choose and their order of execution. The level lower than the strategic level is the tactical level. At this level, pedestrians choose a route to reach the area of each activity. The route is influenced by many factors including the available walking time, the distance to walk, and the degree of congestion of the road, etc. The last and lowest one is the operational level. This level covers those behaviors and actions pedestrians take to avoid imminent collisions with others and obstacles.

The majority of models for pedestrian dynamics describe the movement of pedestrians at the operational level. The decisions at strategical and tactical levels are often considered as external inputs of the operational model. The studies in the current dissertation focus on models at the operational level. A general categorization of pedestrian models at the operational level is based on the scale of analyzed quantities. According to the scale from large to small, models are classified into macroscopic, mesoscopic, and microscopic models.

Macroscopic models treat the crowd as a whole and describe the movement of crowds using averaged quantities, such as density, velocity, or flow. These models neither distinguish individual pedestrians nor consider individual behavior [12], but

they can provide an understanding of the overall behavior of crowds. Therefore, macroscopic models are often used for scenarios of large crowds where individual differences could be neglected. Since there are many similarities between the dynamics of crowds and fluids, a lot of macroscopic models of pedestrian dynamics are developed on the basis of fluid mechanics [13, 14, 15, 16, 17, 18, 19, 20]. Under the assumption of conservation of mass and momentum, these models are usually constituted by a set of continuity equations. However, it is obvious that the movement of crowds does not satisfy these classical continuum assumptions. The network-based model [21, 22, 23, 24] is another type of macroscopic model, which uses networks to represent pedestrians' transport in buildings. Each node in the network represents a facility in the building, e.g., rooms, corridors, halls. These nodes are connected by edges, which corresponds to the connection of these facilities. Network-based models are generally used to determine the optimal evacuation route. However, it can also be combined with microscopic and mesoscopic models to consider the interaction between pedestrians.

Mesoscopic models also use averaged quantities to describe the movement of crowds. However, different from macroscopic models, in mesoscopic models, the behavior of individual pedestrians is described by probability distributions of their positions and velocities. To distinguish between the macroscopic and mesoscopic models more clearly, it is recommended to read [12, 25, 26, 27]. The development of mesoscopic models is inspired by the kinetic theory of gases [12, 28, 29, 30]. The mesoscopic model is also a tool to connect the macroscopic and the microscopic models, the relevant works can be found in [31, 32].

Compared with macroscopic and mesoscopic models, microscopic models focus on the movement of each pedestrian. Pedestrians are represented as particles, also called "agents", which influence each other's movement. Since the movement of each agent needs to be calculated, the microscopic models are computationally expensive to some extent, especially when the scale of crowds is big. However, microscopic models can naturally take into account the heterogeneity and stochasticity of pedestrians' behavior. Moreover, they are suitable to study the interaction between pedestrians and describe their dynamics in simple scenarios.

In recent years, many microscopic models have been developed for describing pedestrian dynamics. In microscopic models, the calculation of the new position of agents usually requires solving differential equations. However, there are also some models that determine the new positions of agents directly according to their current situation, such as desired directions and the positions of neighbors, instead of solving

differential equations. A typical model that falls into this category is the cellular automata (CA) model, which is discrete in space and time. The two-dimensional space is divided into cells of a specific size. Each cell can only be occupied by one agent. In some case, finer discretization are used, where agents occupy more than one cell [33]. At each time step, whether agents moving to the neighboring cell or staying in the current cell is specified by a set of rules in combination with probability. CA models were firstly applied for describing the movement of vehicles on streets and highways, then they were gradually adapted to model the movement of pedestrians [34, 35, 36, 37, 38]. In subsequent developments, various concepts are continuously introduced into the CA model to more accurately describe pedestrian dynamics, e.g., floor field [39, 40], friction parameters [41, 42], anticipation mechanism [43, 44], and game theory [45, 46]. The lattice gas model is similar to the CA models. Agents are located at cross points in the lattices gas model instead of cells in the CA model [47, 48, 49, 50, 51, 52]. The space-discreteness of CA and lattice gas models leads to lower computational costs compared to other microscopic models continuous in space. However, spatial discretization also brings limitations, especially in complex scenarios. For instance, the size of the geometry, the maximum density of agents, and the velocity of agents are all limited by the size and type of cells.

Based on the underlying mechanism used to determine the movement of agents, microscopic models requiring solving differential equations can be divided into two main categories, which are acceleration-based and velocity-based models [53].

Most of the acceleration-based models are continuous in space. The interactions between pedestrians and infrastructure are described by forces, so acceleration-based models are also called force-based models. Based on Newton's second law, the movement of an agent is determined by the acceleration proportional to the force applied to it. The most famous model in this category is the social force model [54], which adopts three force terms to describe the pedestrian movement: the driving force prompts pedestrians to move at their desired velocity, the repulsion force from neighbors and borders to keep distance, and the attractive force from persons or objects. Two additional contact forces are introduced later for dense crowd [55]. The model is widely used to investigate the pedestrian dynamics in the bottleneck scenario [56, 57]. In some studies [58, 59], a group force is also introduced to describe the movement of pedestrians in groups. Furthermore, the model is extended in different ways to better reproduce the movement of pedestrians in bidirectional flow situations [60, 61, 62]. Another force-based model that has been extensively studied is the centrifugal force model [63]. Chraibi et al. [64] generalized the model and introduced an elliptical

volume exclusion of agents. Besides circular and elliptical agents, in [65, 60] each agent is represented by three overlapping disks. Since agents in force-based models are driven by forces, they show some unrealistic behavior, such as overlapping and oscillation. These limitations are detailed discussed in [53, 64, 66].

Velocity-based models are also continuous in space, but the movement of the agent is determined by velocity directly. The velocity of agents is determined by the position and velocity of their neighbors as well as their surroundings. Therefore, calculating the new position of agents only need to solve first-order differential equations. Velocity obstacle models are typically velocity-based model, and it is initially proposed for robot motion planning in a time-varying environment [67]. The velocity obstacle of an agent is the set of the agent's velocities that would cause collisions with obstacles (both static and moving) at some future time. See Figure 1.1. Velocities outside the velocity obstacles are called avoidance velocities. Then the new velocities of agents are selected by a specific rule from the set of avoidance velocities, for example, the highest avoidance velocity along the line to the goal. In subsequent studies, models based on different forms of velocity obstacles have been proposed [68, 69, 70, 71, 72]. Models based on velocity obstacles mainly focus on the collision avoidance of agents. They can reproduce several self-organization phenomena of pedestrians and avoid gridlock in some situations, however, these models are usually not designed for reproducing the fundamental diagram (FD) of pedestrian flows. Tordeux et al. [73] proposed a model to describe pedestrian dynamics, where the moving direction and speed of an agent are calculated separately. The model is called the collision-free speed model (CSM). The direction of movement is determined by the desired direction of the agent and the influence from surrounding neighbors. The speed is a function of the distance to the closest neighboring agent in the direction of movement, which is directly given from a special representation of the FD. The model is overlapping-free, and the speed function reflects the relationship between the speed and the distance to the front agent. Therefore, the model can easily reproduce the FD of pedestrians in single-lane scenarios. Since the model has few parameters and its structure is clear, it is suitable to further develop the model by considering both physical and psychological factors of pedestrians. This model is introduced in publication I. Moreover, the studies in other publications included in this dissertation are all based on this model.

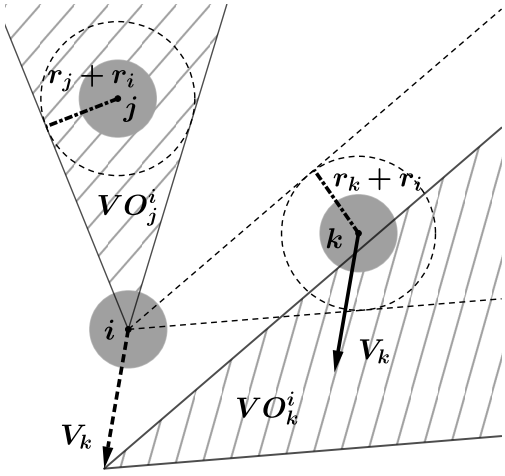

Figure 1.1: Velocity obstacles (hatched areas) of agent i . Velocity obstacle VO^i_j is the set of velocities that would cause collisions with agent j (static). Velocity obstacle VO^i_k is the set of velocities that would cause collisions with agent k (moving with velocity V_k). r_i, r_j, and r_k are the radius of the three agents.

1.3 Verification and validation

Verification and validation are two essential components in the process of developing a model. Verification is the process of determining that a model complies with the developer's conceptual description and specifications. Validation of a model is the process of assessing how well the model can reproduce the movement of real pedestrians. Therefore, the data sets of pedestrian movement obtained from different scenarios are indispensable for developing and enhancing a model. Many researchers are dedicated to collect data on pedestrian movement from the field study [74, 75, 76, 77] and controlled experiment [78, 79, 80, 81]. The data from the field study is collected directly from public places, such as streets and train stations. While in the controlled experiment, pedestrians move in artificially designed scenarios according to predefined rules. Therefore, to some extent, field studies are considered by many researchers to be more realistic than controlled experiments. However, the controlled experiment also has its advantages. Compared to the field study where the pedestrian movement is affected by many factors, the controlled experiment allows to better control the environment of the experiments, e.g., the width of the doors and corridors, which is

more suitable to analyze the effect of a single factor. Nowadays, the movement of pedestrians is usually first recorded in the form of videos, then the position of each pedestrian at each frame is extracted for further studies. Since pedestrians are usually marked with the colored cap or code marker in the controlled experiment, it is easier to extract their positions than in the field study [82].

With the extracted trajectories of pedestrians, the movement of pedestrians can be described by different quantities, e.g., speed (v), density (ρ), and specific flow ($J_s = \rho \cdot v$). The relationship between these quantities is called the fundamental diagram (FD), which is probably the most important and widely used relationship to validate models that are used to describe transport properties of pedestrian streams quantitatively. The two relationships that are often used to validate models are density-speed $v(\rho)$ and density-specific flow $J_s(\rho)$. Several researchers collected the relationship between density and speed from the field study [83, 84, 85, 76, 77]. Although the same qualitative trend has been observed, that is the speed of pedestrians decreases with increasing density, there are still differences between the relationship obtained from these studies. The reason behind the difference is that the FD is influenced by many factors, e.g, culture and population differences, the motivation of pedestrians, the type of measured pedestrian flow (uni- and multi-directional), and the type of facilities (corridor, bottleneck, stairs). To analyze the effect of every single factor and avoid the influence of other factors, many well-designed controlled experiments are performed. For instance, the single-file movement [78, 86, 87, 88, 89, 90], unidirectional flow in straight corridors [91], bidirectional flow in straight corridors [92, 93, 94, 95], and four-directional crossing flow [96].

The bottleneck is another important scenario related to the movement of pedestrians. When the incoming flow is sufficiently large, congestions can occur in front of the bottleneck. The relationship between the capacity and the width of the bottleneck has been discussed a lot and it is often used to validate models. The flow through the bottleneck shows a linear growth with increasing the width of the bottleneck in experiments [81, 97, 80, 98]. Besides the width of the bottleneck, the flow inside the bottleneck is also influenced by many other factors, e.g., the length of the bottleneck [99], the obstacle in front of the bottleneck [100, 101], and the motivation of pedestrians [97, 102, 103].

Besides FD and bottleneck flow, self-organization phenomena, which is an important characteristic of pedestrian dynamics, can also be used to validate models. Self-organization is a process where some form of overall order in the crowd arises

spontaneously from local interactions between individual pedestrians, e.g., stop-and-go waves [77, 104], zipper effect [79, 81], clogging and lane formation. In this dissertation, clogging and lane formation are mainly studied.

Clogging is a typical phenomenon occurred in front of the bottleneck. See Figure 1.2(a)[1]. It is mentioned above that the flow through a bottleneck is influenced by the motivation of pedestrians. This is because clogging occurs when dense crowds move through the bottleneck with high motivation. Clogging is often expressed as the jamming arch formed by several pedestrians in front of the bottleneck, which significantly decreases the flow through the bottleneck. In publication II, the phenomenon is studied through simulations and related studies are introduced.

(a) (b)

Figure 1.2: The self-organization phenomena in laboratory experiments. (a) Clogging. (b) Lane formation.

Lane formation is another phenomenon that occurs in bidirectional pedestrian streams, where pedestrians self-organize into dynamically varying and separated lanes. See Figure 1.2(b)[2]. Unlike car traffic, where stable lanes are predetermined by the restrictions given by the infrastructure, in pedestrian dynamics lanes are formed dynamically and naturally with neither external synchronization nor any prior agreement between the pedestrians. Lane formation is also assumed to be a reason for the difference between the FD of uni- and bidirectional flows. In publication III, the phenomenon is investigated through simulations and related literature are reviewed.

[1] `http://ped.fz-juelich.de/da/2018crowdqueue`
[2] `http://ped.fz-juelich.de/da/2009unidirOpen`

1.4 Objectives

The main goal of this dissertation is to develop a microscopic model that can reproduce the FD of both uni- and bidirectional pedestrian flow, as well as self-organization phenomena including clogging and lane-formation. The model is based on the structure of the CSM and focuses on the operational navigation of agents. It means the model is velocity-based, first-order, and continues in space.

For this purpose, the development of the model is structured in three steps. The first step is developing a model that is able to mitigate the unrealistic oscillation in the CSM, as well as to reproduce the FD of unidirectional pedestrian flow in straight corridors. This model considers several basic behaviors of pedestrians, which are: agents move toward the target without backward movement, change the direction of movement smoothly to avoid collision with neighbors, and adjust speed based on the distance to the closest neighboring agent in front.

The model proposed in the first step is insufficient for reproducing clogging and lane-formation quantitatively, as the factors of pedestrians, which are related to these self-organization phenomena, are not considered fully. Therefore, the second step is determining the ignored "relevant factors" of the basic model by analyzing the simulations of the proposed model in the bottleneck and bidirectional flow scenarios. In the bottleneck scenarios, it is investigated how the motivation of pedestrians and their tendency of queuing affect the occurrence of clogging. Moreover, the effect of factors such as parameters of the spatial boundaries is also investigated. While in bidirectional flow scenarios, the action predicting changes of neighboring pedestrians' positions and the strategy of following others are considered, their influence on the formation of lanes is studied.

The final step is extending the model proposed in the first step according to the analysis result of the second step. The model proposed in this step can reproduce the FD of both uni- and bi-directional pedestrian flows. Moreover, this model is able to describe clogging and lane-formation closer to reality.

Besides the studies related to the main goal, an application of the CSM is also covered in this dissertation. The effectiveness of control measures in German supermarkets during COVID-19 is evaluated through simulations.

Chapter 2

Research questions and results

In publication I, a modified model of the CSM is proposed for mitigating unrealistic oscillations of the agents in the simulation. The model is then used to study clogging in bottleneck scenarios (publication II) and lane formation in bidirectional flow scenarios (publication III). The model is extended with an anticipation mechanism to reproduce bidirectional flow more realistically (publication III). Furthermore, an application of the CSM, which is related to the control measures during COVID-19 period, is given in publication IV. The investigated questions and main results of each publication are given below.

2.1 Publication I: The basic model

The CSM is a model continuous in space based on first-order equations describing microscopically pedestrian dynamics [73].

It consists of two components for determining the direction of movement and speed of agents, respectively. The sub-model for the direction of movement considers the desired direction of agents and the impact of their neighbors. In analogy to most force-based models, the strength of the influence from a neighbor to an agent is a function of the distance between the two agents, and the direction of the vector describing this effect points from the neighbor to the agent. However, unlike force-based models, where accelerations of agents are calculated, the speed of an agent is determined directly by a speed function according to the distance to the closest neighboring agent in front. The structure of the model, especially the sub-model for speed, guarantees the volume exclusion of agents. Although the model is simple, the property of volume exclusion is enough to qualitatively reproduce several self-organization phenomena in pedestrian dynamics, e.g., clogging and lane formation. Besides, since the speed sub-model is based on the relationship between speed and distance to the front agent, it

is suitable to reproduce the FD of pedestrians. This model has a clear structure and few parameters, which are beneficial to further extensions.

The interaction among agents has been described in the CSM. However, the influence of walls and obstacles was neglected in the definition of the model, which hinders the implementation of the model in more scenarios. Therefore, in publication I, this gap is closed before introducing further extensions. After that, the FD of single-lane movement and unidirectional flow in a two-dimensional corridor are used to validate the model. It is found that, when the shape of agents is dynamic elliptical instead of circular, the reproduced FD in the two-dimensional corridor fits the experimental data better.

Adopting elliptical agents reveals another deficiency of the CSM that is the strong fluctuation of agents' direction of movement. Besides, the sub-model for the direction of movement, which is inspired from the force-based model, also inherits the oscillation caused by the frequently backward movement of agents. Therefore, generalized collision-free velocity model (GCVM) is proposed. A dynamical vision area is introduced to identify the neighbors who have an impact on the direction of movement of agents. The vector describing the influence from neighbors to an agent is redefined as a unit vector perpendicular to the desired direction of the agent. Moreover, a new relaxation time parameter is used to smooth the turning process of agents. Compared to the CSM, the unrealistic oscillation of agents is significantly reduced in the GCVM. Furthermore, the GCVM can reproduce a more realistic distribution of agents in front of the bottleneck.

2.2 Publication II: Clogging in the bottleneck

Although a series of extensions have been made on the CSM, the volume exclusion property is reserved in the GCVM, which results in the occurrence of prolonged clogs in front of the bottlenecks with a small width. Clogging is a phenomenon that several pedestrians mutually block each other in front of the bottleneck when high density and high motivation coincide. Since the flexibility and elasticity of the human body, the clog of pedestrians is usually temporary in time. However, the volume exclusion of agents in the simulation results in clogs interrupting flow for a longer time than reality, and sometimes even stable clogs occur.

In publication II, to quantitatively study the clogging phenomenon in the simulation, the formation of the minimal clog in the GCVM is defined as two agents whose directions of movement point toward each other but the distance between them is too

small for them to move. Besides, space and time conditions are adopted to identify prolonged clogs that interrupt the flow longer than a predefined threshold. By analyzing the number of prolonged clogs and the time lapse between two consecutive agents passing the bottleneck, the effect of various factors on the occurrence of prolonged clogs is studied.

The investigated factors are categorized as parameters of the spatial boundaries, algorithmic factors related to the implementation of the model, and the parameters of the movement model. Parameters of the spatial boundaries include the width and the position of the bottleneck exit. As the width of the exit increases the number of prolonged clogs and the probability of clogs sustaining a longer time both decrease. Besides, when locating the exit adjacent to the lateral wall of the bottleneck, the number of prolonged clogs is significantly less than with the other locations. For algorithmic factors, the update methods and the size of the time step are considered as may having an effect. However, the simulation results obtained with different update methods and values of time step do not show significant differences, which comes to the conclusion that the clog in the GCVM is not an algorithmic issue.

Last, the effect of model parameters is studied. The investigated parameters cover the slope of the speed-headway relationship, the free speed of agents, the strength and range of the impact from neighbors in the direction of movement, and the shapes of agents. An increased slope of the speed-headway relationship leads to a smaller distance between agents, which corresponds to the scenario with a higher level of motivation. Increasing the slope results in the increase of both the free flow rate and the number of prolonged clogs in simulations. Since the free speed of agents only determines the maximal speed agents can achieve when the distance to the closest agent in front is far enough, a higher free speed does not affect the movement of agents at congested conditions. Consequently, a higher free speed leads to a lower number of prolonged clogs, as agents move faster in low density situations. A greater impact from neighbors on the direction of movement makes agents being more stimulated to deviate from their desired directions, so agents tend to queue when this impact is low. It results in that the number of prolonged clogs increases with increasing influence from neighbors on the direction of movement. Furthermore, with performing simulations where pedestrians are modeled as disks with different radius, it is found that the number of prolonged clogs decreases when the ratio between the width of the exit and the radius of agents increases. However, the number of prolonged clogs is not affected by the absolute values of the width and the radius if the ratio of them remains the same.

The analysis in publication II reveals that the GCVM can qualitatively describe the clogging of pedestrians in front of the bottleneck to a certain extent. However, a further extension for the GCVM to break the volume exclusion of agents in congested situations is inevitable for better describing the clogging phenomenon, for example, introducing the strategy of pushing others. The structure of a new model that considers the strategy of pushing others is discussed in chapter 3.

2.3 Publication III: Lane formation and anticipation

To eliminate the oscillation of agents in the CSM, the backward movement of agents is abandoned, which results in a side effect that jamming appears at a lower density in bidirectional flow scenarios in the GCVM than in the CSM. Actually, jamming would not occur at such a low density in bidirectional pedestrian flow. Instead, pedestrians follow others who move in the same direction as them and form separate lanes to avoid collision with agents moving in the opposite direction. This phenomenon is called lane-formation, which is based on a stimulus-response mechanism and strategies of navigation in a fast-changing environment. Due to the combination of the volume exclusion and the agents' ability to change their moving direction, the CSM and the GCVM can qualitatively reproduce lane formation as observed in the system of inanimate particles. However, they are not sufficient for a quantitative description of the phenomenon.

In publication III, the anticipation velocity model (AVM) is proposed for reproducing lane formation more realistically. Compared to the GCVM, the action predicting changes of neighboring pedestrians' positions and the strategy of following others are covered in this model. Although jamming is not completely eliminated in the bidirectional flow scenarios, the critical density where jamming occurs in the AVM is higher than in the CSM and the GCVM. Besides, the definition of an order parameter is used to quantitatively describe the formation of lanes at transient states. The AVM leads much faster to the formation of lanes than the CSM and the GCVM, which is much closer to the experimental result. Finally, the AVM is validated with the FD of uni- and bidirectional flow. The difference between the FD of uni- and bidirectional flow is also reproduced well. Moreover, the course of lane formation in time and the shape of the formed lanes in the simulations with the AVM are similar to in the experiments.

Compared to the CSM and the GCVM, the AVM reproduces the bidirectional pedestrian flow more realistically, which proves the significance of considering pedestrian's anticipation and the strategy of following others into the model. However, forming lanes is not the only strategy adopted by pedestrians to avoid collisions. Sometimes, pedestrians choose to cooperate with others to avoid the occurrence of collisions in advance, which should be also considered into the model. The structure of a new model that considers the strategy of cooperating with others is discussed in chapter 3.

2.4 Publication IV: Application

In addition to the above studies about the CSM and its extensions, the CSM is applied to study the effectiveness of the measures taken by German supermarkets during the COVID-19 period. Since the COVID-19 spreads primarily from person to person through small droplets produced by coughing, sneezing, or speaking of an infected person, reducing close contact among people is one of the recommended measures to prevent infection.

To slow down the transmission of the disease, supermarkets in Germany took measures to reduce the contact of customers. For instance, restricting the number of customers, asking them to keep social distance and enter with a shopping cart. In publication IV, the effectiveness of these measures is quantitatively evaluated through numerical simulations with the CSM. First, an index based on the distance between agents is defined to reflect the degree of contact between them. The lower the distance between two agents leads to the higher the degree of contact. Then a virtual supermarket is built based on a real one nearby the city Jülich in Germany, which represents the typical structure of a German medium-sized supermarket. Simulations are performed in this virtual supermarket with four scenarios adopting different control measures. The first two situations only consider the restriction of agents' number, where the maximum number of agents in the supermarket at the same time is 50 in scenario 1 and 30 in scenario 2. Scenario 3 takes into account the rule of 1.5 m social distance, and scenario 4 uses larger agents to represent the customer with a shopping cart.

In each scenario, the total number of agents enter the supermarket for shopping is the same. By analyzing the accumulated time spent by all the agents for shopping and the average degree of contact between agents in the four scenarios, the following results are obtained. The limitation on the number of customers in the supermarket slightly

increases the accumulated time for shopping, but it significantly reduces the contact among agents. Moreover, keeping a social distance is also effective at reducing the contact among agents and not influence the accumulated time for shopping. However, entering the supermarket with shopping carts influences neither the degree of contact nor the accumulated time for shopping. In addition, it is also observed that agents contact each other more in the area with the crossing structure than in other areas. Therefore, reducing the crossing structure in the supermarket may be also an effective measure to reduce the contact among customers.

Although the results of this study may change with the structure of the virtual supermarket scenario and the behavior of agents in simulations, this study presents a framework to evaluate the effectiveness of control measures adopted in indoor scenarios during the COVID-19 period.

Chapter 3

Discussion and outlook

In this dissertation, three microscopic models for pedestrian dynamics are developed and studied, which are the collision-free speed model (CSM), the generalized collision-free velocity model (GCVM), and the anticipation velocity model (AVM). The three models are velocity-based models and have the same structure, which consists of a sub-model for the direction of movement (operational navigation) and a sub-model for speed. However, they perform differently as different sub-models are adopted for operational navigation.

The CSM is the simplest among these three models, and it is also the only one of the three models in which agents can move backward. Actually, it was observed that backward movement can indeed reduce the occurrence of gridlock in scenarios, where multi-directional flow and high density come together. However, this backward movement is also a reason for the unrealistic oscillation in the simulation, which is hardly observed in real pedestrian movement. In reality, pedestrians only move backward actively when having a very strong tendency to give way to others, which is a kind of cooperative behavior realized by communication. In addition, pedestrians sometimes move backward passively in scenarios with high motivation, which can be attributed to the pushing from others. The backward movement in the CSM occurs frequently and is caused by the inappropriate description of pedestrians' waiting behavior, which does not well match the two situations described above.

Therefore, the backward movement is removed in the GCVM by modifying the direction of the vector that describes the impact of neighbors on the direction of movement. Removing the backward movement leads to a more realistic simulation without oscillation, but as mentioned before it also results in more gridlock in scenarios with multi-directional flow. This is because collisions among agents occur more frequently in multi-directional flow scenarios, hence they need to move backward and make space in order to dissolve these already formed collisions. However, if we carefully observe

the movement of pedestrians, we notice that they prefer to avoid collisions in advance before they even happen.

Pedestrians usually avoid collisions by using a stimulus-response mechanism to anticipate changes in the environment. Therefore, the AVM introduces two new features based on the GCVM, which are the action anticipating changes of neighboring pedestrians' positions and the strategy of following others. It is realized by calculating the influence of neighbors using their future positions and direction of movement. In bidirectional flow scenarios, agents in the simulation with the AVM form lanes more realistically and faster than with the other two models. It shows that covering anticipation into the model is significant for reproducing the collision avoidance of pedestrians.

However, as in real life, only considering anticipation is not enough to avoid all collisions in the simulation, especially in high-density situations. From the observation in the experiment, there are two main strategies adopted by pedestrians for avoiding or solving collisions. The first strategy is observed frequently in front of bottlenecks, where pedestrians with high motivation push others away and so obtain some space to move. Pushing is a typical strategy for solving formed collisions. It means a pedestrian can still move even in situations with limited space, which is realized by breaking the volume exclusion to some extent or changing postures via turning the body, moving shoulders, etc. However, in most daily situations pedestrians rarely push others, as pushing is often linked to impoliteness and rudeness. Instead, most pedestrians prefer to avoid collisions in advance by giving away space to others, who may be potentially on the collision course. This strategy can be interpreted as a form of "cooperation", where pedestrians who have enough space to move choose to wait in place or move slightly backward and signal other people to go first. In fact, pedestrians choose different strategies by perceiving the surrounding environment to avoid or solve collisions. However, in all three models, detached from the situation, agents can only choose the same strategy defined in each model. For instance, the speed of an agent is determined by the distance to the agent in front, which is not always in accordance with reality. Therefore, for future research, we propose a new structure of the model for pedestrian dynamics as shown in Figure 3.1.

In the new structure, agents first perceive the actual situations, which includes the position, velocity, motivation, and cooperation signal from others. Then the prediction of future situations is made according to the current situations. Three optional methods for predicting future situations are considered, which are: the future position, the time to collision, and the distance to collision. Afterward, the strategy

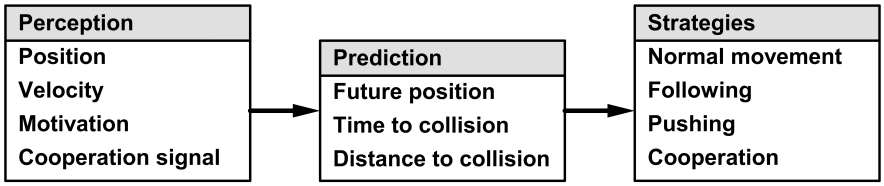

Figure 3.1: A new structure of the model for pedestrian dynamics.

adopted by an agent is the result of a combination of perception, prediction, and self-property of the agent. According to the different situations, agents choose different strategies, i.e., normal movement, following, pushing, and cooperation. Future works include defining the situation, when agents adapt each strategy and how they will move when they adopt the corresponding strategy.

References

[1] Carol E Nicholson and B Roebuck. The investigation of the hillsborough disaster by the health and safety executive. *Safety Science*, 18(4):249–259, 1995.

[2] Dirk Helbing and Pratik Mukerji. Crowd disasters as systemic failures: analysis of the love parade disaster. *EPJ Data Science*, 1(1):1–40, 2012.

[3] Jingbo Zhou, Hongbin Pei, and Haishan Wu. Early warning of human crowds based on query data from baidu maps: Analysis based on shanghai stampede. In *Big data support of urban planning and management*, pages 19–41. Springer, 2018.

[4] Wikipedia contributors. 2021 meron crowd crush — Wikipedia, the free encyclopedia. `https://en.wikipedia.org/w/index.php?title=2021_Meron_crowd_crush&oldid=1040040470`, 2021. [Online; accessed 31-August-2021].

[5] Jun Zhang. *Pedestrian fundamental diagrams: Comparative analysis of experiments in different geometries*, volume 14. Forschungszentrum Jülich, 2012.

[6] Rodrigo Machado Tavares. Prescriptive codes vs. performance-based codes: which one is the best fire safety code for the brazilian context. *Safety science monitor*, 12(1):1–10, 2008.

[7] Vitaly M Predtechenskii and Anatolii Ivanovich Milinskii. *Planning for foot traffic flow in buildings*. National Bureau of Standards, US Department of Commerce, and the National Science Foundation, 1978.

[8] Stefan Buchmueller and Ulrich Weidmann. Parameters of pedestrians, pedestrian traffic and walking facilities. *IVT Schriftenreihe*, 132, 2006.

[9] Morgan J Hurley, Daniel T Gottuk, John R Hall Jr, Kazunori Harada, Erica D Kuligowski, Milosh Puchovsky, John M Watts Jr, CHRISTOPHER J WIECZOREK, et al. *SFPE handbook of fire protection engineering*. Springer, 2015.

[10] World Health Organization. Q&A on coronaviruses (COVID-19). https://www.who.int/emergencies/diseases/novel-coronavirus-2019/question-and-answers-hub/q-a-detail/q-a-coronaviruses.

[11] Serge P Hoogendoorn and Piet HL Bovy. Pedestrian route-choice and activity scheduling theory and models. *Transportation Research Part B: Methodological*, 38(2):169–190, 2004.

[12] Serge Hoogendoorn and Piet HL Bovy. Gas-kinetic modeling and simulation of pedestrian flows. *Transportation Research Record*, 1710(1):28–36, 2000.

[13] Roger L Hughes. A continuum theory for the flow of pedestrians. *Transportation Research Part B: Methodological*, 36(6):507–535, 2002.

[14] Vincenzo Coscia and Cinzia Canavesio. First-order macroscopic modelling of human crowd dynamics. *Mathematical Models and Methods in Applied Sciences*, 18(supp01):1217–1247, 2008.

[15] Nicola Bellomo and Christian Dogbe. On the modelling crowd dynamics from scaling to hyperbolic macroscopic models. *Mathematical Models and Methods in Applied Sciences*, 18(supp01):1317–1345, 2008.

[16] Christian Dogbé. On the numerical solutions of second order macroscopic models of pedestrian flows. *Computers & Mathematics with Applications*, 56(7):1884–1898, 2008.

[17] Bertrand Maury, Aude Roudneff-Chupin, and Filippo Santambrogio. A macroscopic crowd motion model of gradient flow type. *Mathematical Models and Methods in Applied Sciences*, 20(10):1787–1821, 2010.

[18] Benedetto Piccoli and Andrea Tosin. Time-evolving measures and macroscopic modeling of pedestrian flow. *Archive for Rational Mechanics and Analysis*, 199(3):707–738, 2011.

[19] Rinaldo M Colombo, Mauro Garavello, and Magali Lécureux-Mercier. A class of nonlocal models for pedestrian traffic. *Mathematical Models and Methods in Applied Sciences*, 22(04):1150023, 2012.

[20] Christian Dogbe. On the modelling of crowd dynamics by generalized kinetic models. *Journal of Mathematical Analysis and Applications*, 387(2):512–532, 2012.

[21] Luc G Chalmet, Richard L Francis, and Patsy B Saunders. Network models for building evacuation. *Management science*, 28(1):86–105, 1982.

[22] Steve Gwynne, Edward R Galea, M Owen, Peter J Lawrence, and Lazaros Filippidis. A review of the methodologies used in the computer simulation of evacuation from the built environment. *Building and environment*, 34(6):741–749, 1999.

[23] Gregor Lämmel, Hubert Klüpfel, and Kai Nagel. *The MATSim network flow model for traffic simulation adapted to large-scale emergency egress and an application to the evacuation of the Indonesian city of Padang in case of a tsunami warning*. Emerald Group Publishing Limited, 2009.

[24] Ren-Yong Guo, Hai-Jun Huang, and SC Wong. Collection, spillback, and dissipation in pedestrian evacuation: A network-based method. *Transportation research part B: methodological*, 45(3):490–506, 2011.

[25] José A Carrillo, Massimo Fornasier, Giuseppe Toscani, and Francesco Vecil. Particle, kinetic, and hydrodynamic models of swarming. In *Mathematical modeling of collective behavior in socio-economic and life sciences*, pages 297–336. Springer, 2010.

[26] Nicola Bellomo and Abdelghani Bellouquid. On the modeling of crowd dynamics: Looking at the beautiful shapes of swarms. *Networks & Heterogeneous Media*, 6(3):383, 2011.

[27] Emiliano Cristiani, Benedetto Piccoli, and Andrea Tosin. *Multiscale modeling of pedestrian dynamics*, volume 12. Springer, 2014.

[28] LF Henderson. The statistics of crowd fluids. *nature*, 229(5284):381–383, 1971.

[29] Leroy F Henderson. On the fluid mechanics of human crowd motion. *Transportation research*, 8(6):509–515, 1974.

[30] Dirk Helbing. A fluid-dynamic model for the movement of pedestrians. *Complex Systems*, 6:391–415, 1992.

[31] Cécile Appert-Rolland, J Cividini, Hendrik-Jan Hilhorst, and Pierre Degond. Pedestrian flows: from individuals to crowds. *Transportation Research Procedia*, 2:468–476, 2014.

[32] Pierre Degond, Cécile Appert-Rolland, Mehdi Moussaid, Julien Pettré, and Guy Theraulaz. A hierarchy of heuristic-based models of crowd dynamics. *Journal of Statistical Physics*, 152(6):1033–1068, 2013.

[33] Ansgar Kirchner, Hubert Klüpfel, Katsuhiro Nishinari, Andreas Schadschneider, and Michael Schreckenberg. Discretization effects and the influence of walking speed in cellular automata models for pedestrian dynamics. *Journal of Statistical Mechanics: Theory and Experiment*, 2004(10):P10011, 2004.

[34] Minoru Fukui and Yoshihiro Ishibashi. Self-organized phase transitions in cellular automaton models for pedestrians. *Journal of the physical society of Japan*, 68(8):2861–2863, 1999.

[35] Minoru Fukui and Yoshihiro Ishibashi. Jamming transition in cellular automaton models for pedestrians on passageway. *Journal of the Physical Society of Japan*, 68(11):3738–3739, 1999.

[36] Victor J Blue and Jeffrey L Adler. Emergent fundamental pedestrian flows from cellular automata microsimulation. *Transportation Research Record*, 1644(1):29–36, 1998.

[37] Victor J Blue and Jeffrey L Adler. Cellular automata microsimulation of bidirectional pedestrian flows. *Transportation Research Record*, 1678(1):135–141, 1999.

[38] Victor J Blue and Jeffrey L Adler. Modeling four-directional pedestrian flows. *Transportation research record*, 1710(1):20–27, 2000.

[39] Carsten Burstedde, Kai Klauck, Andreas Schadschneider, and Johannes Zittartz. Simulation of pedestrian dynamics using a two-dimensional cellular automaton. *Physica A: Statistical Mechanics and its Applications*, 295(3-4):507–525, 2001.

[40] Ansgar Kirchner and Andreas Schadschneider. Simulation of evacuation processes using a bionics-inspired cellular automaton model for pedestrian dynamics. *Physica A: statistical mechanics and its applications*, 312(1-2):260–276, 2002.

[41] Ansgar Kirchner, Katsuhiro Nishinari, and Andreas Schadschneider. Friction effects and clogging in a cellular automaton model for pedestrian dynamics. *Physical review E*, 67(5):056122, 2003.

[42] Daichi Yanagisawa, Ayako Kimura, Akiyasu Tomoeda, Ryosuke Nishi, Yushi Suma, Kazumichi Ohtsuka, and Katsuhiro Nishinari. Introduction of frictional and turning function for pedestrian outflow with an obstacle. *Physical Review E*, 80(3):036110, 2009.

[43] Yushi Suma, Daichi Yanagisawa, and Katsuhiro Nishinari. Anticipation effect in pedestrian dynamics: Modeling and experiments. *Physica A: Statistical Mechanics and its Applications*, 391(1-2):248–263, 2012.

[44] Stefan Nowak and Andreas Schadschneider. Quantitative analysis of pedestrian counterflow in a cellular automaton model. *Physical review E*, 85(6):066128, 2012.

[45] S Bouzat and MN Kuperman. Game theory in models of pedestrian room evacuation. *Physical Review E*, 89(3):032806, 2014.

[46] Anton von Schantz and Harri Ehtamo. Spatial game in cellular automaton evacuation model. *Physical Review E*, 92(5):052805, 2015.

[47] Masakuni Muramatsu, Tunemasa Irie, and Takashi Nagatani. Jamming transition in pedestrian counter flow. *Physica A: Statistical Mechanics and its Applications*, 267(3-4):487–498, 1999.

[48] Masakuni Muramatsu and Takashi Nagatani. Jamming transition in two-dimensional pedestrian traffic. *Physica A: Statistical Mechanics and its Applications*, 275(1-2):281–291, 2000.

[49] Masakuni Muramatsu and Takashi Nagatani. Jamming transition of pedestrian traffic at a crossing with open boundaries. *Physica A: Statistical Mechanics and its Applications*, 286(1-2):377–390, 2000.

[50] Yusuke Tajima and Takashi Nagatani. Clogging transition of pedestrian flow in t-shaped channel. *Physica A: Statistical Mechanics and its Applications*, 303(1-2):239–250, 2002.

[51] S Maniccam. Effects of back step and update rule on congestion of mobile objects. *Physica A: statistical mechanics and its applications*, 346(3-4):631–650, 2005.

[52] Ryoichi Nagai and Takashi Nagatani. Jamming transition in counter flow of slender particles on square lattice. *Physica A: Statistical Mechanics and its Applications*, 366:503–512, 2006.

[53] Mohcine Chraibi, Antoine Tordeux, Andreas Schadschneider, and Armin Seyfried. Modelling of pedestrian and evacuation dynamics. *Encyclopedia of Complexity and Systems Science*, pages 1–22, 2018.

[54] Dirk Helbing and Peter Molnar. Social force model for pedestrian dynamics. *Physical review E*, 51(5):4282, 1995.

[55] Dirk Helbing, Illés Farkas, and Tamas Vicsek. Simulating dynamical features of escape panic. *Nature*, 407(6803):487–490, 2000.

[56] Daniel Ricardo Parisi and Claudio Oscar Dorso. Microscopic dynamics of pedestrian evacuation. *Physica A: Statistical Mechanics and its Applications*, 354:606–618, 2005.

[57] Daniel Ricardo Parisi and Claudio Oscar Dorso. Morphological and dynamical aspects of the room evacuation process. *Physica A: Statistical Mechanics and its Applications*, 385(1):343–355, 2007.

[58] Mehdi Moussaïd, Niriaska Perozo, Simon Garnier, Dirk Helbing, and Guy Theraulaz. The walking behaviour of pedestrian social groups and its impact on crowd dynamics. *PloS one*, 5(4):e10047, 2010.

[59] Song Xu and Henry Been-Lirn Duh. A simulation of bonding effects and their impacts on pedestrian dynamics. *IEEE Transactions on Intelligent Transportation Systems*, 11(1):153–161, 2009.

[60] Alastair Smith, Christopher James, Richard Jones, Paul Langston, Edward Lester, and John Drury. Modelling contra-flow in crowd dynamics dem simulation. *Safety Science*, 47(3):395–404, 2009.

[61] Jooyong Lee, Taewan Kim, Jin-Hyuk Chung, and Jinho Kim. Modeling lane formation in pedestrian counter flow and its effect on capacity. *KSCE Journal of Civil Engineering*, 20(3):1099–1108, 2016.

[62] Yan-Qun Jiang, Bo-Kui Chen, Bing-Hong Wang, Weng-Fai Wong, and Bing-Yang Cao. Extended social force model with a dynamic navigation field for bidirectional pedestrian flow. *Frontiers of Physics*, 12(5):124502, 2017.

[63] WJ Yu, R Chen, Li-Yu Dong, and SQ Dai. Centrifugal force model for pedestrian dynamics. *Physical Review E*, 72(2):026112, 2005.

[64] Mohcine Chraibi, Armin Seyfried, and Andreas Schadschneider. Generalized centrifugal-force model for pedestrian dynamics. *Physical Review E*, 82(4):046111, 2010.

[65] Paul A Langston, Robert Masling, and Basel N Asmar. Crowd dynamics discrete element multi-circle model. *Safety Science*, 44(5):395–417, 2006.

[66] Gerta Köster, Franz Treml, and Marion Gödel. Avoiding numerical pitfalls in social force models. *Physical Review E*, 87(6):063305, 2013.

[67] Paolo Fiorini and Zvi Shiller. Motion planning in dynamic environments using velocity obstacles. *The International Journal of Robotics Research*, 17(7):760–772, 1998.

[68] Jur Van den Berg, Ming Lin, and Dinesh Manocha. Reciprocal velocity obstacles for real-time multi-agent navigation. In *2008 IEEE International Conference on Robotics and Automation*, pages 1928–1935. IEEE, 2008.

[69] Jur Van Den Berg, Stephen J Guy, Ming Lin, and Dinesh Manocha. Reciprocal n-body collision avoidance. In *Robotics research*, pages 3–19. Springer, 2011.

[70] Stephen J Guy, Ming C Lin, Dinesh Manocha, et al. Modeling collision avoidance behavior for virtual humans. In *AAMAS*, volume 2010, pages 575–582, 2010.

[71] Stephen J Guy, Jatin Chhugani, Sean Curtis, Pradeep Dubey, Ming C Lin, and Dinesh Manocha. Pledestrians: A least-effort approach to crowd simulation. In *Symposium on computer animation*, pages 119–128, 2010.

[72] Stephen J Guy, Sean Curtis, Ming C Lin, and Dinesh Manocha. Least-effort trajectories lead to emergent crowd behaviors. *Physical review E*, 85(1):016110, 2012.

[73] Antoine Tordeux, Mohcine Chraibi, and Armin Seyfried. Collision-free speed model for pedestrian dynamics. In *Traffic and Granular Flow'15*, pages 225–232. Springer, 2016.

[74] Ulrich Weidmann. Transporttechnik der fußgänger: transporttechnische eigenschaften des fußgängerverkehrs, literaturauswertung. *IVT Schriftenreihe*, 90, 1993.

[75] Z Fang, JP Yuan, Yu-Chun Wang, and Siu Ming Lo. Survey of pedestrian movement and development of a crowd dynamics model. *Fire safety journal*, 43(6):459–465, 2008.

[76] Masamitsu Mōri and Hiroshi Tsukaguchi. A new method for evaluation of level of service in pedestrian facilities. *Transportation Research Part A: General*, 21(3):223–234, 1987.

[77] Dirk Helbing, Anders Johansson, and Habib Zein Al-Abideen. Dynamics of crowd disasters: An empirical study. *Physical review E*, 75(4):046109, 2007.

[78] Armin Seyfried, Bernhard Steffen, Wolfram Klingsch, and Maik Boltes. The fundamental diagram of pedestrian movement revisited. *Journal of Statistical Mechanics: Theory and Experiment*, 2005(10):P10002, 2005.

[79] Serge P Hoogendoorn and Winnie Daamen. Pedestrian behavior at bottlenecks. *Transportation science*, 39(2):147–159, 2005.

[80] Ryoichi Nagai, Masahiro Fukamachi, and Takashi Nagatani. Evacuation of crawlers and walkers from corridor through an exit. *Physica A: Statistical Mechanics and its Applications*, 367:449–460, 2006.

[81] Armin Seyfried, Oliver Passon, Bernhard Steffen, Maik Boltes, Tobias Rupprecht, and Wolfram Klingsch. New insights into pedestrian flow through bottlenecks. *Transportation Science*, 43(3):395–406, 2009.

[82] M Boltes, J Zhang, A Tordeux, A Schadschneider, and A Seyfried. Empirical results of pedestrian and evacuation dynamics. *Encyclopedia of complexity and systems science*, pages 1–29, 2018.

[83] BD Hankin and Richard A Wright. Passenger flow in subways. *Journal of the Operational Research Society*, 9(2):81–88, 1958.

[84] SJ Older. Movement of pedestrians on footways in shopping streets. *Traffic engineering & control*, 10(4), 1968.

[85] Francis P Navin and Robert J Wheeler. Pedestrian flow characteristics. *Traffic Engineering, Inst Traffic Engr*, 39, 1969.

[86] Ujjal Chattaraj, Armin Seyfried, and Partha Chakroborty. Comparison of pedestrian fundamental diagram across cultures. *Advances in complex systems*, 12(03):393–405, 2009.

[87] Xuan Liu, Weiguo Song, and Jun Zhang. Extraction and quantitative analysis of microscopic evacuation characteristics based on digital image processing. *Physica A: Statistical Mechanics and its Applications*, 388(13):2717–2726, 2009.

[88] Shuchao Cao, Jun Zhang, Daniel Salden, Jian Ma, Ruifang Zhang, et al. Pedestrian dynamics in single-file movement of crowd with different age compositions. *Physical Review E*, 94(1):012312, 2016.

[89] Asja Jelić, Cécile Appert-Rolland, Samuel Lemercier, and Julien Pettré. Properties of pedestrians walking in line: Fundamental diagrams. *Physical review E*, 85(3):036111, 2012.

[90] Rudina Subaih, Mohammed Maree, Mohcine Chraibi, Sami Awad, and Tareq Zanoon. Experimental investigation on the alleged gender-differences in pedestrian dynamics: A study reveals no gender differences in pedestrian movement behavior. *IEEE Access*, 8:33748–33757, 2020.

[91] Jun Zhang, Wolfram Klingsch, Andreas Schadschneider, and Armin Seyfried. Transitions in pedestrian fundamental diagrams of straight corridors and t-junctions. *Journal of Statistical Mechanics: Theory and Experiment*, 2011(06):P06004, 2011.

[92] Tobias Kretz, Anna Grünebohm, Maike Kaufman, Florian Mazur, and Michael Schreckenberg. Experimental study of pedestrian counterflow in a corridor. *Journal of Statistical Mechanics: Theory and Experiment*, 2006(10):P10001, 2006.

[93] Jun Zhang, Wolfram Klingsch, Andreas Schadschneider, and Armin Seyfried. Ordering in bidirectional pedestrian flows and its influence on the fundamental diagram. *Journal of Statistical Mechanics: Theory and Experiment*, 2012(02):P02002, 2012.

[94] Claudio Feliciani and Katsuhiro Nishinari. Empirical analysis of the lane formation process in bidirectional pedestrian flow. *Physical Review E*, 94(3):032304, 2016.

[95] Jun Zhang, Qiao Wang, Yanghui Hu, Shuchao Cao, Long Xia, and Weiguo Song. The effect of a directional split flow ratio on bidirectional pedestrian streams at signalized crosswalks. *Journal of Statistical Mechanics: Theory and Experiment*, 2018(7):073408, 2018.

[96] Shuchao Cao, Armin Seyfried, Jun Zhang, Stefan Holl, and Weiguo Song. Fundamental diagrams for multidirectional pedestrian flows. *Journal of Statistical Mechanics: Theory and Experiment*, 2017(3):033404, 2017.

[97] Helen C Muir, David M Bottomley, and Claire Marrison. Effects of motivation and cabin configuration on emergency aircraft evacuation behavior and rates of egress. *The International Journal of Aviation Psychology*, 6(1):57–77, 1996.

[98] Tobias Kretz, Anna Grünebohm, and Michael Schreckenberg. Experimental study of pedestrian flow through a bottleneck. *Journal of Statistical Mechanics: Theory and Experiment*, 2006(10):P10014, 2006.

[99] Jack Liddle, Armin Seyfried, Wolfram Klingsch, Tobias Rupprecht, Andreas Schadschneider, and Andreas Winkens. An experimental study of pedestrian congestions: influence of bottleneck width and length. *arXiv preprint arXiv:0911.4350*, 2009.

[100] Dirk Helbing, Lubos Buzna, Anders Johansson, and Torsten Werner. Self-organized pedestrian crowd dynamics: Experiments, simulations, and design solutions. *Transportation science*, 39(1):1–24, 2005.

[101] Ángel Garcimartín, Diego Maza, José Martín Pastor, Daniel R Parisi, César Martín-Gómez, and Iker Zuriguel. Redefining the role of obstacles in pedestrian evacuation. *New Journal of Physics*, 20(12):123025, 2018.

[102] Ángel Garcimartín, Daniel R Parisi, Jose M Pastor, César Martín-Gómez, and Iker Zuriguel. Flow of pedestrians through narrow doors with different competitiveness. *Journal of Statistical Mechanics: Theory and Experiment*, 2016(4):043402, 2016.

[103] Juliane Adrian, Armin Seyfried, and Anna Sieben. Crowds in front of bottlenecks at entrances from the perspective of physics and social psychology. *Journal of the Royal Society Interface*, 17(165):20190871, 2020.

[104] Armin Seyfried, Andrea Portz, and Andreas Schadschneider. Phase coexistence in congested states of pedestrian dynamics. In *International Conference on Cellular Automata*, pages 496–505. Springer, 2010.

Publication I

Info: Xu Q, Chraibi M, Tordeux A, Zhang J. Generalized collision-free velocity model for pedestrian dynamics. Physica A: Statistical Mechanics and its Applications, 2019, 535: 122521.

Note: The collision-free velocity model (CVM) in this publication is equivalent to the collision-free speed model (CSM) in other parts of the dissertation.

Generalized Collision-free Velocity Model for Pedestrian Dynamics

Qiancheng Xu[a,*], Mohcine Chraibi[a], Antoine Tordeux[b], Jun Zhang[c]

[a]*Institute for Advanced Simulation, Forschungszentrum Jülich GmbH, 52425 Jülich, Germany*
[b]*School of Mechanical Engineering and Safety Engineering, University of Wuppertal, 42119 Wuppertal, Germany*
[c]*State Key Laboratory of Fire Science, University of Science and Technology of China, 230027 Hefei, China*

Abstract

The collision-free velocity model is a microscopic pedestrian model, which despite its simplicity, reproduces fairly well several self-organization phenomena in pedestrian dynamics. The model consists of two components: a direction sub-model that combines individual desired moving direction and neighbor's influence to imitate the process of navigating in a two-dimensional space, and an intrinsically collision-free speed sub-model which controls the speed of the agents with respect to the distance to their neighbors.

In this paper we generalize the collision-free velocity model by introducing the influence of walls and extending the distance calculations to velocity-based ellipses. Besides, we introduce enhancements to the direction sub-module that smooth the direction changes of pedestrians in the simulation; a shortcoming that was not visible in the original model due to the symmetry of the circular shapes. Moreover, the introduced improvements mitigate backward movements, leading to a more realistic distribution of pedestrians especially in bottleneck scenarios.

We study by simulation the effects of the pedestrian's shape by comparing the fundamental diagram in narrow and wide corridors. Furthermore, we validate our generalized approach by investigating the flow through bottlenecks with varying exit's widths.

Keywords: Collision-free velocity model, pedestrian dynamics, dynamical ellipse, fundamental diagram, validation

1. Introduction

Nowadays, the scale of crowd activities is getting bigger with the constant increase in the world population and the convenience of transport. Although these events usually are

*corresponding author

Email addresses: q.xu@fz-juelich.de (Qiancheng Xu), m.chraibi@fz-juelich.de (Mohcine Chraibi), tordeux@uni-wuppertal.de (Antoine Tordeux), junz@ustc.edu.cn (Jun Zhang)

carefully planned before they are held, the probability of accidents cannot be neglected, especially when the number of participants is considerably high. Besides, in some complex buildings, such as train stations, airports, stadiums, and commercial malls, crowd density can be relatively high, in particular during rush hours. For increasing the comfort and usability of these facilities, simulations of pedestrian dynamics may help during the design of buildings and even after their construction to identify potential bottlenecks and mitigate their effects [1, 2].

In general, models used to describe pedestrian dynamics can be categorized according to their scale of definition into macroscopic models, mesoscopic models, and microscopic models. Microscopic models describe individual trajectories of pedestrians while macroscopic models rely on aggregated quantities e.g. density, velocity, and flow to describe pedestrian dynamics in partial differential equation systems [3, 4, 5, 6]. For instance, recent macroscopic approaches rely on mean-field game theory and the coupling of Hamilton-Jacobi-Bellman and Fokker-Planck equations [7, 8, 9, 10]. The intermediate scale between microscopic and macroscopic classes is mesoscopic. Kinetic models [11, 12, 13, 14, 15] describing the crowd through distribution functions with Boltzmann-type equations and discrete queuing models [16, 17, 18] belong to the mesoscopic modeling category. Mesoscopic models can take in consideration behavior heterogeneity [18, 19, 20] or stochastic components in the interaction. Generally speaking, macroscopic and mesoscopic models consider pedestrian flow as a continuum and deal with large modeling scales, while microscopic models operate at local scales. Yet a systematic classification of model features according to the model form is difficult. We refer to [21, 22, 23, 24, 25, 26, 27] for overviews of modeling approaches for pedestrian dynamics.

We aim in this article to tackle pedestrians' interactions as well as their granular aspects (e.g. pedestrian shape and collision-free property) and to describe their dynamics locally in simple geometries such as corridors and bottlenecks. Objectives are mainly addressed on the microscopic modeling scale.

Microscopic models are largely used in traffic engineering to simulate pedestrian dynamics. They describe pedestrians individually and can naturally take into account the heterogeneity and stochasticity of the pedestrians' behavior. Most of the models can reproduce fairly well several collective phenomena in pedestrian dynamics [26, 28, 29]. After more than 50 years of development, many kinds of microscopic models exist in the literature. We can distinguish between cellular automate models [30, 31, 32, 33, 34] (0th order models), velocity models [35, 36, 37, 38] (1st order models) and force-based models [39, 40, 41, 42] (2nd order models). While the former models are discrete in space and computationally fast, the later models are continuous in space and hence are easier to be used in complex geometries. Whether continuous models are computationally expensive depends not only on the order of the model but also on its definition. However, generally speaking, first-order models are less expensive since their numerical solution involves only one integration step, while two integration steps are required for second-order models. Furthermore, for numerical reasons fine discretization generally requires small integration time steps. In any case, microscopic models remain however generally much more computationally expensive than continuum pedestrian models.

In this paper, we focus on the extension of the collision-free velocity model introduced in [36]. The collision-free velocity model (for short CVM) is a velocity-model, composed of a speed and a direction sub-models. Unlike most force-based models, CVM, being a first-order model, is by definition collision-free.

We generalize the CVM by considering the influence of walls and integrating two extensions. First, we change the shape of agents from circle to dynamical ellipse. In the original model, circles are used to express the projection of the pedestrian's body on the two-dimensional plane. However, many references and researches indicate that a dynamical ellipse can represent pedestrian's shape more accurately since the space a pedestrian occupied is influenced by the length of the legs during the motion and the lateral swaying of the body [40]. Therefore, we generalize CVM by extending the distance calculation to velocity-based ellipse and compare the simulation results with the original model (circles). After introducing the first extension, an unnatural "shaking" was observed during the simulation, which is caused by the zero-order direction sub-model. We propose a new first-order direction sub-model, designed to stabilize the direction changes of pedestrians in the simulation.

For the sake of completeness, we briefly introduce the original CVM in section 2. The generalization of the model from circle-based to an ellipse-based definition and the new direction sub-model are presented in section 3. In section 4, the comparison between the simulation results of a circle and a velocity-based ellipse is given and the performances of the new direction sub-model are compared to the original CVM. Finally, we give a summary of the extensions and discuss limitations of the model as well as future research directions in the concluding section 5.

2. Collision-free velocity model

In the original model, the moving direction and speed of each pedestrian are updated at each time step. Moving direction of a pedestrian is obtained by superposing the influence of the surrounding pedestrians and the desired moving direction. The value of the speed depends on the minimum spacing in the moving direction. In Figure 1 (borrowed from [36]), pedestrians are modeled as circles with constant diameter ℓ. X_i, X_j and X_k are positions of pedestrians i, j and k. The original CVM is described as

$$\dot{X}_i(X_i, X_j, \dots) = V_i(X_i, X_j, \dots) \cdot \vec{e}_i(X_i, X_j, \dots), \tag{1}$$

where V_i is the speed of pedestrian i and $\vec{e}_i$ is the moving direction.

Moving direction $\vec{e}_i$ is obtained from the direction sub-model

$$\vec{e}_i(X_i, X_j, ...) = u_1 \cdot \Big(\vec{e}_i^{\,0} + \sum_{j \in N_i} R(s_{i,j}) \cdot \vec{e}_{i,j} \Big), \tag{2}$$

where u_1 is a normalization constant such that $||\vec{e}_i|| = 1$, $\vec{e}_i^{\,0}$ is the desired direction towards a certain goal, N_i is the set containing all the neighbours of the pedestrian i, $\vec{e}_{i,j}$ is the

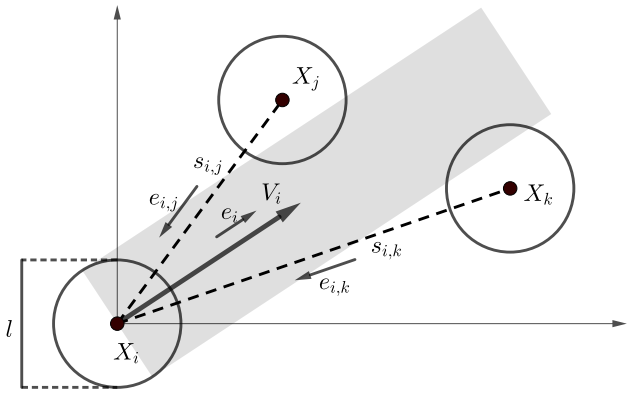

Figure 1: Notations used in the collision-free velocity model. ℓ is the size of agents, X_i, X_j and X_k are positions of pedestrians, $\vec{e}_i$ is the moving direction of pedestrian i and V_i is the moving speed, $s_{i,j}$ and $s_{i,k}$ are distances between the centers of pedestrians, $\vec{e}_{i,j}$ and $\vec{e}_{i,k}$ and the unit vector from X_j and X_k to X_i.

unit vector from the center of the pedestrian j towards the center of the pedestrian i. The function

$$R(s_{i,j}) = k \cdot \exp\Big(\frac{\ell - s_{i,j}}{D}\Big), \tag{3}$$

is used to describe the influence that neighbours act on the moving direction of pedestrian i. The strength coefficient $k > 0$ and the distance coefficient $D > 0$ calibrate the function accordingly. As mentioned before, ℓ is the diameter of the circle used to represent the pedestrians and $s_{i,j}$ is the distance between the centers of pedestrian i and j.

After obtaining the moving direction $\vec{e}_i$, the speed model

$$V_i(s_{i,j}) = \min\Big\{V_i^0, \max\big\{0, \frac{s_i - \ell}{T}\big\}\Big\}, \tag{4}$$

is used to determine the scale of velocity V_i in the direction $\vec{e}_i$. In Eq. 4, V_i^0 is the desired speed of pedestrian i, which depends on various environmental factors such as the existence of stairs or smoke produced by a fire.

$$s_i = \min_{j \in J_i} s_{i,j}, \tag{5}$$

is the distance between the center of pedestrian i and the center of the closet pedestrian in front of pedestrian i, when pedestrian i moving in the direction $\vec{e}_i$. The definition of set J_i in Eq. 5 is

$$J_i = \Big\{j, \vec{e}_i \cdot \vec{e}_{i,j} \le 0 \text{ and } \big|\vec{e}_i^{\perp} \cdot \vec{e}_{i,j}\big| \le \frac{\ell}{s_{i,j}}\Big\}, \tag{6}$$

where $\vec{e}_i^{\perp} \cdot \vec{e}_i = 0$. J_i is the set of all pedestrians overlapping with the grey area in Figure 1. The only coefficient in the speed model is $T > 0$ which is used to adjust the gap between pedestrians.

The above-mentioned definition of the CVM describes specifically interactions among pedestrians. However, the influence of walls and obstacles has been left from the definition of the model. In this work, we close this gap by only considering straight walls. If the shape of the wall in the simulation is irregular, then we will approximate it to a few straight walls. In Figure 2, X_i, $\vec{e}_i$ and V_i have the same definitions as in Figure 1. Besides, there are two walls in the figure, wall v and w. C_v and C_w are the closest points in wall v and w to the center of pedestrian i respectively. $\vec{e}_{i,v}$ and $\vec{e}_{i,w}$ are the unit vectors from C_v and C_w to X_i. $s_{i,v}$ and $s_{i,w}$ are the distances from C_v and C_w to X_i. The angle between $\vec{e}_i$ and $-\vec{e}_{i,v}$ is α_v and the angle between $\vec{e}_i$ and $-\vec{e}_{i,w}$ is α_w.

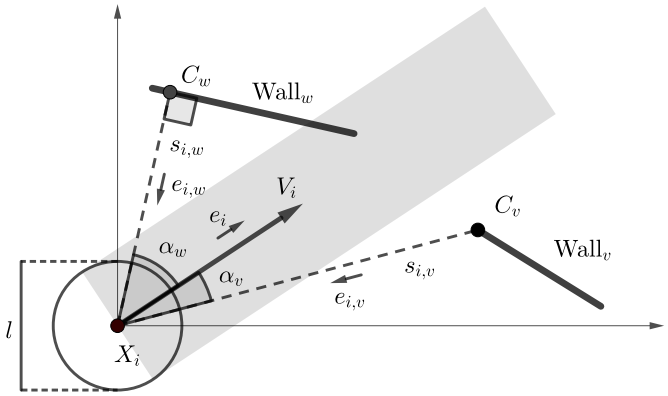

Figure 2: Notations used in the collision-free velocity model when calculating the influence of walls. ℓ, X_i, $\vec{e}_i$, V_i are the size, position, moving direction and moving speed of pedestrian i, C_v and C_w are the closest points in wall v and w to X_i, $\vec{e}_{i,v}$ and $\vec{e}_{i,w}$ are the unit vectors from C_v and C_w to X_i, $s_{i,v}$ and $s_{i,w}$ are the distances from C_v and C_w to X_i, α_v is the angle between $\vec{e}_i$ and $-\vec{e}_{i,v}$, α_w is the angle between $\vec{e}_i$ and $-\vec{e}_{i,w}$.

After introducing the influence of walls, the direction model becomes

$$\vec{e}_i = u_2 \cdot \Big(\vec{e}_i^{\,0} + \sum_{j \in N_i} R(s_{i,j}) \cdot \vec{e}_{i,j} + \sum_{v \in W_i} R_w(s_{i,v}) \cdot \vec{e}_{i,v} \Big), \tag{7}$$

where u_2 is a normalization constant such that $||\vec{e}_i|| = 1$, W_i is the set of walls nearby pedestrian i, and

$$R_w(s_{i,v}) = k_w \cdot \exp\Big(\frac{\frac{\ell}{2} - s_{i,v}}{D_w} \Big), \tag{8}$$

where $k_w > 0$ and $D_w > 0$ are used to calibrate the function accordingly.

To avoid overlaps of pedestrians with walls, walls should not only influence pedestrian's moving direction but also their speed. The expanded speed model is

$$V_i = \min\Big\{ V_i^0, \max\big\{0, \frac{s_i - \ell}{T}\big\}, \max\big\{0, \frac{sw_i}{T}\big\} \Big\}, \tag{9}$$

where the definitions of s_i, ℓ, T are same as in Eq. 4 and

$$sw_i = \min_{v \in JW_i} \frac{s_{i,v} - \frac{\ell}{2}}{\cos \alpha_v}, \tag{10}$$

where JW_i is the set containing all the walls in the moving direction of pedestrian i (grey area in Figure 2).

3. Generalization of the collision-free velocity model

In this section we introduce extensions of the CVM. We also show how every extension influences the resulting dynamics and eventually enhances the simulation results.

3.1. From circle to ellipse

We generalize the collision-free velocity model by extending the distance calculations to velocity-based ellipses. The plane view of the pedestrian i's body is represented by an ellipse [43]. The major semi-axis a_i and minor semi-axis b_i of the ellipse represent the space requirement in the direction of motion and along the shoulder axis respectively.

In [40] the semi-axis along the walking direction is defined as

$$a_i = a_{\min} + \tau_a V_i, \tag{11}$$

where V_i is the speed of pedestrian i, while $a_{\min} > 0$ and $\tau_a > 0$ are two parameters.

The idea that the semi-axis of the ellipse along the walking direction vary with speed is derived from the fact that the spacing a pedestrian needed in her moving direction has a positive correlation with her speed [44]. This, in turn, is also the role of parameter T which is defined in the speed sub-model to adjust the gap between agents. We conclude that in our model T and τ_a model the same behavior of pedestrians even if their physical interpretations are different.

This becomes apparent after performing a basic stability analysis of the model. Assuming an one-dimensional system in steady-state , we can derive from the speed sub-model in Eq. 4 the following relation

$$V_{\text{steady}} = \frac{1/\rho_{\text{steady}} - 2 \cdot a_{\min}}{\tilde{T}}, \tag{12}$$

where V_{steady} and ρ_{steady} are the speed and the density of pedestrians flow in steady state, and $\tilde{T} = T + 2\tau_a$. Hence, the parameter τ_a and the parameter T in speed sub-model have the same influence on the dynamics. To confirm our assumption we perform numerical simulations by varying these two parameters while maintaining a constant value of $\tilde{T}$. We can observe from Figure 3 that although the values of τ_a are different in these simulations, the results obtained are almost identical when $\tilde{T}$ is constant. In the spirit of Occam's razor, we dispense with parameter τ_a and opt for a constant semi-axis a_i.

The other semi-axis along the shoulder axis b_i is defined according to [40] as a linear function:

$$b_i = b_{\max} - (b_{\max} - b_{\min}) \frac{V_i}{V_i^0}, \tag{13}$$

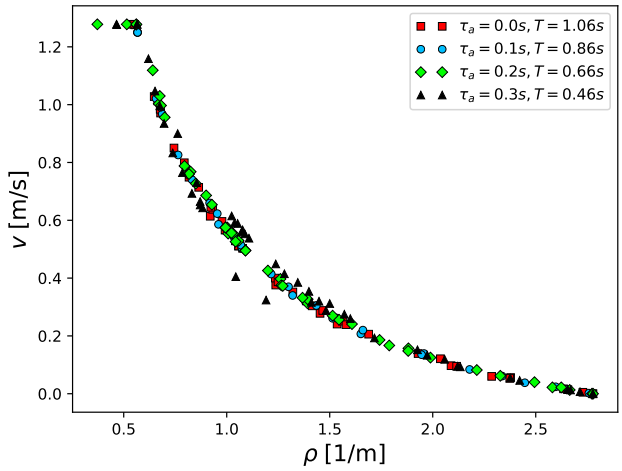

Figure 3: The fundamental diagram obtained in 1D simulations with $\tilde{T} = 1.06$.

with $b_{\min}$ is the minimal semi-width when pedestrian i reaches the desired speed V_i^0 and $b_{\max}$ is the maximum semi-width reached when pedestrian i is not moving [40].

We found in simulations with the CVM that this linear relationship does not provide satisfactory results. Hence we introduce a new non-linear function inspired by the observation that pedestrians often reduce their occupied space in the vertical direction of motion by turning their body to walk faster and pass through narrow gaps that are smaller than the width of their shoulder.

We set

$$b_i = b_{\min} + \frac{b_{\max} - b_{\min}}{1 + e^{\beta \cdot (V_i - \gamma)}}, \tag{14}$$

which is a Sigmoid function, where the maximum semi-width $b_{\max}$ is equal to the half of a static pedestrian's width and $b_{\min}$ is equal to the half of a moving pedestrian's minimum width. Parameters β and γ are used to adjust the shape of the function as shown in Figure 4 which shows the curves of the function for different parameter values.

After defining the semi-axes of the ellipse, we extend the distance calculations from circle to velocity-based ellipse (Figure 5). The ellipses in the full line describe non-moving pedestrians, while the ellipses in the dashed line represent the pedestrians at the desired velocity. $d_{i,j}$ is the distance between ellipses used to represent pedestrian i and j, which is defined as the distance between the borders of ellipses i and j, along a line connecting their centers. $d_{i,v}$ is the distance between the wall v and pedestrian i, which is defined as the distance between the C_v (the closest points in wall v to the center of pedestrian i) and the border of ellipse used to present pedestrian i, along a line connecting the center of pedestrian i and C_v.

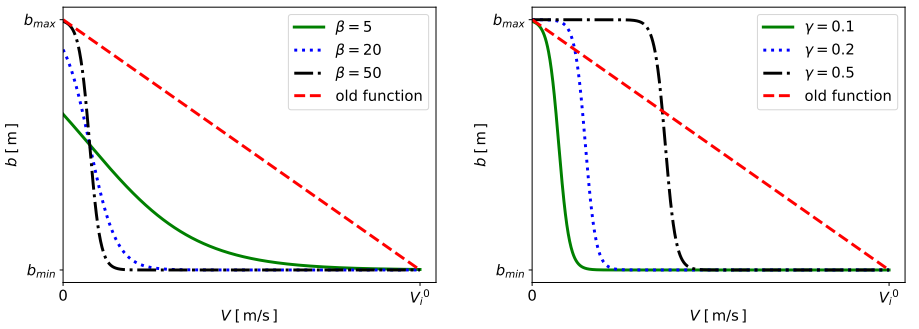

(a) $\gamma = 0.1$ (b) $\beta = 50$

Figure 4: The new function of b with different β and γ, the left figure shows the curves of the function with same $\gamma = 0.1$ but different β while the right figure shows the curves of the function with same $\beta = 50$ but different γ.

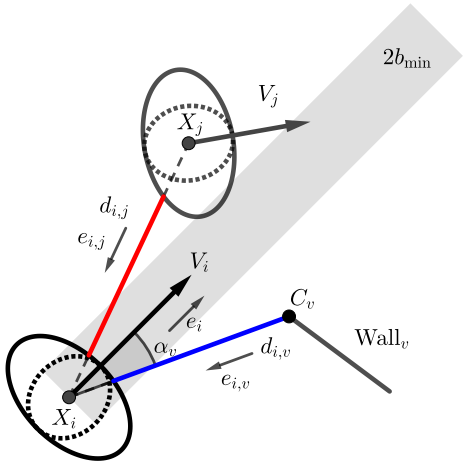

Figure 5: Notations used in the collision-free velocity model after extending the distance calculations between pedestrians from circle to velocity-based ellipse. $d_{i,j}$ is the length of red segment and $d_{i,v}$ is the length of blue segment. X_i and X_j are positions of pedestrians, C_v is the closet point in wall v to X_i, V_i and V_j are moving speeds of pedestrians, $\vec{e}_i$ is the moving direction of pedestrian i, $\vec{e}_{i,j}$ and $\vec{e}_{i,v}$ are the unit vectors from X_j and C_v to X_i, α_v is the angle between $\vec{e}_i$ and $-\vec{e}_{i,v}$.

In the new equation of motion, the influence of the agents' shape is added as follows: The moving direction $\vec{e}_i$ is calculated by Eq. 7, but the new definition of functions

$$R(d_{i,j}) = k \cdot \exp\Big(\frac{d_{i,j}}{D}\Big), \quad R_w(d_{i,v}) = k_w \cdot \exp\Big(\frac{d_{i,v}}{D_w}\Big), \tag{15}$$

are used. Then the speed V_i is obtained by

$$V_i = \min\left\{V_i^0, \max\left\{0, \frac{d_i}{T}\right\}, \max\left\{0, \frac{dw_i}{T}\right\}\right\}, \tag{16}$$

where

$$d_i = \min_{j \in J_i} d_{i,j}, \quad dw_i = \min_{v \in JW_i} \frac{d_{i,v}}{\cos\alpha_v}. \tag{17}$$

Here J_i and JW_i are the sets containing all pedestrians and walls in the direction of movement (i.e. the pedestrians and walls overlap with the grey area in Figure 5). We set the width of the grey area to $2b_{\min}$ in the case of a velocity-based ellipse. The comparisons between the models describing agents with different shapes are given in section 4.

3.2. New direction sub-model

After generalizing the model to ellipses, some unrealistic phenomena during simulation become visible. First of all, backward movements occur very often, which is not realistic especially in evacuation scenarios. Second, an unnatural "shaking" appears during simulation, which is due to a strong fluctuation of the ellipse's orientation.

In the original model, the moving direction of pedestrian i is calculated by combining individual desired moving direction $\vec{e}_i^{\,0}$ and the neighbors' influence. Since the direction of neighbor's influence is from the center of pedestrians or closest point on the wall towards the center of the pedestrian i, the influence can be divided into two parts, one is the projection on $\vec{e}_i^{\,0}$ and the other one is perpendicular to the projection part. The direction of the projection part is the reason for backward movements. Pedestrians hardly choose a moving direction whose projection on $\vec{e}_i^{\,0}$ is in the inverse direction of $\vec{e}_i^{\,0}$. And the cause of the "shaking" is that pedestrians turn to $\vec{e}_i$ directly after calculation in the original model (0th order model).

Therefore, our solution has two parts, the projection of neighbors' influence on $\vec{e}_i^{\,0}$ is always equal to zero, and introducing a smoothing process (e.g. a relaxation process) in the direction sub-model. Based on this idea, we propose a new direction sub-model as shown in Figure 6, where $\vec{e}_i^{\,0}$ is the desired moving direction of the pedestrian i and $\vec{e}_i$ is the actual moving direction, $\vec{e}_{i,j}^{\,N}$ and $\vec{e}_{i,v}^{\,N}$ are the new directions used to calculate the influence of the pedestrians j and walls v act on pedestrian i respectively.

The new direction sub-model uses two steps to calculate the moving direction of a pedestrian. First, we use

$$\vec{E}_i = u_3 \cdot \left(\vec{e}_i^{\,0} + \sum_{j \in N_i} R(d_{i,j}) \cdot \vec{e}_{i,j}^{\,N} + \sum_{v \in W_i} R_w(d_{i,v}) \cdot \vec{e}_{i,v}^{\,N}\right), \tag{18}$$

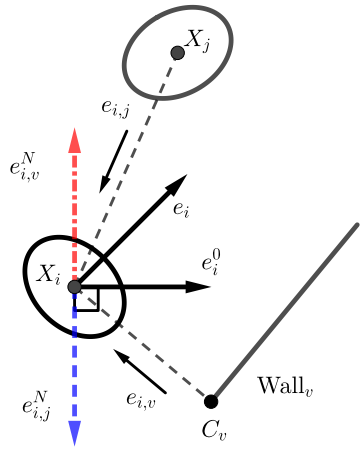

Figure 6: Notations used in the new direction sub-model. the direction of influence from pedestrian j to pedestrian i is vector represented by red chain line and the direction of influence from wall v to pedestrian i is vector represented by the blue dashed line. X_i and X_j are positions of the pedestrians, C_v is the closet point in wall v to X_i, $\vec{e}_i{}^0$ and $\vec{e}_i$ are the desired moving direction and the actual moving direction of the pedestrian i, $\vec{e}_{i,j}$ and $\vec{e}_{i,v}$ are the unit vectors from X_j and C_v to X_i, $\vec{e}^{\,N}_{i,j}$ and $\vec{e}^{\,N}_{i,v}$ are the directions used to calculate the influence of the pedestrians j and walls v act on pedestrian i respectively.

to calculate the optimal moving direction of the pedestrian i, u_3 is a normalization constant such that $||\vec{E}_i|| = 1$. The repulsive function $R(d_{i,j})$ and $R_w(d_{i,v})$ are given in Eq. 15 and the definition of $\vec{e}^{\,N}_{i,j}$ and $\vec{e}^{\,N}_{i,v}$ are

$$\vec{e}^{\,N}_{i,j} = \begin{cases} \vec{e}_i{}^{0\perp} & \text{if } C_j > 0, \\ \vec{e}_i{}^{0\perp} \text{ or } -\vec{e}_i{}^{0\perp} & \text{if } C_j = 0, \\ -\vec{e}_i{}^{0\perp} & \text{if } C_j < 0. \end{cases} \qquad \vec{e}^{\,N}_{i,v} = \begin{cases} \vec{e}_i{}^{0\perp} & \text{if } C_v > 0, \\ \vec{e}_i{}^{0\perp} \text{ or } -\vec{e}_i{}^{0\perp} & \text{if } C_v = 0, \\ -\vec{e}_i{}^{0\perp} & \text{if } C_v < 0. \end{cases} \tag{19}$$

where

$$C_j = \vec{e}_{i,j} \cdot \vec{e}_i{}^{0\perp}, \quad C_v = \vec{e}_{i,v} \cdot \vec{e}_i{}^{0\perp}. \tag{20}$$

Here, $\vec{e}_i{}^{0\perp}$ is the vector obtained by rotating desired moving direction $\vec{e}_i{}^0$ for 90° counter-clockwise. According to Eq. 19, influence from pedestrians and walls are decided not only by their position but also by the desired moving direction of the pedestrian i. If the centers of pedestrians or the closest points in walls to the center of the pedestrian i are located in the left area to $\vec{e}_i{}^0$, the direction of influence is defined as right side perpendicular vector of $\vec{e}_i{}^0$ and vice versa. It should be noticed that there might be an extremely rare case when C_j or C_v is equal to zero. In this case, the influence direction is decided by multiple factors, e.g. culture, gender. To simplify the model, the direction of influence is randomly chosen from $\vec{e}_i{}^{0\perp}$ and $-\vec{e}_i{}^{0\perp}$ in this case, corresponding to pedestrians avoiding front obstacles from the sides.

Then, we introduce a new relaxation time parameter τ in the direction sub-model, which is represented as

$$\frac{d\vec{e_i}(t)}{dt} = \frac{\vec{E_i}(t) - \vec{e_i}(t)}{\tau}, \tag{21}$$

where $\vec{e_i}$ is the moving direction of the pedestrian i and $\vec{E_i}$ is the optimal moving direction calculated by Eq. 18. In this step, we change the direction sub-module from zero-order to first-order, which does not change the global first-order property of the original CVM. By adjusting τ, a pedestrian can turn to its moving direction smoothly.

Besides, we use a dynamical vision area in this paper, which is the hatching area in Figure 7. Only the pedestrians and walls located in Area_i, which is the dynamical vision area of the pedestrian i, influence the moving direction of the pedestrian i. The set contains all neighbors of the pedestrian i in Area_i is

$$N_i^{\text{Area}} = \left\{ j, \vec{e_i} \cdot \vec{e}_{i,j} < 0 \text{ or } \vec{e_i}^{\,0} \cdot \vec{e}_{i,j} < 0 \right\}. \tag{22}$$

Here $\vec{e}_{i,j}$ is the vector from the center of neighbors towards the center of the pedestrian i. As for the walls, only when two vertices of a wall are both in Area_i, this wall influences the moving direction of the pedestrian i. Vision area of the pedestrian i is decided by his desired moving direction $\vec{e_i}^{\,0}$ and his actual moving direction $\vec{e_i}$. This means a pedestrian choose the best moving direction according to the neighbors and walls located in the half area in front of his moving direction and the half area in front of his desired moving direction. The dynamical vision area is based on the idea that pedestrians will turn their heads to obtain the environmental information of the areas in front of their desired moving directions if their actual moving directions deviate from the desired moving directions. Using this dynamical vision area can eliminate some unrealistic block occurred between agents when using fixed vision area in the simulation.

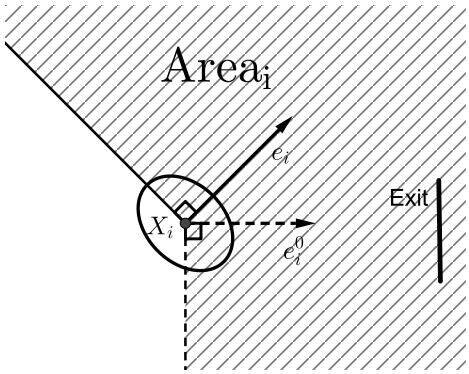

Figure 7: Dynamical vision area. X_i is the position, Area_i is the hatching area, $\vec{e_i}^{\,0}$ is the desired moving direction towards the exit, and $\vec{e_i}$ is the actual moving direction of pedestrian i.

These enhancements can almost eliminate the phenomena of backward movement and "shaking" in the simulation, as shown in Figure 8.

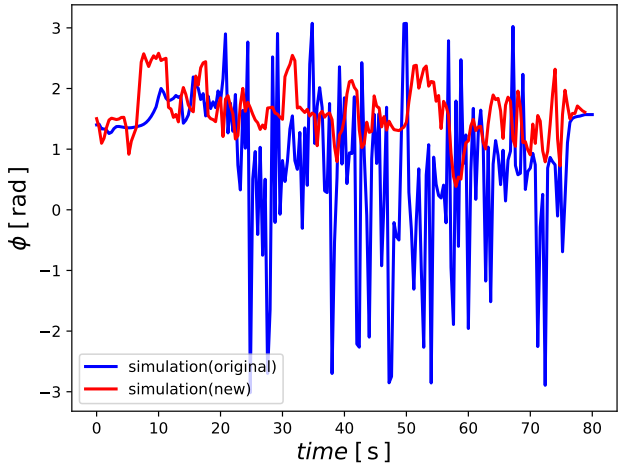

Figure 8: Time series of the angle between the moving direction of a pedestrian and the x-axis (ϕ).

ϕ is defined as the angle between the moving direction of a pedestrian and the x-axis. As we can see in Figure 8, the blue line (original model) shows a strong fluctuation of the angle over time compared with the red line (our extension).

In the next section, we further show a systematic comparison of both models.

4. Simulation results

In this section, the comparisons and analysis of models with different shapes and different direction sub-models are given. Preliminary simulation analysis has shown that the model can satisfy standards addressed in [45, 46] for basic movements of single pedestrians. We aim in this section to extend the validity of the model in regard to fundamental diagrams and collective behaviors in straight corridors and bottlenecks. The simulations in this section are executed with Euler scheme using a time step $\Delta t = 0.05\ s$. The update of the pedestrians is parallel in each step.

First, we perform simulations in a 26 m corridor with periodic boundary condition and measure the 1D fundamental diagram in a two meters long area located in the middle of the corridor. The shape of agents in these simulations, as well as the direction sub-model, are insignificant for the outcome of the simulation since pedestrians can not overtake others walking in front. Hence, we can focus on the validation of the speed sub-model and the relation between the speed and the required spacing in front.

The values of parameters are shown in Table 1. The desired speed of the pedestrians is 1.34 m/s. The shape of agents is circular with a constant radius a. The value of a is 0.18 m and the value of T is 1.06 s, which are obtained from the linear relationship of required length and velocity [44].

	V^0 (m/s)	a (m)	T (s)	k	D (m)	k_w	D_w (m)
1D	1.34	0.18	1.06	3.0	0.1	6.0	0.05

Table 1: Parameters of CVM in one-dimensional scenario

The simulation results in the 1D case are shown in Figure 9. We realize that the obtained 1D fundamental diagram fit well with the experimental data.

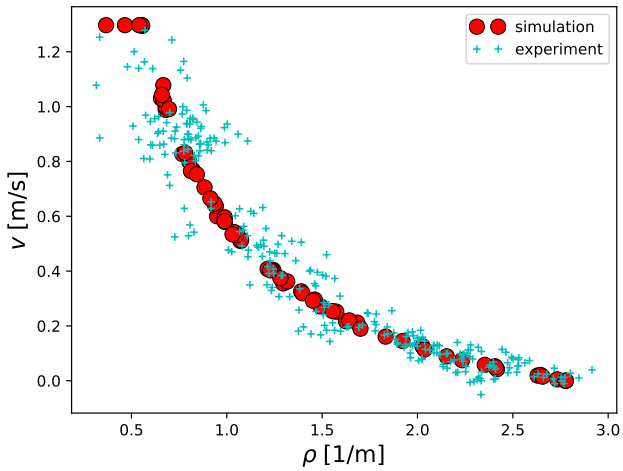

Figure 9: Velocity-density relation (fundamental diagram) in one-dimensional scenario, compared with experimental data [47].

In the second step, we investigate the effect of the agent's shape on the two-dimensional fundamental diagram. The simulation scenario is a 26×1.8 m^2 corridor with periodic boundary conditions. We measure the 2D fundamental diagram of models which describing agent with different shapes. We use three kinds of shapes here, circles with constant radius, ellipses with constant a and variable b as defined in Eq. 13 and ellipses with constant a and variable b as defined in Eq. 14.

The value of V^0, a, T and parameters in direction sub-model are the same as in the one-dimensional case. Table 2 summarizes the value of other parameters.

The simulation results of the 2D case are shown in Figure 10. From Figure 10, we can get the result that the shape of agents in the model influence the fundamental diagram

	$b_{\min}$ (m)	$b_{\max}$ (m)	b function	β	γ
constant circle	\	\	\	\	\
original ellipse	0.15	0.25	(13)	\	\
new ellipse	0.15	0.25	(14)	50	0.1

Table 2: Parameters of CVM in two-dimensional scenario

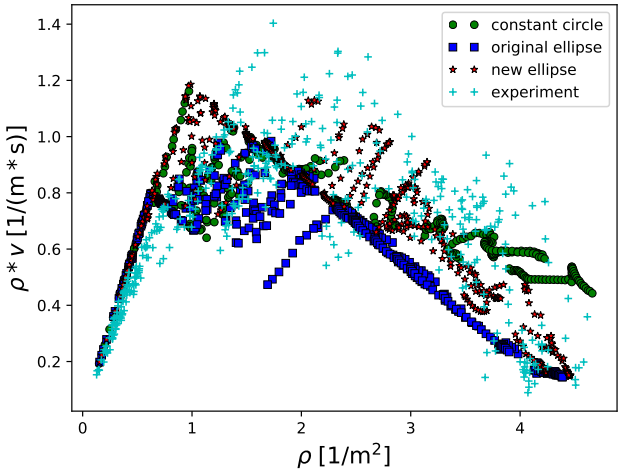

Figure 10: Relation between flow and density (fundamental diagram) in two-dimensional scenario, compared with experimental data obtained in the Hermes-project [48].

in the two-dimensional scenario, especially in the high-density area. The results obtained with constant circle and ellipse with variable b defined as Eq. 13 both have deviation with experimental data in the high-density area while using ellipse with variable b defined as Eq. 14 can obtain 2D fundamental diagram which is closer to the experimental results. That means the new function for b we proposed has a positive impact on the simulation result.

Then, we perform simulations in bottleneck scenarios [47]. We measure the relation between the flow in the middle of the bottleneck and the width of the bottleneck which is adjusted from 1.0 m to 2.5 m in our simulations. As we mentioned before, we can observe some unusual behavior during the simulation. Besides, we observe that the distribution of pedestrians in front of the bottleneck is different from the experiment. The new direction sub-model proposed in the previous section can eliminate these unusual phenomena.

In order to compare the simulation results of original and new direction sub-model fairly, we adjust the value of the parameter T to make the flow-width relation obtained from the simulation results as close to the relation obtained from experimental data as possible. The

shape of the pedestrian in original and new model are both the new dynamical ellipse we proposed in previous section, the value of a, $b_{\min}$, $b_{\max}$, β and γ are given in Table 2, the value of k, D, k_w, D_w are provided in Table 1. The desired speeds of the pedestrians are Gaussian distributed with a mean of 1.34 m/s and a standard deviation of 0.26 m/s [49]. After validation, the value of T in the original model is 0.5 s and in the new model is 0.45 s. The value of new parameter τ introduced in new direction sub-model is 0.3 s. The relations obtained are shown in Figure 11 and compared with experimental data. In Figure 11 we can find the relation obtained from simulation results of the original and new model both very close to the experimental data.

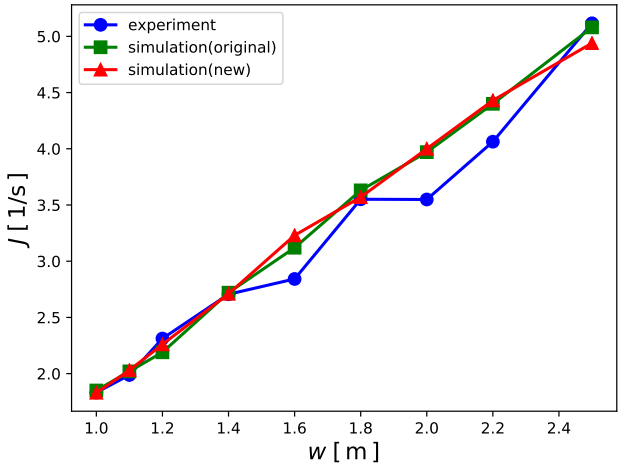

Figure 11: Relation between the flow in the middle of the bottleneck and the width of bottleneck, compared with experimental data[23].

Since the purpose of our extension is to eliminate backward movement and shaking phenomenon. We compare two indexes to prove that our extensions are useful. The first one is the backward movement proportion

$$O = \frac{\sum_{i=1}^{N} \sum_{k=0}^{M_i} O_i(k \cdot \Delta t)}{\sum_{i=1}^{N} M_i}, \tag{23}$$

where Δt is the time step size in the simulation, $M_i * \Delta t$ is the simulation duration of

pedestrian i, N is the number of pedestrians in the simulation and

$$O_i(t) = \begin{cases} 1, & \vec{e}_i(t) \cdot \vec{e}_i^{\,0}(t) < 0 \\ 0, & \text{else} \end{cases}, \tag{24}$$

where $\vec{e}_i(t)$ is the moving direction of pedestrian i. This definition means that when the angle between the actual moving direction and the desired moving direction of a pedestrian is greater than 90 degrees, we regard it as a backward movement.

We calculate the proportion of backward movement from the simulation results of the original model and new model in bottleneck scenarios with different widths from 1.0 m to 2.5 m. The results are shown and compared in Figure 12.

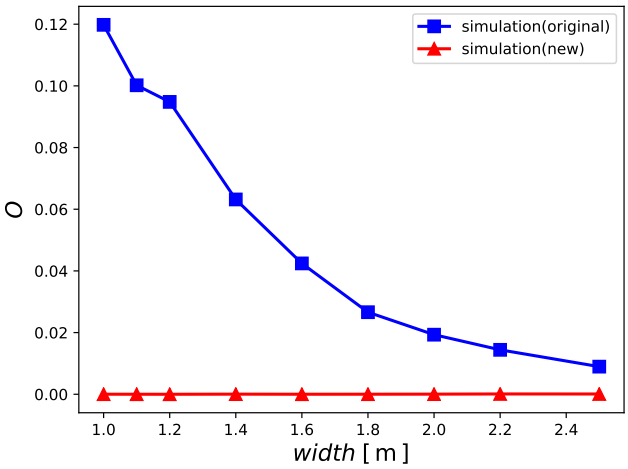

Figure 12: Proportion of backward movement in bottleneck scenarios with different widths from 1.0 m to 2.5 m.

From Figure 12, we can find that the proportion of backward movement significantly decreases in the new model compared to the original model. Therefore our extension eliminates the unrealistic backward movement.

The second index is the average angular variation in moving direction per pedestrian per frame, which is presented as

$$S_{average} = \frac{\sum_{i=1}^{N} \sum_{k=1}^{M_i} S_i(k \cdot \Delta t)}{\sum_{i=1}^{N} (M_i - 1)} \tag{25}$$

with

$$S_i(t) = \left| \angle \left[\vec{e}_i(t), \vec{e}_i t - \Delta t) \right] \right|, \tag{26}$$

where the definition of $\angle \left[\vec{e}_i(t), \vec{e}_i t - \Delta t) \right]$ is the angle between $\vec{e}_i(t)$ and $\vec{e}_i(t - \Delta t)$. The definition of moving direction $\vec{e}_i(t)$ is the same as before. $S_i(t)$ is the absolute value of the angle between moving direction in the current time step and the previous one. We compare this index for the new model and the original model. The results are presented in Figure 13.

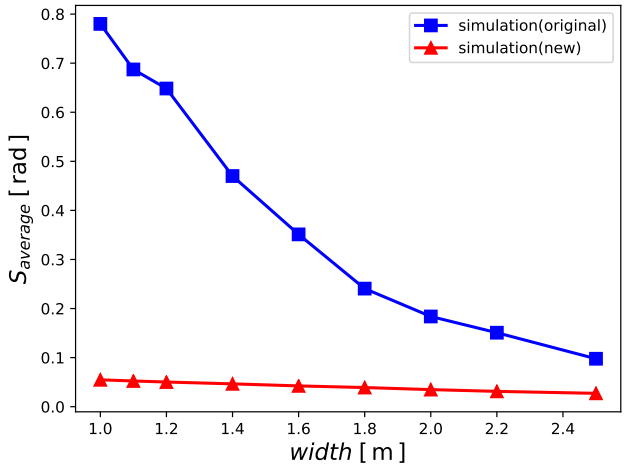

Figure 13: Average angular variation in moving direction per pedestrian per frame in bottleneck scenarios with different widths from 1.0 m to 2.5 m.

It can be observed in Figure 13 that in the new model the pedestrians change less their direction than the pedestrians in the original model, which is in line with the fact that pedestrians prefer to keep their direction instead of changing it. Compared within the original model, agents no longer shake frequently.

Finally, we compare the spatiotemporal profile of bottleneck flow when the width is 1.2 m. In simulations, we initialise pedestrians in the same positions and at the same times as in the experiment, in order to eliminate the impact of pedestrians' initial distribution. The profiles obtained from the experiment, the original speed model as well as the new model are shown in Figure 14. Although profiles obtained from new model are still somewhat different from the experimental results, a visible enhancement can be observed. The pedestrians do not deviate strongly from the exit as it can be observed with the original model.

5. Conclusion

In this paper we enhance and generalize the collision-free model [36] by introducing new components that lead to better dynamics. We firstly complete the collision-free velocity

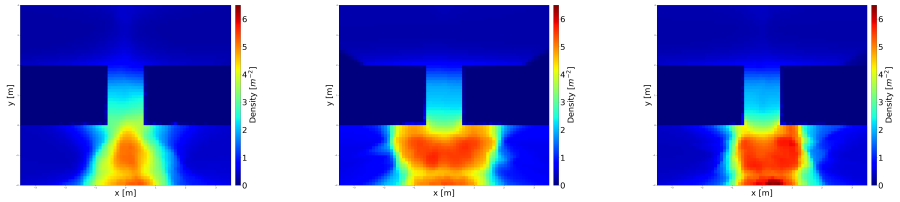

(a) density, experiment (b) density, original model (c) density, new model

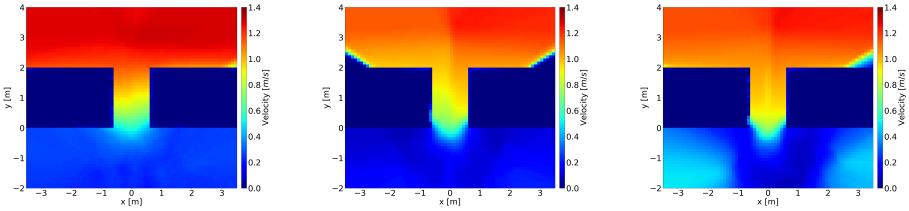

(d) velocity, experiment (e) velocity, original model (f) velocity, new model

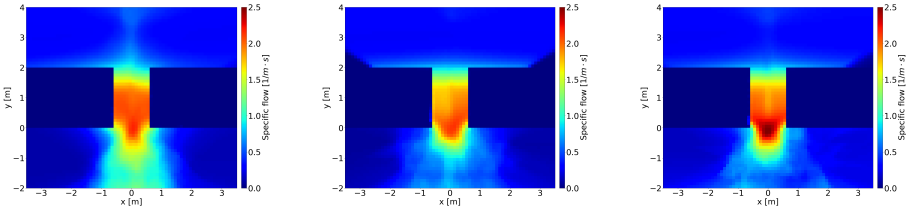

(g) Specific flow, experiment (h) Specific flow, original model (i) Specific flow, new model

Figure 14: Spatiotemporal profile of bottleneck flow, the width of bottleneck is 1.2 m. Pedestrians pass through the bottleneck from bottom to top.

model by introducing the influence of walls. Then, we generalize the definition of the model in order to consider dynamical ellipse shapes of pedestrian's projection on the 2D space, instead of the originally used circular shapes. Hereby, we define the semi-axes of the ellipses such that the two-dimensional fundamental diagram is well reproduced with respect to experimental data. After introducing a new direction sub-model, we show quantitatively that the unrealistic behavior of the agents during simulations with the original model could be mitigated. Simulation results show that the new direction sub-model can remove unrealistic backward movement and undesired shaking behaviors without compromising the benefits of the original model.

Our validation of the model was systematic, going from the fundamental diagram in narrow corridors (1D) through fundamental diagrams in wide corridors (2D) to the flow-width relation in bottlenecks. Although the generalized model produces better results, there are still some problems that have not been solved yet. First of all, in bottleneck scenarios with small widths, a jamming arch may arise. Here, the collision-free nature of the model favors excessive blocking of agents in front of the exit. Further investigations are necessary to identify an appropriate mechanism for mitigating the effects of arching. Besides, more detailed validations will be done in future work.

Acknowledgments

Qiancheng Xu thanks the funding support from the China Scholarship Council (Grant NO.201706060186). Mohcine Chraibi thanks the support from the Visiting Professor International Project at the University of Science and Technology of China (2019A VR35).

References

[1] A. Seyfried, O. Passon, B. Steffen, M. Boltes, T. Rupprecht, W. Klingsch, New insights into pedestrian flow through bottlenecks, Transportation Science 43 (3) (2009) 395–406.

[2] D. C. Duives, W. Daamen, S. P. Hoogendoorn, State-of-the-art crowd motion simulation models, Transportation research part C: emerging technologies 37 (2013) 193–209.

[3] R. L. Hughes, A continuum theory for the flow of pedestrians, Transportation Research Part B: Methodological 36 (6) (2002) 507–535.

[4] J. A. Carrillo, S. Martin, M.-T. Wolfram, An improved version of the Hughes model for pedestrian flow, Mathematical Models and Methods in Applied Sciences 26 (04) (2016) 671–697.

[5] B. Piccoli, A. Tosin, Time-evolving measures and macroscopic modeling of pedestrian flow, Archive for Rational Mechanics and Analysis 199 (3) (2011) 707–738.

[6] S. P. Hoogendoorn, F. L. van Wageningen-Kessels, W. Daamen, D. C. Duives, Continuum modelling of pedestrian flows: From microscopic principles to self-organised macroscopic phenomena, Physica A: Statistical Mechanics and its Applications 416 (2014) 684 – 694.

[7] A. Lachapelle, M.-T. Wolfram, On a mean field game approach modeling congestion and aversion in pedestrian crowds, Transportation Research Part B: Methodological 45 (10) (2011) 1572–1589.

[8] M. Burger, M. D. Francesco, P. A. Markowich, M.-T. Wolfram, Mean field games with nonlinear mobilities in pedestrian dynamics, Discrete & Continuous Dynamical Systems - B 19 (2014) 1311.

[9] A. Aurell, B. Djehiche, Mean-field type modeling of nonlocal crowd aversion in pedestrian crowd dynamics, SIAM Journal on Control and Optimization 56 (1) (2018) 434–455.

[10] Y. Achdou, J.-M. Lasry, Contributions to Partial Differential Equations and Applications, Springer International Publishing, Cham, 2019, Ch. Mean Field Games for Modeling Crowd Motion, pp. 17–42.

[11] N. Bellomo, A. Bellouquid, On the modelling of vehicular traffic and crowds by kinetic theory of active particles, in: Mathematical modeling of collective behavior in socio-economic and life sciences, Springer, 2010, pp. 273–296.
[12] C. Dogbe, On the modelling of crowd dynamics by generalized kinetic models, Journal of Mathematical Analysis and Applications 387 (2) (2012) 512–532.
[13] N. Bellomo, D. Clarke, L. Gibelli, P. Townsend, B. Vreugdenhil, Human behaviours in evacuation crowd dynamics: from modelling to "big data" toward crisis management, Physics of life reviews 18 (2016) 1–21.
[14] N. Bellomo, L. Gibelli, N. Outada, On the interplay between behavioral dynamics and social interactions in human crowds, Kinetic & Related Models 12 (2019) 397.
[15] A. Elmoussaoui, P. Argoul, M. E. Rhabi, A. Hakim, Discrete kinetic theory for 2d modeling of a moving crowd: Application to the evacuation of a non-connected bounded domain, Computers & Mathematics with Applications 75 (4) (2018) 1159–1180.
[16] A. Treuille, S. Cooper, Z. Popović, Continuum crowds, ACM Trans. Graph. 25 (3) (2006) 1160–1168.
[17] K. Rahman, N. A. Ghani, A. A. Kamil, A. Mustafa, M. K. Chowdhury, Modelling pedestrian travel time and the design of facilities: A queuing approach, PLoS ONE 8(5) (2013) e63503.
[18] A. Tordeux, G. Lämmel, F. S. Hänseler, B. Steffen, A mesoscopic model for large-scale simulation of pedestrian dynamics, Transportation Research Part C: Emerging Technologies 93 (2018) 128 – 147.
[19] G. Puppo, M. Semplice, A. Tosin, G. Visconti, Fundamental diagrams in traffic flow: The case of heterogeneous kinetic models, Communications in mathematical sciences 14 (2016) 643–669.
[20] G. Visconti, M. Herty, G. Puppo, A. Tosin, Multivalued fundamental diagrams of traffic flow in the kinetic Fokker-Planck limit, Multiscale Modeling & Simulation 15 (2017) 1267–1293.
[21] N. Bellomo, A. Bellouquid, D. Knopoff, From the microscale to collective crowd dynamics, Multiscale Modeling & Simulation 11 (3) (2013) 943–963.
[22] E. Cristiani, B. Piccoli, A. Tosin, Multiscale modeling of pedestrian dynamics, Vol. 12, Springer, 2014.
[23] N. Bellomo, L. Gibelli, Toward a mathematical theory of behavioral-social dynamics for pedestrian crowds, Mathematical Models and Methods in Applied Sciences 25 (13) (2015) 2417–2437.
[24] N. Bellomo, C. Dogbe, On the modeling of traffic and crowds: A survey of models, speculations, and perspectives, SIAM review 53 (3) (2011) 409–463.
[25] N. Bellomo, A. Bellouquid, On multiscale models of pedestrian crowds from mesoscopic to macroscopic, Commun. Math. Sci 13 (7) (2015) 1649–1664.
[26] M. Chraibi, A. Tordeux, A. Schadschneider, A. Seyfried, Modelling of pedestrian and evacuation dynamics, Encyclopedia of Complexity and Systems Science (2018) 1–22.
[27] L. Gibelli, N. Bellomo, Crowd Dynamics – Theory, Models, and Safety Problems, Vol. 1, Springer, 2019.
[28] D. Helbing, I. J. Farkas, P. Molnar, T. Vicsek, Simulation of pedestrian crowds in normal and evacuation situations, Pedestrian and evacuation dynamics 21 (2) (2002) 21–58.
[29] A. Schadschneider, A. Seyfried, Empirical results for pedestrian dynamics and their implications for modeling, Networks & Heterogeneous Media 6 (2011) 545.
[30] V. J. Blue, J. L. Adler, Cellular automata microsimulation for modeling bi-directional pedestrian walkways, Transportation Research Part B: Methodological 35 (3) (2001) 293–312.
[31] C. Burstedde, K. Klauck, A. Schadschneider, J. Zittartz, Simulation of pedestrian dynamics using a two-dimensional cellular automaton, Physica A: Statistical Mechanics and its Applications 295 (3-4) (2001) 507–525.
[32] M. Fukui, Y. Ishibashi, Self-organized phase transitions in cellular automaton models for pedestrians, Journal of the physical society of Japan 68 (8) (1999) 2861–2863.
[33] A. Kirchner, A. Schadschneider, Simulation of evacuation processes using a bionics-inspired cellular automaton model for pedestrian dynamics, Physica A: statistical mechanics and its applications 312 (1-2) (2002) 260–276.
[34] M. Muramatsu, T. Irie, T. Nagatani, Jamming transition in pedestrian counter flow, Physica A: Statistical Mechanics and its Applications 267 (3-4) (1999) 487–498.

[35] A. Tordeux, A. Seyfried, Collision-free nonuniform dynamics within continuous optimal velocity models, Physical Review E 90 (4) (2014) 042812.
[36] A. Tordeux, M. Chraibi, A. Seyfried, Collision-free speed model for pedestrian dynamics, in: Traffic and Granular Flow'15, Springer, 2016, pp. 225–232.
[37] B. Maury, J. Venel, A discrete contact model for crowd motion, ESAIM: Mathematical Modelling and Numerical Analysis 45 (1) (2011) 145–168.
[38] S. Paris, J. Pettré, S. Donikian, Pedestrian reactive navigation for crowd simulation: a predictive approach, in: Computer Graphics Forum, Vol. 26, Wiley Online Library, 2007, pp. 665–674.
[39] D. Helbing, P. Molnar, Social force model for pedestrian dynamics, Physical review E 51 (5) (1995) 4282.
[40] M. Chraibi, A. Seyfried, A. Schadschneider, Generalized centrifugal-force model for pedestrian dynamics, Physical Review E 82 (4) (2010) 046111.
[41] D. R. Parisi, M. Gilman, H. Moldovan, A modification of the social force model can reproduce experimental data of pedestrian flows in normal conditions, Physica A: Statistical Mechanics and its Applications 388 (17) (2009) 3600–3608.
[42] A. Johansson, D. Helbing, P. K. Shukla, Specification of the social force pedestrian model by evolutionary adjustment to video tracking data, Advances in complex systems 10 (supp02) (2007) 271–288.
[43] J. J. Fruin, Pedestrian planning and design, Tech. rep., New York: Elevator World (1971).
[44] A. Seyfried, B. Steffen, W. Klingsch, M. Boltes, The fundamental diagram of pedestrian movement revisited, Journal of Statistical Mechanics: Theory and Experiment 2005 (10) (2005) P10002.
[45] R. e.V., Guideline for microscopic evacuation analysis, URL `https://rimeaweb.files.wordpress.com/2016/06/rimea_richtlinie_3-0-0_-_d-e.pdf` acceded on 01.07.2019 (2016).
[46] E. Ronchi, E. D. Kuligowski, P. A. Reneke, R. D. Peacock, D. Nilsson, The process of verification and validation of building fire evacuation models, US Department of Commerce, National Institute of Standards and Technology, 2013.
[47] A. Seyfried, M. Boltes, J. Kähler, W. Klingsch, A. Portz, T. Rupprecht, A. Schadschneider, B. Steffen, A. Winkens, Enhanced empirical data for the fundamental diagram and the flow through bottlenecks, in: Pedestrian and Evacuation Dynamics 2008, Springer, 2010, pp. 145–156.
[48] S. Holl, A. Seyfried, Hermes-an evacuation assistant for mass events, Inside 7 (1) (2009) 60–61.
[49] S. Buchmüller, U. Weidmann, Parameters of pedestrians, pedestrian traffic and walking facilities, IVT Schriftenreihe 132 (2006).

Publication II

Info: Xu Q, Chraibi M, Seyfried A. Prolonged clogs in bottleneck simulations for pedestrian dynamics. Physica A: Statistical Mechanics and its Applications, 2021, 573: 125934.

Prolonged Clogs in Bottleneck Simulations for Pedestrian Dynamics

Qiancheng Xu[a,*], Mohcine Chraibi[a], Armin Seyfried[a,b]

[a]*Institute for Advanced Simulation, Forschungszentrum Jülich, 52425 Jülich, Germany*
[b]*School of Architecture and Civil Engineering, University of Wuppertal, 42119 Wuppertal, Germany*

Abstract

This article studies clogging phenomena using a velocity-based model for pedestrian dynamics. First, a method to identify prolonged clogs in simulations was introduced. Then bottleneck simulations were implemented with different initial and boundary conditions. The number of prolonged clogs were analyzed to investigate the decisive factors causing this phenomenon. Moreover, the time lapse between two consecutive agents passing the exit, and the trajectories of agents were analyzed. The influence of three type of factors was studied: parameters of the spatial boundaries, algorithmic factors related to implementation of the model, and the movement model. Parameters of the spatial boundaries include the width and position of the bottleneck exit. Algorithmic factors are the update methods and the size of the time step. Model parameters cover several parameters describing the level of motivation, the strength and range of impact among agents, and the shape of agents. The results show that the occurrence of prolonged clogs is closely linked to parameters of the spatial boundaries and the movement model but has virtually no correlation with algorithmic factors.

Keywords: bottleneck, clogging, pedestrian dynamics, simulations, velocity-based model

1. Introduction

Clogging is a phenomenon that usually arises when particles pass through narrow bottleneck structures [1]. It is often expressed as the jamming arch formed by several interactive particles in front of the bottleneck, which significantly decreases or even stops the flow through the bottleneck.

The phenomenon occurs in different systems of inert particles such as granular material in the silo [1, 2, 3], dense suspension of colloidal particles [4, 5, 6, 7] or electrons on the surface of liquid helium [8, 9]. This type of clogging is usually stable if there is no external disturbance to break the balance between the particles that form the clogging [1, 10]. Clogging can also

*corresponding author

Email addresses: q.xu@fz-juelich.de (Qiancheng Xu), m.chraibi@fz-juelich.de (Mohcine Chraibi), a.seyfried@fz-juelich.de (Armin Seyfried)

be observed in the movement of animals [11] and humans [12] when congestion and high motivation coincide, for instance, when a large number of passengers at a train station enter carriages through a narrow train door with high motivation, or when fans at entrances to a concert hall are all trying to get in and find places near the stage [13].

Unlike with the clogging of inert particles, clogging in systems with humans is temporary. The duration of clogs depends on the motivation level of the pedestrians involved in the clogging [5, 11, 12, 13]. Although the clogging of humans may last a relatively long time in some extreme cases and sometimes even leads to severe injuries [14, 15], in most normal cases, its duration is short even in competitive situations [13]. In the literature, the short-term nature of the clogs is often attributed to the fluctuation in the load to the humans in the clog. This fluctuation, in turn, may be the result of the flexibility and elasticity of the human body. Moreover, some clogs are avoided before forming, through complex steering mechanisms that include cognitive processes and control of the body.

However, microscopic models based on physical principles merely focus on guaranteeing volume exclusion. They do not take the above-mentioned factors sufficiently into account, which could lead to prolonged clogs (clogs interrupting flow for a long time) or even stable clogs similar to inert particles. One study, [16], examined this phenomenon using a cellular automaton (CA) model. A friction parameter was introduced for an improved description of the clogging of pedestrians. In another study, [17], the friction parameter was extended to a function of the number of agents in clogging for a more realistic result of the pedestrian outflow through the exit. The effect of queuing and pushing behavior in front of the bottleneck on the overall dynamics of the crowd is explored using another CA model in [18], where a local pushing mechanism is used [19]. Another global pushing mechanism is proposed in [20]. Furthermore, game theory is combined with CA models in some studies to better reproduce the movement of pedestrians [21, 22]. Prolonged clogs and stable clogs can also be observed in the social force models for pedestrian dynamics by increasing the desired velocity of the agents [23]. Introducing random behavioral variations is important to mitigate these clogs in simulations [24, 25]. Further studies [26, 27] used the social force model to study the effect of desired velocity and the exit door on the duration of clogs. Clogs caused by higher desired velocity in force-based models result in lower flow through bottlenecks, a phenomenon also known as "faster-is-slower" [24, 26, 27, 28, 29].

In this paper, we focus on prolonged clogs occurring in the generalized collision-free velocity model (GCVM) [30], a first-order microscopic model for pedestrian dynamics. It is based on the collision-free speed model [31], and strictly follows the principle of volume exclusion to guarantee that there is no overlap among agents. Therefore, clogs that result in long-term interruption of flow occur frequently in simulations of bottlenecks, particularly in narrow exits. We aim to quantify these prolonged clogs by exploring decisive factors behind their occurrence in the bottleneck scenario, to purposefully improve the GCVM for reproducing pedestrians' movement more realistically. The effect of three types of factors is examined in this study. The first category includes two parameters of the spatial boundaries, i.e., the width and the position of the bottleneck exit. The second category consists of algorithmic factors related to the implementation of the GCVM, including the time step size and the update scheme (e.g., sequential or parallel update) for the agents in the simulations.

Third, several model parameters such as the strength of impact among agents in the GCVM, and the shapes of the agents are analyzed. The results are used to ascertain the relationship between these factors and the occurrence of prolonged clogs.

This paper is organized as follows. Section 2 introduces the bottleneck scenario for the simulations. In section 3, we briefly define the GCVM and introduce the method used for identifying prolonged clogs in numerical simulations. Section 4 compares simulation results obtained with various factors and shows the corresponding analysis. Finally, we conclude with a discussion in section 5.

2. The bottleneck scenario for simulations

The bottleneck scenario for simulations in this study is shown in Figure 1. It is composed of three parts separated by red dashed segments. The source area, a $8\,\mathrm{m} \times 8\,\mathrm{m}$ square in gray, the moving area, a rectangular room with an area of $10\,\mathrm{m} \times 8\,\mathrm{m}$, and the exit, a corridor measuring $2\,\mathrm{m} \times w$. In section 4 different values of w and d (the position of the exit with respect to the lower horizontal wall) are used to determine the effect of the structure of the bottleneck has on the occurrence of the prolonged clogs.

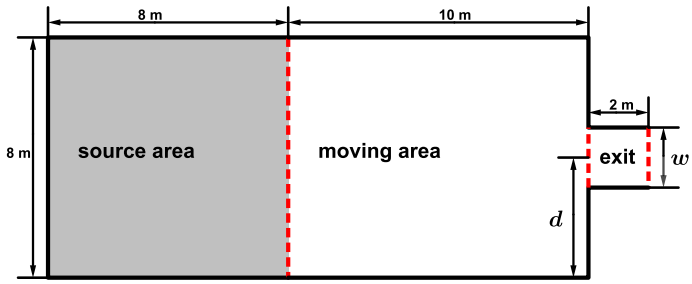

Figure 1: The bottleneck scenario for simulations.

In order to determine the decisive factors behind the appearance of prolonged clogs, simulations are implemented in the bottleneck scenario with different initial and boundary conditions. In each simulation, 400 agents are generated with a constant rate at random positions in the source area and these move through the moving area to leave the scenario by the exit. During this process, clogs may appear, leading to an interruption of the bottleneck flow. A clog interrupting the flow longer than the time threshold T_w is identified as a prolonged clog. Since prolonged clogs can last a long time and so as to ensure that the blockage does not stop the dynamics of the system, resulting in an impractically long simulation time, we manually solve them by moving one of the agents involved in the clog to free space in the source area. The details of this manual clog-solving procedure will be elaborated in the next section. The number of prolonged clogs in each simulation is recorded. Then the results of

different simulations are compared to explore the relationship between these factors and the occurrence of prolonged clogs.

The model for pedestrian dynamics and the approach to identify clogs are presented in the following section.

3. Introducing the model and identifying prolonged clogs

We begin this section with a brief introduction to the GCVM, which is the model used in this study. It is defined as

$$\dot{X}_i(X_i, X_j, \dots) = \vec{e}_i(X_i, X_j, \dots) \cdot V_i(X_i, X_j, \dots), \tag{1}$$

where X_i is the position of agent i, V_i is a scalar denoting its speed, and $\vec{e}_i$ is a unit vector representing its direction of movement.

The direction of movement $\vec{e}_i$ is calculated first by using the equation

$$\vec{e}_i = u \cdot \left(\vec{e}_i^{\,0} + \sum_{j \in J_i} k \cdot \exp\left(\frac{-s_{i,j}}{D}\right) \cdot \vec{n}_{i,j} + \vec{w}_i \right). \tag{2}$$

Here, u is a normalization constant such that $\|\vec{e}_i\| = 1$. $\vec{e}_i^{\,0}$ is a unit vector representing the desired direction of the agent. This is calculated according to reference lines indicated by the red dashed segments in Figure 1. The vector $\vec{e}_i^{\,0}$ points to the middle of the reference line when agent i is not in the range of the reference line; otherwise, it points to the nearest point on the reference line. More details of the calculation method are given in [32]. J_i is the set of agents that contains all neighbors affecting the moving direction of agent i. The magnitude of the impact from these neighbors is a function of $s_{i,j}$, which is the distance between the edges of agent i and j along the line connecting their centers. Parameters $k > 0$ and $D > 0$ are used to calibrate the strength and range of the impact, respectively. The effect of k and D on the strength of impact is shown in Figure 2(a) and a similar analysis for the effect of k and D can be found in [33]. The direction of the impact from agent j to i is denoted by the unit vector $\vec{n}_{i,j}$, which depends on the relative positions of both agents. $\vec{w}_i$ is the effect from walls and obstacles in the room, which is calculated analogously to the effect from neighbors.

Then the speed on the new moving direction is obtained using the equation

$$V_i = \min\left\{ V_i^0, \max\left\{0, \frac{s_i}{T}\right\}\right\}. \tag{3}$$

The speed is a function of s_i, which is the maximum space of agent i in the new direction of movement $\vec{e}_i$ without overlapping with other agents. In Eq. 3, V_i^0 is the free speed of agent i, the speed that is achieved by moving without interference from other agents. The parameter $T > 0$ is the slope of the speed-headway relationship. The speed functions with different V_i^0 and T are shown in Figure 2(b). The value of T could be used to model the level of motivation in simulations. A decrease of T at constant s_i leads to a smaller distance

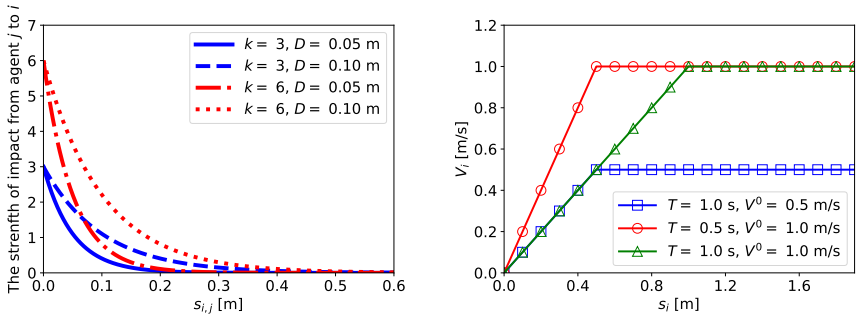

(a) (b)

Figure 2: (a) The effect of k and D on the strength of impact. (b) The speed functions with different V_i^0 and T.

between agent i and the nearest agent in front, which corresponds to behavior with a higher level of motivation. A more detailed introduction to the GCVM can be found in [30].

Since there is no overlapping among agents in the GCVM, the space occupied by one agent is not available to other agents. Therefore, clogging occurs when the direction of movement, $\vec{e}_i$, of two agents point toward each other and the distance $s_{i,j}$ between them is too small for them to move. A representative case is shown in Figure 3(a). It could be formalized by

$$\begin{cases} s_{i,j} & \leq \epsilon, \\ V_i + V_j & \leq \lambda, \\ \vec{e}_{i,j} \cdot \vec{e}_i & < 0, \\ \vec{e}_{i,j} \cdot \vec{e}_j & > 0, \end{cases} \tag{4}$$

where $\vec{e}_{i,j}$ is the unit vector points from the center of agent j to i, ϵ is a threshold used to determine whether the distance between these two agents is small enough to form a clog, and λ is the threshold of speed to ascertain whether these two agents are almost stationary. The last two conditions in Eq. 4 denote that these two agents are moving toward each other. In the present study, ϵ is equal to the radius of agents, and λ is set as $(V_i^0 + V_j^0)/100$. A clog formed by more than two agents contains at least two agents satisfying Eq. 4.

There could be many pairs of agents that satisfy the definition of clogging in Eq. 4 at any time and any place in the simulation. We treat clogs that interrupt the flow longer than time period T_w as prolonged clogs. These prolonged clogs occur almost around exits, as the degree of freedom in the direction of movement is limited by the wall. An example of prolonged clogs is shown in Figure 3(b), a clog consisting of four red agents is formed in front of the bottleneck and interrupts the flow. After $T_w = 2\,\mathrm{s}$, the clog is solved manually by moving one of the agents in the clog. As for clogs that do not interrupt the flow or last less than T_w seconds, we do not destroy them artificially since these can be solved automatically by agents adjusting their direction of movement. A clog formed by two red agents, which

can be automatically solved in $T_w = 2\,\mathrm{s}$, is shown in Figure 3(c).

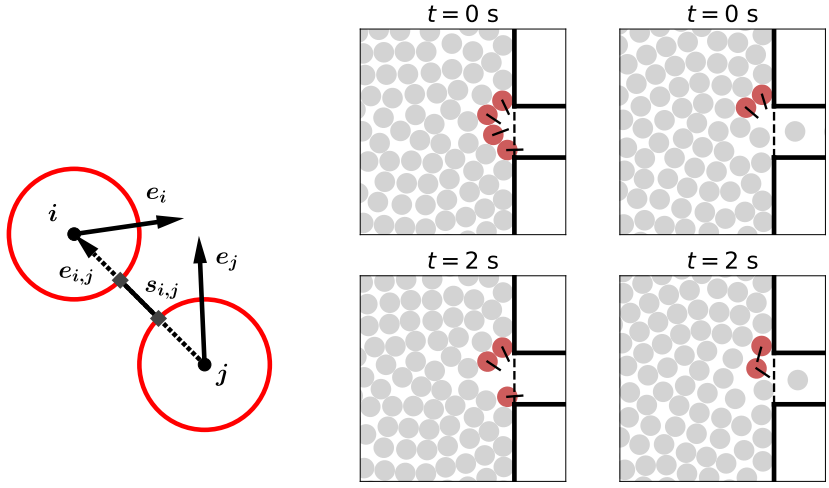

(a) (b) (c)

Figure 3: (a): When two agents are about to cause clogging, $\vec{e}_i$ and $\vec{e}_j$ are directions of movement of agent i and j, $\vec{e}_{i,j}$ is the unit vector points from the center of agent j to i, $s_{i,j}$ is the distance between the edges of agent i and j along the line connecting their centers. (b): A prolonged clog is manually solved after interrupting the flow for 2 s. (c): A clog is solved automatically by agents adjusting their direction of movement.

The flowchart in Figure 4 illustrates how to count the prolonged clogs in simulations, where t is the current time, t_p is the time at which the last agent enters the exit, t_m is the time of the last manual clog-solving process, N_s is the number of prolonged clogs, Δt is the time step size in the simulation, and t_c is the smaller of $t - t_p$ and $t - t_m$.

For each time step of a simulation, a non-zero flow through the measurement line between moving area and exit is an indicator that no prolonged clogs occur. Otherwise, we will check whether t_c is greater than the threshold T_w, and whether there are agents satisfying the definition of clogging in Eq. 4. A prolonged clog is identified if these two conditions are met. It is treated as a new clog if t_p, the time when the last agent crossed the bottleneck, is not less than t_m, the time of the last manual removal of an agent. Regardless of whether the clog is new or already existing, one of the two agents forming the closest clog to the exit is moved manually to free space in the source area. It should be noted that breaking up a prolonged clog may require more than one manual clog-solving process, which results in $t_p < t_m$. The number of prolonged clogs is counted from the beginning of the simulation to the last agent leaving the simulation scenario.

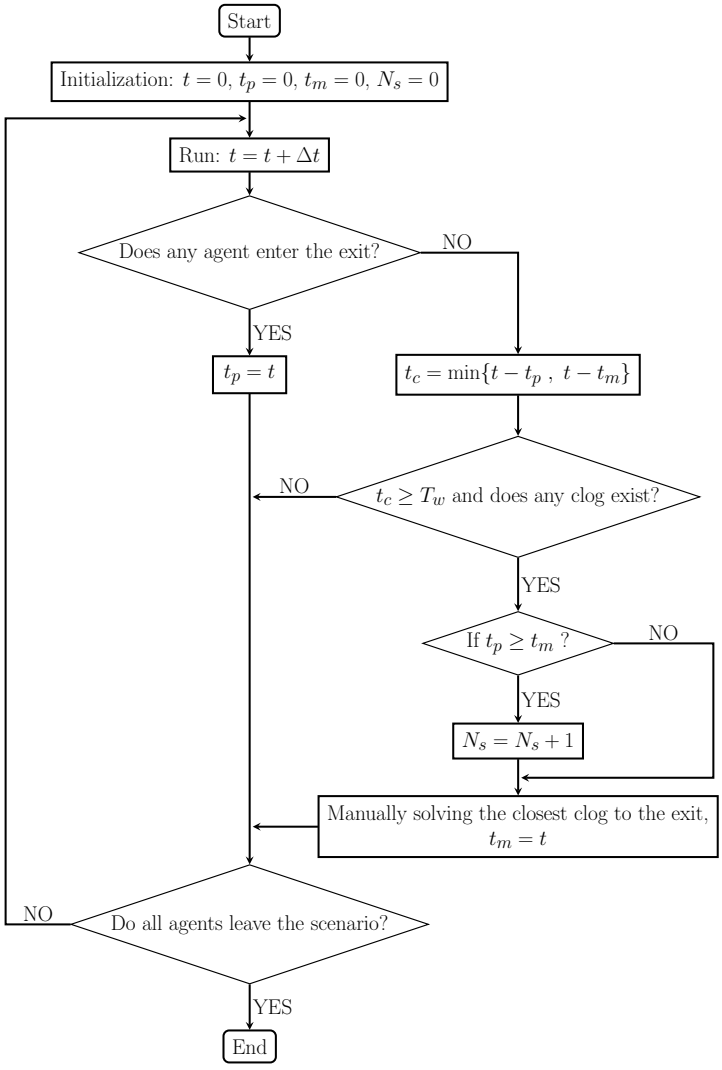

Figure 4: The process of solving and counting prolonged clogs. t is the current time, t_p is the time of the last agent entering the exit, t_m is the time of the last manual clog-solving process, N_s is the number of prolonged clogs, Δt is the time step size in the simulation, t_c is the smaller of $t - t_p$ and $t - t_m$, T_w is the time threshold.

4. Simulation results

In each simulation, one or two factors were selected for variation. The other factors were set to default values as shown in Table 1.

Factors	Default values
Agent generation rate	8 Agents/s
Agent shape	circle ($r = 0.2$ m)
Update method	parallel update
Time step size Δt	0.05 s
w (Figure 1)	0.8 m
d (Figure 1)	4 m
k (Eq. 2)	3
D (Eq. 2)	0.1 m
V_i^0 (Eq. 3)	1.34 m s^{-1}
T (Eq. 3)	0.3 s

Table 1: Default values of factors in simulations. w is the width of the exit, d is the distance between the center of the exit and the lower horizontal wall of the moving area, k and D are parameters used to calibrate the strength and range, respectively, of the impact from neighbors in the movement direction, V_i^0 is the free speed, and T is the slope of the speed-headway relationship.

To improve the efficiency of simulations, a series of simulations were implemented firstly to select the suitable T_w, the time span between the formation, and artificial termination of a prolonged clog for subsequent simulations. We ran simulations in four bottleneck scenarios, where the value of w was 0.8, 1.0, 1.2, and 1.6 m, respectively. For each scenario, simulations with T_w from 0 s to 4 s were implemented. We ran each simulation four times with different distributions of agents in the source area. The relationship between T_w and the mean values of N_s, the number of prolonged clogs, from the four runs are shown in Figure 5, where the error bars indicate the standard deviations. The results in scenarios with a different value of w are represented by different marks and colors. In all four scenarios, N_s dis not change significantly when T_w was longer than 2 s. Therefore, this value for T_w was selected for the following simulations.

In the following, we ran each simulation four times. The mean value of N_s from the four runs reflects the effect of the factors observed on the occurrence of prolonged clogs. Moreover, the time lapse between two consecutive agents entering the exit, and the trajectories of agents were analyzed for the selected factors.

4.1. Parameters of spatial boundaries

The effects of the width and the position of the exit are explored in this subsection. Three exit positions ($d = 4.0$, 2.0, or $w/2$ m) and six widths ($w = 0.8$, 1.0, 1.2, 1.6, 2.0, or 2.5 m) were selected for the simulations. The exit was located in the middle of two lateral walls of the moving area when $d = 4$ m and adjacent to the lower horizontal wall when $d = w/2$.

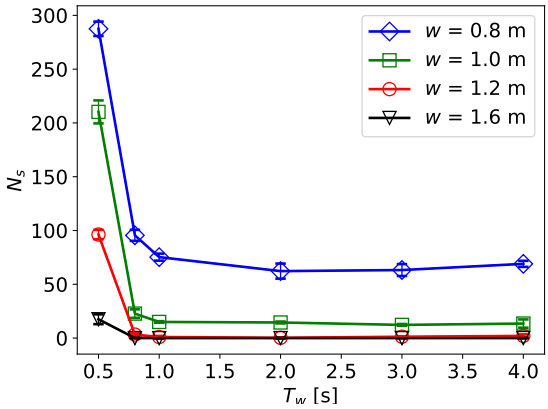

Figure 5: The correlation between N_s (the number of prolonged clogs) and T_w (the time span between the formation and artificial termination of a prolonged clog) for different values of w (the width of the exit). The error bars show the standard deviations.

Figure 6 shows the correlation between N_s and w for different values of d. The position of the exit does not alter the fact that N_s decreases to zero as w increases. Moreover, there is no prolonged clog when the exit is wider than 1.6 m for all three positions. Besides the effect of w, when $d = w/2$ (the exit is adjacent to the lower horizontal wall of the moving area), N_s was significantly less than with the other two locations. We assumed that this difference was caused by the reduced degree of freedom in the possible directions in which agents will move.

In order to quantitatively analyze the influence of the width of the exit (w) on the clogs, we examined the time lapses δ between two consecutive agents passing the exit, for different values of w. The value of δ reflects the sustained time of clogs interrupting the flow. The probability distribution function $P(t > \delta)$, also known as the survival function, is sensitive to changes in the spatial boundaries, e.g. the width of the bottleneck [5, 11, 12, 34]. We analyzed the results of simulations when $d = 4$ m. The survival functions of different values of w are compared in Figure 7(a). It can be observed that the probability of a higher value of δ decreases as w increases. Besides, the occurrence of prolonged clogs leads to plateaus in the survival functions of $w = 0.8$ and $w = 1.0$ m. Basically, in these two cases, the actual values of $\langle\delta\rangle$, the mean time lapse, are unknown as clogs lasting longer than 2 s are manually solved. In fact, the actual value of $\langle\delta\rangle$ without manually removal of clogs may probably tend to infinite. Nevertheless, in order to obtain an estimate for the lower bound of $\langle\delta\rangle$ and study its dependence on w, we treated all $\delta > 2$ s as $\delta = 2$ s in the calculation of the mean value of δ. The correlation between the value of $\langle\delta\rangle$ and w is shown in Figure 7(b). The mean value and standard deviation of δ both decrease with increasing w.

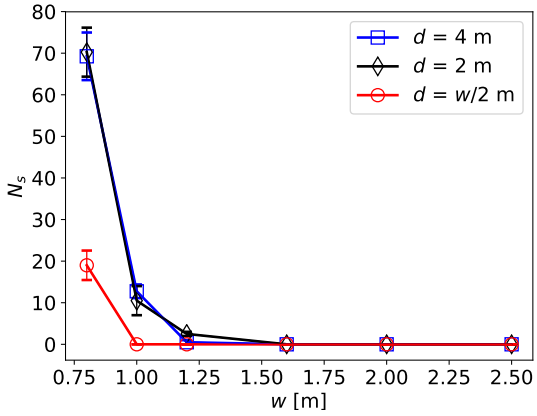

Figure 6: The correlation between N_s (the number of prolonged clogs) and w (the width of the exit) for different values of d (the distance between the center of the exit and the lower horizontal wall of the moving area). The error bars show the standard deviations.

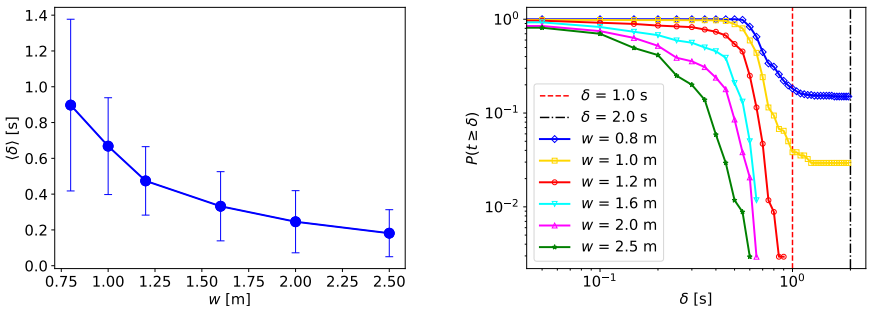

(a) (b)

Figure 7: (a): The survival functions of δ for simulations with different values of w when $d = 4\,\mathrm{m}$. (b): The correlation between the $\langle\delta\rangle$ (the mean time lapse between two consecutive agents entering the exit) and w when $d = 4\,\mathrm{m}$. The error bars show the standard deviations.

4.2. Algorithmic factors

The effect of update methods and the time step sizes Δt to solve the equation of motion are analyzed in this subsection. Two update methods were adopted: the parallel update and the sequential update. When we used the parallel update, the direction of movement, speed and location of all the agents were updated at the same time. When the sequential update was used, the direction of movement, speed and location of agents were updated one by one according to the distance to the exit. The agents near the exit had more effect on the dynamic of the system than the agents further away from the exit. Therefore, the agent with a greater effect, i.e., the agent closer to the exit, was updated first in the sequential update. For each update method, simulations were performed with different values of Δt from 0.01 s to 0.125 s.

The correlation between N_s and Δt for two update methods is shown in Figure 8. The effect of Δt on N_s is marginal for both update methods.

To explain the reason behind the results, an extreme case is considered here where two agents i and j are moving directly toward each other, which means $\vec{e}_i = -\vec{e}_j$. We assume that their direction of movement is fixed, and $s_{i,j} < T \cdot V_i^0$. According to Eq. 3, their speeds V_i and V_j are both equal to $s_{i,j}/T$. They will not overlap and, consequently, form a clog if their speeds satisfy

$$(V_i + V_j) \cdot \Delta t \leq s_{i,j}, \tag{5}$$

which can be transformed to $2 \cdot \Delta t \leq T$. This example illustrates that adopting a lower value of Δt or substituting the sequential update cannot hinder the occurrence of clogging, since the scarcity of available space is not changed.

Therefore, the occurrence of prolonged clogs in the simulations with the GCVM is not an algorithmic issue.

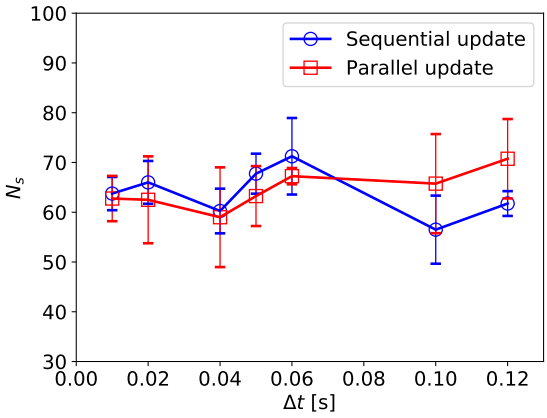

Figure 8: The correlation between N_s (the number of prolonged clogs) and Δt (time step size) for different update methods. The error bars show the standard deviations.

4.3. Parameters of the GCVM

In this subsection, the effect of several parameters in the GCVM is examined, including the slope of the speed-headway relationship T and the free speed V^0 in Eq. 3. The strength and range of the effect of neighbors in the direction of movement, k and D in Eq. 2, and the shapes of agents are also studied.

First, we looked at the effect of T and V^0. We ran simulations with different V^0 (1.34, 3.34, or 5.34 $\mathrm{m\,s^{-1}}$) and different T (0.1, 0.3, 0.5, 0.8, or 1.0 s). The correlation between N_s and T for different values of V^0 is shown in Figure 9(a). For all three values of V^0, as T increased, N_s decreased initially, then remained relatively stable. A decrease in T led to a smaller slope of the speed-headway function, see Eq. 3 and Figure 2(b). With decreasing T agents move closer, which reduces the space available to resolve clogs. This is in accordance with the finding that clogging is more likely to occur in scenarios with higher level of motivation [12, 25, 28, 34].

The level of motivation has been shown to have an effect on the time lapse δ [12, 25, 28]. Figure 9(b) shows the survival functions of δ in the simulations with $V^0 = 3.34\,\mathrm{m\,s^{-1}}$, which is similar to the result of granular media experiment [28]. These survival functions can be approximately separated into two successive regimes by $\delta = 1.2\,\mathrm{s}$. For $\delta \leq 1.2\,\mathrm{s}$, increasing T leads to a higher value of $P(t > \delta)$, while for $\delta > 1.2\,\mathrm{s}$, increasing T reduces $P(t > \delta)$. The mean time lapse $\langle\delta\rangle$ for each regime is shown in Figure 9(c). As we mentioned above, the actual values of $\langle\delta\rangle$ for the region of $\delta > 1.2\,\mathrm{s}$ are unknown as clogs lasting longer than 2 s are manually solved. Therefore, we treated all $\delta > 2\,\mathrm{s}$ as $\delta = 2\,\mathrm{s}$ in the calculation of the mean value of δ. The obtained values are the lower bound of the real ones. Decreasing T can be interpreted as increasing the level of motivation, which results in an increase in the free flow rate ($\delta \leq 1.2\,\mathrm{s}$) as well as an increase in the probability of clogging ($\delta > 1.2\,\mathrm{s}$).

However, a higher value of V^0, which can be interpreted as the expression of a higher motivation level, leads to lower values of N_s. We analyzed the results of simulations with $T = 0.8\,\mathrm{s}$. The survival functions of different values of V^0 are compared in Figure 9(d). The probability of a higher value of δ decreases as V^0 increases. According to Eq. 3, the speed of agents in the GCVM depends on the overlapping-free spaces in their directions of movement. Although a higher V^0 increases the maximum possible speed of agents, it has little effect in congested areas due to limited space. Therefore, the effect of V^0 in the GCVM on the motivation level of present simulations is marginal, as most of the investigated situations represent congested conditions. Moreover, a higher V^0 allows agents to move faster in low density situations, which results in the reduction of N_s. Note, that in force-based models [25] the driving force increases with increasing V^0, hence V^0 can have an effect in congested situations as well.

Then we examined the effect of k and D. Higher values of k and larger D led to agents being more stimulated to deviate from their desired directions. We ran simulations with different values of k (0.2, 0.5, 1, 2, 3, 4, 5, or 6) and different values of D (0.01, 0.02, 0.05, or 0.1 m). The correlation between N_s and k for different values of D is shown in Figure 10.

It can be seen that N_s increases with increasing k and increasing D. We assume the reason for this is that lower values of k and D decrease the neighbor's impact on agents, which leads to the queuing behavior. We show in Figure 11(a) the trajectories of agents

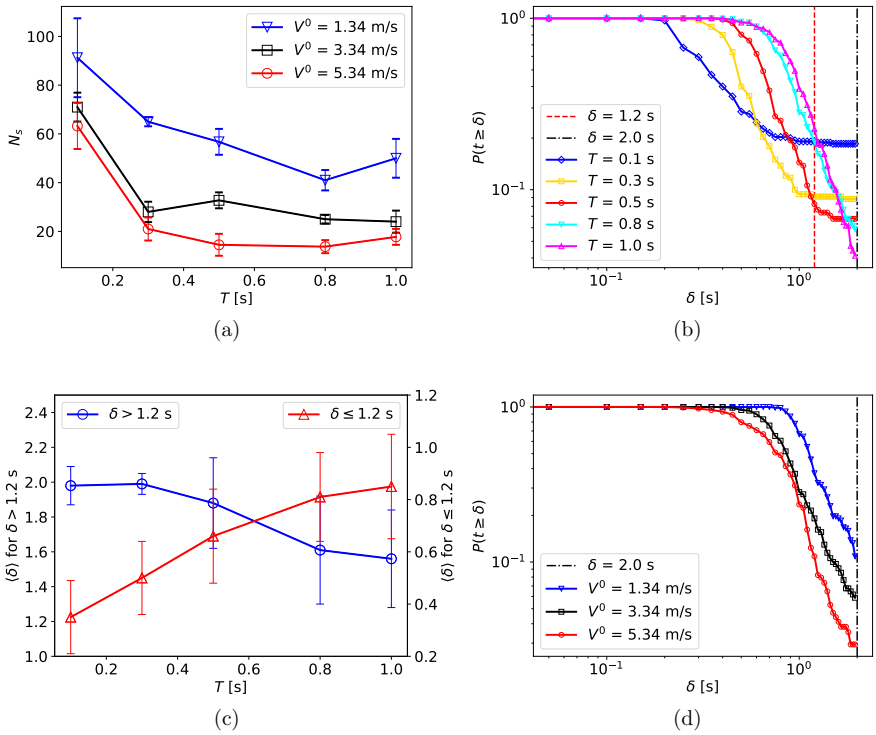

Figure 9: (a): The correlation between N_s (the number of prolonged clogs) and T (the slope of the speed-headway relation) for different values of V^0 (the free speed). The error bars show the standard deviations. (b): The survival functions of δ (the time lapse between two consecutive agents entering the exit) in the simulations with different values of T when $V^0 = 3.34\,\mathrm{m\,s^{-1}}$. (c): The mean time lapse $\langle\delta\rangle$ versus T when $V^0 = 3.34\,\mathrm{m\,s^{-1}}$, for $\delta \leq 1.2\,\mathrm{s}$ and $\delta > 1.2\,\mathrm{s}$, respectively. (d): The survival functions of δ (the time lapse between two consecutive agents entering the exit) in the simulations with different values of V^0 when $T = 0.8\,\mathrm{s}$.

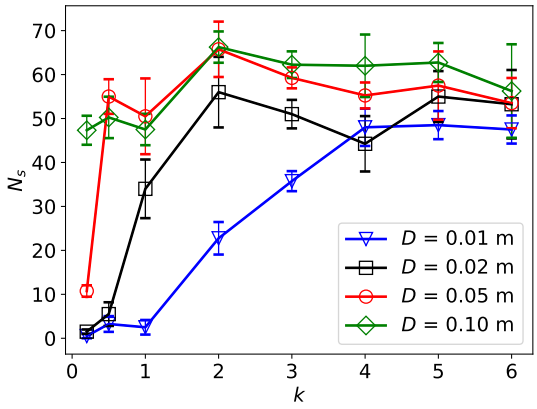

Figure 10: The correlation between N_s (the number of prolonged clogs) and k for different values of D. The error bars show the standard deviations.

in the simulation when k is 0.2 and D is 0.01 m, which shows a strong queuing behavior. When the impact among agents increased consistently, agents began to deviate from their desired direction until the queuing behavior was broken. Figure 11(b) shows the trajectories of agents in the simulation when k is 3 and D is 0.01 m.

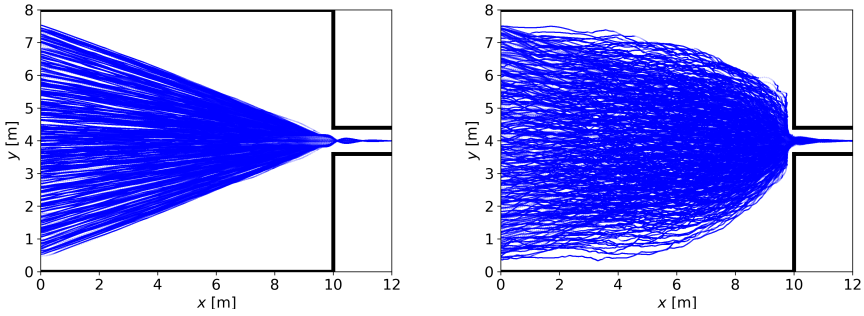

Figure 11: (a): Trajectories of agents when k is 0.2 and D is 0.01 m. (b): Trajectories of agents when k is 3.0 and D is 0.01 m.

The final factor analyzed was the shapes of agents. In the previous sections, a pedestrian's shape was modeled as circles with a constant radius. To study the influence of the shape, we also performed simulations where pedestrians were modeled as velocity-based ellipses [30]. The length of the semi-axis along the walking direction is a constant value a. The length of

the other semi-axis along the shoulder equals b, which is defined as

$$b = b_{\min} + \frac{b_{\max} - b_{\min}}{1 + e^{\beta \cdot (V - \gamma)}} , \tag{6}$$

where $b_{\max}$ is the maximum value which is equal to half of a static pedestrian's width, $b_{\min}$ is equal to the half of a moving pedestrian's minimum width, V is the speed of the agent, and parameters β and γ are used to adjust the shape of the function.

Simulations in this part are performed with three constant circles with different radius values r (0.15, 0.20, or 0.25 m) and a velocity-based ellipse ($a = 0.20\,\mathrm{m}$, $b_{\min} = 0.15\,\mathrm{m}$, $b_{\max} = 0.25\,\mathrm{m}$, $\beta = 50$, $\gamma = 0.1$). Figure 12(a) shows the correlation between N_s and w for different shapes. The result of the ellipse is close to the result of the circle with $r = 0.20\,\mathrm{m}$, which is between the result of the smallest circle ($r = 0.15\,\mathrm{m}$) and of the biggest circle ($r = 0.25\,\mathrm{m}$). The possible explanation of this result is that the shape of the dynamic ellipse varies with the speed of agents. For example if the speed of an agent is $0.1\,\mathrm{m\,s^{-1}}$, the dynamic ellipse becomes a circle with $r = 0.2\,\mathrm{m}$. Which means that in high density situations the agents tend to have a circular shape instead.

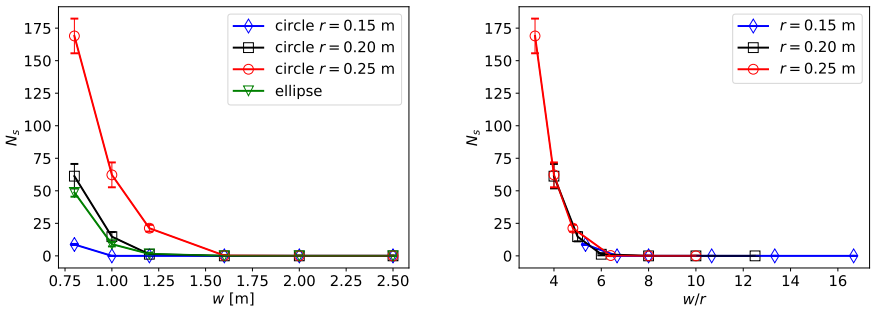

(a) (b)

Figure 12: (a) The correlation between N_s (the number of prolonged clogs) and w (the width of the exit) for different shapes of agents. The error bars show the standard deviations. (b) The correlation between N_s and w/r for different r (the radius of agents). The error bars show the standard deviations.

A finding in [35] is that the probability of clogs stopping the flow decreases with an increasing ratio between the size of the orifice and the size of the beads. Therefore, we plot Figure 12(b) with w/r (the ratio between the width of the exit and the radius of the agents) as the horizontal axis. It seems that the number of prolonged clogs is not affected by the absolute values of w and r, provided that w/r remains the same.

5. Conclusion

In the present paper, we focus on prolonged clogs that occur in bottleneck scenarios with the GCVM. A general definition of prolonged clogs has been given. Then a series of

simulations in a bottleneck scenario were implemented to analyze the effect of various factors on the occurrence of prolonged clogs.

From the simulation results, the following conclusions can be drawn. First, the number of prolonged clogs decreases as the width of the exit increases. Second, the occurrence of prolonged clogs cannot be eliminated by adopting a smaller time step size or updating the positions of agents sequentially. Third, a decrease in T in the GCVM leads to smaller distance between agents, which corresponds to a behavior with a higher level of motivation. Meanwhile, decreasing T reduces the space available for agents to resolve clogs, which increases the number of prolonged clogs. This is in accordance with the fact that clogging is more likely to occur in scenarios with a higher level of motivation. Fourth, reducing the degree of freedom in the possible directions in which agents will move can reduce or even eliminate the occurrence of prolonged clogs. For instance, this can be facilitated by the queuing behavior in Figure. 11(a) as well as by locating the exit adjacent to the lower horizontal wall of the moving area. Finally, when the ratio between the width of the exit and the radius of agents increases, the number of prolonged clogs decreases.

Acknowledgments

The authors are grateful to the HGF Knowledge-transfer project under Grant No. WT-0105. Qiancheng Xu thanks the funding support from the China Scholarship Council (Grant NO. 201706060186).

References

[1] I. Zuriguel, Invited review: Clogging of granular materials in bottlenecks, Papers in Physics 6 (2014) 060014–060014.

[2] R. Arévalo, I. Zuriguel, Clogging of granular materials in silos: effect of gravity and outlet size, Soft Matter 12 (1) (2016) 123–130.

[3] R. Hidalgo, C. Lozano, I. Zuriguel, A. Garcimartín, Force analysis of clogging arches in a silo, Granular Matter 15 (6) (2013) 841–848.

[4] M. van Hecke, Jamming of soft particles: geometry, mechanics, scaling and isostaticity, Journal of Physics: Condensed Matter 22 (3) (2009) 033101.

[5] I. Zuriguel, D. R. Parisi, R. C. Hidalgo, C. Lozano, A. Janda, P. A. Gago, J. P. Peralta, L. M. Ferrer, L. A. Pugnaloni, E. Clément, et al., Clogging transition of many-particle systems flowing through bottlenecks, Scientific reports 4 (2014) 7324.

[6] A. Guariguata, M. A. Pascall, M. W. Gilmer, A. K. Sum, E. D. Sloan, C. A. Koh, D. T. Wu, Jamming of particles in a two-dimensional fluid-driven flow, Physical review E 86 (6) (2012) 061311.

[7] D. Genovese, J. Sprakel, Crystallization and intermittent dynamics in constricted microfluidic flows of dense suspensions, Soft Matter 7 (8) (2011) 3889–3896.

[8] D. G. Rees, I. Kuroda, C. A. Marrache-Kikuchi, M. Höfer, P. Leiderer, K. Kono, Point-contact transport properties of strongly correlated electrons on liquid helium, Physical review letters 106 (2) (2011) 026803.

[9] D. Rees, H. Totsuji, K. Kono, Commensurability-dependent transport of a wigner crystal in a nanoconstriction, Physical review letters 108 (17) (2012) 176801.

[10] C. Lozano, G. Lumay, I. Zuriguel, R. Hidalgo, A. Garcimartín, Breaking arches with vibrations: the role of defects, Physical review letters 109 (6) (2012) 068001.

[11] A. Garcimartín, J. Pastor, L. Ferrer, J. Ramos, C. Martín-Gómez, I. Zuriguel, Flow and clogging of a sheep herd passing through a bottleneck, Physical Review E 91 (2) (2015) 022808.
[12] A. Garcimartín, D. R. Parisi, J. M. Pastor, C. Martín-Gómez, I. Zuriguel, Flow of pedestrians through narrow doors with different competitiveness, Journal of Statistical Mechanics: Theory and Experiment 2016 (4) (2016) 043402.
[13] J. Adrian, A. Seyfried, A. Sieben, Crowds in front of bottlenecks at entrances from the perspective of physics and social psychology, Journal of the Royal Society Interface 17 (165) (2020) 20190871.
[14] P. S. Taylor, The Hillsborough Stadium Disaster: 15 April 1989; Inquiry by the Rt Hon Lord Justice Taylor; Final Report; Presented to Parliament by the Secretary of State for the Home Department by Command of Her Majesty January 1990, HM Stationery Office, 1990.
[15] B. Krausz, C. Bauckhage, Loveparade 2010: Automatic video analysis of a crowd disaster, Computer Vision and Image Understanding 116 (3) (2012) 307–319.
[16] A. Kirchner, K. Nishinari, A. Schadschneider, Friction effects and clogging in a cellular automaton model for pedestrian dynamics, Physical review E 67 (5) (2003) 056122.
[17] D. Yanagisawa, A. Kimura, A. Tomoeda, R. Nishi, Y. Suma, K. Ohtsuka, K. Nishinari, Introduction of frictional and turning function for pedestrian outflow with an obstacle, Physical Review E 80 (3) (2009) 036110.
[18] M. Fischer, G. Jankowiak, M.-T. Wolfram, Micro-and macroscopic modeling of crowding and pushing in corridors, Networks & Heterogeneous Media 15 (3) (2020) 405.
[19] C. A. Yates, A. Parker, R. E. Baker, Incorporating pushing in exclusion-process models of cell migration, Physical Review E 91 (5) (2015) 052711.
[20] A. A. Almet, M. Pan, B. D. Hughes, K. A. Landman, When push comes to shove: exclusion processes with nonlocal consequences, Physica A: Statistical Mechanics and its Applications 437 (2015) 119–129.
[21] A. von Schantz, H. Ehtamo, Spatial game in cellular automaton evacuation model, Physical Review E 92 (5) (2015) 052805.
[22] X. Zheng, Y. Cheng, Conflict game in evacuation process: A study combining cellular automata model, Physica A: Statistical Mechanics and its Applications 390 (6) (2011) 1042–1050.
[23] D. Helbing, I. Farkas, T. Vicsek, Simulating dynamical features of escape panic, Nature 407 (6803) (2000) 487.
[24] D. Helbing, L. Buzna, A. Johansson, T. Werner, Self-organized pedestrian crowd dynamics: Experiments, simulations, and design solutions, Transportation science 39 (1) (2005) 1–24.
[25] R. C. Hidalgo, D. R. Parisi, I. Zuriguel, Simulating competitive egress of noncircular pedestrians, Physical Review E 95 (4) (2017) 042319.
[26] D. R. Parisi, C. O. Dorso, Microscopic dynamics of pedestrian evacuation, Physica A: Statistical Mechanics and its Applications 354 (2005) 606–618.
[27] D. R. Parisi, C. O. Dorso, Morphological and dynamical aspects of the room evacuation process, Physica A: Statistical Mechanics and its Applications 385 (1) (2007) 343–355.
[28] J. M. Pastor, A. Garcimartín, P. A. Gago, J. P. Peralta, C. Martín-Gómez, L. M. Ferrer, D. Maza, D. R. Parisi, L. A. Pugnaloni, I. Zuriguel, Experimental proof of faster-is-slower in systems of frictional particles flowing through constrictions, Physical Review E 92 (6) (2015) 062817.
[29] G. A. Patterson, P. I. Fierens, F. S. Jimka, P. König, A. Garcimartín, I. Zuriguel, L. A. Pugnaloni, D. R. Parisi, Clogging transition of vibration-driven vehicles passing through constrictions, Physical review letters 119 (24) (2017) 248301.
[30] Q. Xu, M. Chraibi, A. Tordeux, J. Zhang, Generalized collision-free velocity model for pedestrian dynamics, Physica A: Statistical Mechanics and its Applications (2019) 122521.
[31] A. Tordeux, M. Chraibi, A. Seyfried, Collision-free speed model for pedestrian dynamics, in: Traffic and Granular Flow'15, Springer, 2016, pp. 225–232.
[32] M. Chraibi, Validated force-based modeling of pedestrian dynamics, Vol. 13, Forschungszentrum Jülich, 2012, chapter 5.2.3.
[33] B. Hein, Agent-based modelling for crowding and queuing in front of bottlenecks, Master's thesis, University of Wuppertal, chapter 3.4.2 (2019).

[34] A. Garcimartín, I. Zuriguel, J. Pastor, C. Martín-Gómez, D. Parisi, Experimental evidence of the "faster is slower" effect, Transportation Research Procedia 2 (2014) 760–767.
[35] I. Zuriguel, A. Garcimartín, D. Maza, L. A. Pugnaloni, J. Pastor, Jamming during the discharge of granular matter from a silo, Physical Review E 71 (5) (2005) 051303.

Publication III

Info: Xu Q, Chraibi M, Seyfried A. Anticipation in a velocity-based model for pedestrian dynamics. Transportation research part C: emerging technologies, 2021, 133: 103464.

Anticipation in a velocity-based model for pedestrian dynamics

Qiancheng Xu[a,*], Mohcine Chraibi[a], Armin Seyfried[a,b]

[a]*Institute for Advanced Simulation, Forschungszentrum Jülich, 52425 Jülich, Germany*
[b]*School of Architecture and Civil Engineering, University of Wuppertal, 42119 Wuppertal, Germany*

Abstract

Lane formation in bidirectional pedestrian streams is based on a stimulus-response mechanism and strategies of navigation in a fast-changing environment. Although microscopic models that only guarantee volume exclusion can qualitatively reproduce this phenomenon, they are not sufficient for a quantitative description. To quantitatively describe this phenomenon, a minimal anticipatory collision-free velocity model is introduced. Compared to the original velocity model, the new model reduces the occurrence of gridlocks and reproduces the movement of pedestrians more realistically. For a quantitative description of the phenomenon, the definition of an order parameter is used to describe the formation of lanes at transient states and to show that the proposed model compares relatively well with experimental data. Furthermore, the model is validated by the experimental fundamental diagrams of bidirectional flows.

Keywords: anticipation, velocity-based model, pedestrian dynamics, bidirectional flow, lane formation

1. Introduction

In bidirectional flow situations, pedestrians self-organize into dynamically varying and separated lanes [1, 2, 3, 4, 5, 6]. Although the mechanisms behind this apparently organized separation of the crowd are not known for certain and in many cases may seem random, we observe that this formation leads to a reduction in collisions and thus increases the speed. Unlike with car traffic, where stable lanes are predetermined by the restrictions established by the infrastructure, in pedestrian dynamics, lanes are formed dynamically and naturally with neither external synchronization nor any prior agreement between pedestrians.

We also see lane formation in systems of inanimate particles [7, 8, 9], where models ensuring volume exclusion are sufficient to reproduce the phenomenon. Therefore, with a simple social force model considering the repulsion between particles, Helbing et al. [10]

*corresponding author

Email addresses: q.xu@fz-juelich.de (Qiancheng Xu), m.chraibi@fz-juelich.de (Mohcine Chraibi), a.seyfried@fz-juelich.de (Armin Seyfried)

qualitatively reproduced the lane formation in a corridor with periodic boundary conditions. They attributed two reasons to this phenomenon, the sideways movement, which separates agents moving in opposite directions, and the weak interaction between agents moving in the same lane, which maintains the lanes that have been formed [2].

However, pedestrians usually avoid collisions by using a stimulus-response mechanism to anticipate changes in the environment. In this context, we consider anticipation as the prediction of the path of neighboring pedestrians by perceiving their past or current movement and taking this information into account to avoid collisions. The effect of anticipation on the movement of pedestrians in bidirectional flows has been discussed and addressed in several works to date. For instance, Suma et al. [11] conducted a bidirectional flow experiment where participants are asked to use cell phones (weak anticipation) or move cautiously (excessive anticipation), to study how anticipation affects the movement of pedestrians. They found anticipation significantly affects the time it takes for pedestrians to pass through the corridor, and there is an optimal degree of anticipation to realize the minimum passing time. However, since the scale of the experiment was small, the lane formation was not analyzed quantitatively. Murakami et al. [12] performed the bidirectional experiment in a corridor with open boundary conditions, and they observed that the sideways movement of pedestrians before lane formation can be described in terms of the Lévy walk process. Therefore, the authors suggested that this sideways movement is strongly related to lane formation. Moreover, they assumed the most likely action underlying the sideways movement is anticipation. The relationship between anticipation and lane formation is further studied in [13] through a larger scale bidirectional flow experiment, where pedestrians distracted by cell phones are located at different positions to represent situations with different degrees of anticipation. They found anticipation favors the formation of lanes in bidirectional flow situations. As a part of the anticipation process, the strategy selected by pedestrians in bidirectional flow situations is also related to the formation of lanes. It was observed in experiments that preferring to follow other pedestrians moving in the same direction is a strategy to promote and stable the formation of lanes [14, 15, 16]. In addition, lane formation is also influenced by the effect of various factors, such as flow ratio [17] and heterogeneity of agents [16]. Therefore, models based solely on volume exclusion, such as the one in [10], are oversimplified and not suitable for quantitatively reproducing the lane formation in pedestrian systems.

To give a more realistic picture of the behavior of agents in the bidirectional flow simulation, the process of anticipation was considered in several recent models. Suma et al. [11] proposed an anticipation floor field cellular automata model. The transition probability of agents is calculated by considering the cells occupied by other agents currently, as well as the cells that are expected to be occupied by other agents in the future. The model was analyzed in [18] by using an order parameter, which is originally used to detect lanes of particles in a colloidal suspension [19]. Quantitative analysis showed that the model with anticipation can reproduce lane formation in higher density situations than the model without anticipation, but the model is not calibrated with experimental data. Zanlungo et al. [20] introduced anticipation into the social force model. Instead of using the current distance between agents, the repulsion force from one agent to another is calculated by using their future distance determined by the time to collision. The result of calibration shows that introducing antic-

ipation improves the model's capability to reproduce pedestrian trajectories. However, the influence of anticipation on lane formation was not studied in this work. Through statistical analysis of pedestrian trajectories, Karamouzas et al. [21] found that the time to collision is more suitable to describe the interaction energy between pedestrians than the distance between them. Based on the power law relationship between the interaction energy and the time to collision, a force-based model is developed, which can reproduce several self-organization phenomena including lane formation. However, a quantitative analysis of the lane formation was not conducted using this model. Moreover, although the model was validated with experimental data by comparing the data from [22], the calibration process did not distinguish the uni- and bidirectional flow. Bailo et al. [23] also proposed a microscopic model based on the time to collisions. The model is able to reproduce the lane formation in bidirectional flow situations, but it hasn't been tested in scenarios with different densities. Besides, the model was not calibrated with the experimental data. Seitz [24] proposed four simple cognitive heuristics to describe pedestrian behavior and investigated the possible heuristics related to lane formation. It was found that only the model with "follower" heuristics can reproduce lane formation, which corresponds to the strategy of following other agents moving in the same direction. This work shows that considering the correct cognitive heuristics is significant and maybe also enough for reproducing self-organization phenomena, which provides a direction for developing models in the future.

Besides lane formation, another phenomenon related to bidirectional flow is the jamming transition, also called gridlock, appearing at a critical density. Muramatsu et al. [25] used a lattice gas model without backstepping to study the jamming transition in bidirectional pedestrian flow with open boundary conditions. They found the jamming transition does not depend on the corridor size but it is affected by the strength of the drift (the preference to move in the desired direction) and the traffic rule adopted (such as keep to the right). Fang et al. [26] adopted a cellular automata model with backstepping and the right-hand side rule. They observed the critical density of jamming transition increases with a higher probability of backstepping. Nowak et al. [18] studied the phenomenon with the anticipation floor field cellular automata model proposed in [11]. They discovered the anticipation mechanism in the model suppresses the formation of jamming (facilitating the formation of lanes), which leads to an increase in the critical density of the jamming transition. However, the jamming transition is only observed in computer simulations.

Furthermore, the fundamental diagram is used to analyze bidirectional streams. In some early studies summarized in [15], it is believed that there is no clear or only a small difference between uni- and bidirectional flows. Helbing et al. [27] concluded that bidirectional flows are more efficient than unidirectional flows. The possible reason behind this is better coordination between people in bidirectional situations (lane formation). Kretz et al. [28] also found that pedestrians use space more efficiently in bidirectional situations. Subsequently, Zhang et al. [15] carried out both uni- and bidirectional flow experiments under laboratory conditions. A clear difference between the fundamental diagrams of uni- and bidirectional flows is observed when the density is higher than $1.0\,\mathrm{m}^{-2}$. The specific flow reaches a peak with increasing density in the unidirectional flow, whereas a plateau is formed in the bidirectional flow. However, there are no experimental data for densities higher than

$4.5\,\mathrm{m}^{-2}$.

In order to reproduce bidirectional flow quantitatively, the anticipation velocity model (AVM) for pedestrian dynamics is proposed. The action anticipating changes of neighboring pedestrians' positions and the strategy of following others are covered in this model. The new model is compared to two similar models from the literature, the collision-free speed model [29] and generalized collision-free velocity model [30], and we highlight the reasons behind the difference. Moreover, we use the AVM to study the jamming transition, lane formation, and fundamental diagrams in bidirectional flow scenarios. In the following section, the AVM is described.

2. Definition of the anticipation velocity model

In this model, an agent is represented as a disk with a constant radius r. The position and velocity of pedestrian i are denoted by $\vec{x}_i$ and $\vec{v}_i$, respectively, where $\vec{v}_i = \dot{\vec{x}}_i$. Furthermore, $\vec{v}_i = \vec{e}_i \cdot v_i$, where $\vec{e}_i$ and v_i denote the direction of movement and the speed of agent i, respectively. Both variables are modeled differently as explained in the following subsections.

2.1. Submodel for operational navigation

The direction of movement of agent i is determined by its desired direction which is a unit vector denoted by $\vec{e}_i^{\,0}$ pointing towards its target. The determination of the target follows various tactical strategies, which is not the subject of the present study. For operational navigation to avoid collisions and obstructions, in the presence of other agents, the direction of i will deviate from its desired direction $\vec{e}_i^{\,0}$. To consider anticipation, the process can be divided into the following parts: a. perception of the actual situation, b. prediction of a future situation, and c. selection of a strategy leading to an action.

a. Perception of the actual situation: To consider restrictions using visual perception, it is assumed that only agents located in the union of two half-planes, where i is moving or intends to move, affect its direction. The set containing all agents who have an impact on i's direction of movement is

$$N_i(t) = \left\{ j,\ \vec{e}_i(t) \cdot \vec{e}_{i,j}(t) > 0 \text{ or } \vec{e}_i^{\,0}(t) \cdot \vec{e}_{i,j}(t) > 0 \right\}, \tag{1}$$

where $\vec{e}_{i,j}$ denotes the unit vector from i to j.

b. Prediction of a future situation: To consider the prediction, it is assumed that the strength of j's impact on i is a function of the predicted distance between these two agents at a particular time point. Given a time constant t^{a}, which can be interpreted as the prediction time, the predicted distance is defined as

$$s_{i,j}^{\mathrm{a}}(t + t^{\mathrm{a}}) = \max \left\{ 2r,\ \left(\vec{x}_j^{\,\mathrm{a}}(t + t^{\mathrm{a}}) - \vec{x}_i^{\,\mathrm{a}}(t + t^{\mathrm{a}}) \right) \cdot \vec{e}_{i,j}(t) \right\}, \tag{2}$$

where $\vec{x}_i^{\,\mathrm{a}}(t + t^{\mathrm{a}}) = \vec{x}_i(t) + \vec{v}_i(t) \cdot t^{\mathrm{a}}$. See Figure 1.

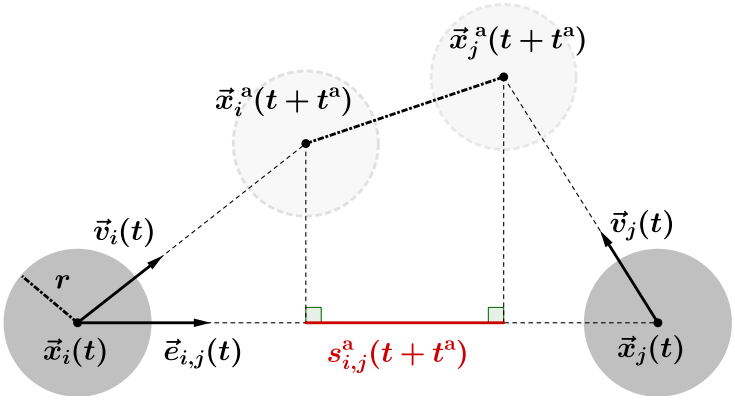

Figure 1: An example of $s^{\mathrm{a}}_{i,j}(t+t^{\mathrm{a}})$, the predicted distance between agents i ($\vec{x}_i$, $\vec{v}_i$) and j ($\vec{x}_j$, $\vec{v}_j$). When pedestrians move towards each other their predicted distance is smaller than the actual distance.

c. Selection of a strategy leading to an action: After the introduction of the predicted distance in Eq. 2, the strength of the impact from agent j on the direction of movement of agent i is defined as

$$R_{i,j}(t) = \alpha_{i,j}(t) \cdot \exp\left(\frac{2r - s^{\mathrm{a}}_{i,j}(t+t^{\mathrm{a}})}{D}\right), \tag{3}$$

where $D > 0$ is a constant parameter used to calibrate the range of the impact from neighbors and $\alpha_{i,j}$ is a directional dependency used to vary the strength of impact from different neighbors (see Eq. 4).

$$\alpha_{i,j}(t) = k\Big(1 + \frac{1 - \vec{e}_i^{\,0}(t) \cdot \vec{e}_j(t)}{2}\Big),\ k > 0, \tag{4}$$

where $\alpha_{i,j}$ is minimal (k) when both vectors $\vec{e}_i^{\,0}$ and $\vec{e}_j$ are aligned and is maximum ($2k$) when they are anti-aligned, which means that agents influence each other's direction strongly in bidirectional scenarios. Here, $\alpha_{i,j}$ means agents have a high tendency to follow the agents who move in the same direction. When this strategy is used, the probability of further conflicts is reduced.

The direction of the impact from agent j on i's direction of the movement is defined as

$$\vec{n}_{i,j}(t) = -\operatorname{sign}\left(\vec{e}^{\,\mathrm{a}}_{i,j}(t+t^{\mathrm{a}}) \cdot \vec{e}_i^{\,0\perp}(t)\right) \cdot \vec{e}_i^{\,0\perp}(t), \tag{5}$$

where $\vec{e}^{\,\mathrm{a}}_{i,j}(t+t^{\mathrm{a}}) = \vec{x}_j^{\,\mathrm{a}}(t+t^{\mathrm{a}}) - \vec{x}_i(t)$. The direction of $\vec{n}_{i,j}$ depends on the predicted position of agent j after a period of time t^{a}. Note that when this predicted position is aligned with

the desired direction of i, the direction of $\vec{n}_{i,j}(t)$ in Eq. 5 is chosen randomly as $\vec{e}_i^{\,0\perp}$ or $-\vec{e}_i^{\,0\perp}$. See Figure 2. This rule prevents agents from moving in the opposite direction to the desired direction.

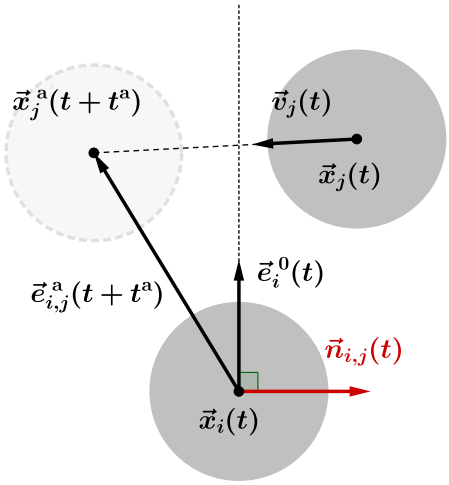

Figure 2: The direction of the impact from j on the direction of movement of i ($\vec{n}_{i,j}$) according to Eq. 5.

Finally, Eq. 3 and Eq. 5 yield the optimal direction of agent i as

$$\vec{e}_i^{\,d}(t) = u\left(\vec{e}_i^{\,0}(t) + \sum_{j\in N_i(t)} R_{j,i}(t)\cdot\vec{n}_{j,i}(t)\right), \tag{6}$$

where u is a normalization constant such that $\|\vec{e}_i^{\,d}\| = 1$. Then, the direction of movement of agent i is updated as

$$\frac{d\vec{e}_i(t)}{dt} = \frac{\vec{e}_i^{\,d}(t) - \vec{e}_i(t)}{\tau}, \tag{7}$$

where τ is a relaxation parameter adjusting the rate of the turning process from the current direction $\vec{e}_i$ to the optimal direction $\vec{e}_i^{\,d}$.

2.2. Submodel for the speed

After obtaining the new direction of the movement according to Eq. 7, the set of neighbors that are imminently colliding with i is defined as

$$J_i = \left\{j,\ \vec{e}_i\cdot\vec{e}_{i,j} \geq 0 \text{ and } \left|\vec{e}_i^{\,\perp}\cdot\vec{e}_{i,j}\right| \leq \frac{2r}{s_{i,j}}\right\}, \tag{8}$$

where $s_{i,j}$ is the current distance between i and j. Therefore, the maximum distance that agent i can move in the direction without overlapping other agents is

$$s_i = \min_{j \in J_i} s_{i,j} - 2r. \tag{9}$$

Finally, the speed of agent i in the new direction is

$$v_i = \min \left\{ v_i^0, \ \max \left\{ 0, \frac{s_i}{T} \right\} \right\}, \tag{10}$$

where v_i^0 is the free speed of agent i, and $T > 0$ is the slope of the speed-headway relationship. The speed submodel used here is the same as in the generalized collision-free velocity model [30].

3. Test with two interacting agents

Binary interaction scenarios with the collision-free speed model (CSM) [29], the generalized collision-free velocity model (GCVM) [30], and the AVM, respectively, are studied to assess the models' ability. The three models adopt the same speed submodel but different submodels for operational navigation. In both the CSM and the GCVM, the strength of the effect from agent j on agent i's direction of movement is a function of the distance between the two agents. As for the direction of this effect, in the CSM it is from j to i, while in the GCVM it is obtained with Eq. 5 ($t_a = 0\,\mathrm{s}$). The parameters of these models are summarized in Table 1.

	r [m]	k Eq. 4	D [m] Eq. 3	T [s] Eq.10	Δt [s]	τ [s] Eq. 7	t^{a} [s]
CSM	0.18	3	0.1	1.06	0.05	\	\
GCVM						0.3	\
AVM							1

Table 1: The parameters of the models in binary interaction simulations. Here, r is the radius of agents, Δt is the time step size, and t_a is the prediction time. The simulation in the present study is conducted using the Euler scheme. Parameter values of the CSM and the GCVM are obtained from [30]. The reason for $t^{\mathrm{a}} = 1\,\mathrm{s}$ in the AVM is discussed in Appendix A.

The first scenario is that agent i walks behind agent j, which is shown in Figure 3(a). The agents have the same desired direction, but the free speed of agent i is higher than that of agent j. The trajectory of the agents in the first scenario is shown in Figure 3(b). In the simulation using the GCVM and the AVM, agent i overtakes agent j by adjusting the direction of movement. In the CSM, however, no overtaking is observed. Moreover, compared to the GCVM, the overtaking in the AVM occurs earlier.

(a)

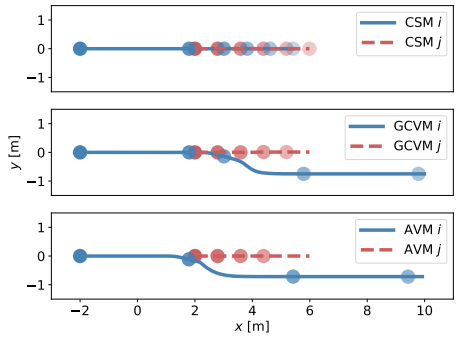

(b)

Figure 3: (a): Scenario 1, agent i walks behind agent j. The two agents have the same desired direction but the free speed of agent i is higher than that of agent j. (b): The trajectory of agents. The position of agents at different times is represented by the disk, and the transparency of these disks increases with increasing time. When the AVM is used, overtaking starts earlier.

The second scenario, more relevant to bidirectional flow, depicts two agents having the same free speed with opposite desired directions (see Figure 4(a)). The trajectory of the agents in the second scenario is shown in Figure 4(b). Here again, it is observed that with the GCVM and the AVM, agents i and j both change their paths to avoid the imminent conflict, although this maneuver occurs earlier in the AVM than in the GCVM. In the CSM, the two agents are unable to pass each other.

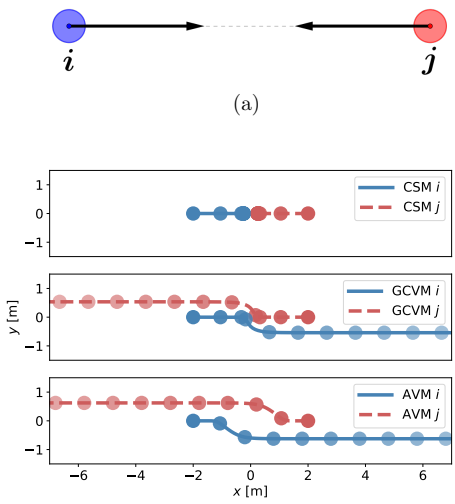

(a)

(b)

Figure 4: (a): Scenario 2, agent i and agent j move toward each other. The two agents have the same free speed but opposite desired directions. (b): The trajectory of agents. The position of agents at different times is represented by the disk, and the transparency of these disks increases with increasing time. Evasive movement starts earlier when the AVM is used.

In the last scenario (see Figure 5(a)), the paths cross at right angles. The free speeds of the two agents are very similar but not quite equal to avoid the symmetric movement of the two agents. The trajectory of the agents in the last scenario is shown in Figure 5(b). When the AVM is used, the agents deviate slightly from the desired direction to the target and avoid collision.

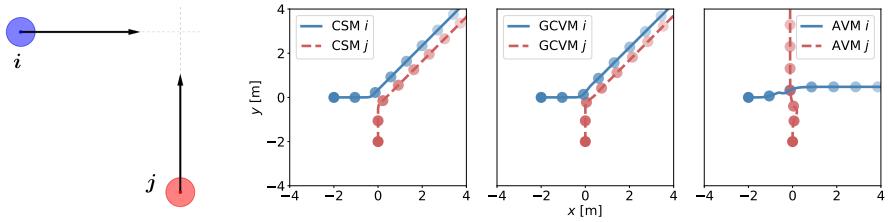

(a)

(b)

Figure 5: (a): Scenario 3, agent i and agent j move across each other's path. The free speeds of the two agents are very close but not equal and their desired directions are perpendicular to each other. (b): The trajectory of agents. The position of agents at different times is represented by the disk, and the transparency of these disks increases with increasing time.

In all cases, it can be concluded that, without introducing noise terms into the models, the movement of agents in the simulation using the AVM is closer to reality than using the CSM and the GCVM, where agents have difficulty overtaking or performing realistic evasive movements.

4. Bidirectional flow simulations with periodic boundary conditions

4.1. States of bidirectional flow

The bidirectional flow simulation is performed for a corridor shown in Figure 6. The width of the corridor is 4 m, which is the same as the experimental setting in [31]. Simulations were also performed in corridors with different widths, and the result is discussed in Appendix B. For the initial conditions of a simulation, the gray waiting areas are separated into grids with a specific size, then the agents are randomly distributed in these grids without overlapping. The same number of agents were placed at the left and the right sides of the corridor. After the simulation starts, agents in the left waiting area move toward the right, and vice versa. Different initial conditions of agents' desired direction $\vec{e}^{\,0}$ were compared before performing the simulations in this section. Since no significant difference could be observed between the simulation results of ordered and unordered initial conditions, agents' desired direction $\vec{e}^{\,0}$ were set parallel to the horizontal walls of the corridor. The free speeds of agents are normally distributed $N \sim (1.55, 0.18^2)\ \mathrm{m\,s^{-1}}$ according to [15]. The effect of the free speed distribution on the simulation results is studied in Appendix C. All simulations presented in this section are performed with periodic boundary conditions in the walking direction of the agents. Each simulation lasts 400 s, which gives a good compromise between the running time of the simulations and the time needed to develop lane formation.

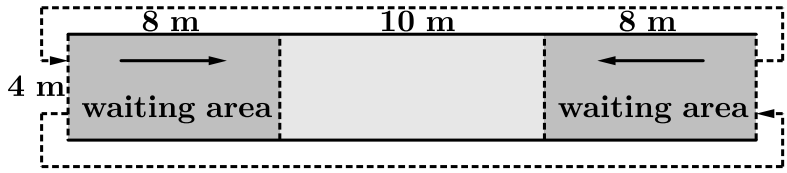

Figure 6: The corridor for bidirectional flow simulations. Dashed arrows outside the corridor represent periodic boundary conditions.

Based on the approach used in [18], the patterns emerging in our simulations are classified into four different states, which are local jamming, global jamming, lane formation, and disorder (see Figure 7). Local jamming and global jamming are both categorized as jamming states, whereas lane formation and disorder are grouped into the moving states. If the average speed of an agent over 10 s is less than $v^0/100$, it is indicated as a static agent. Using this definition, a simulation is considered to be in the jamming state when the number

of static agents in the simulation is equal to or greater than 2 ($N_{\text{static}} \geq 2$); otherwise, the simulation is considered to be in a moving state. Note, although 400 s is usually long enough to reach the steady state of the simulation, the jamming or moving state of a simulation still has a certain probability of being transient. The number of static agents in the four simulations in Figure 7 are 29 (local jamming), 80 (global jamming), 0 (lane formation), and 0 (disorder), respectively.

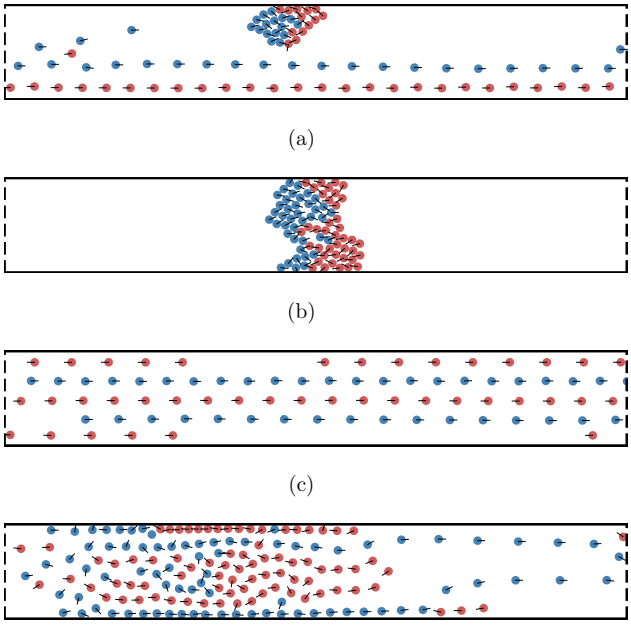

Figure 7: Different states of bidirectional flow simulations with periodic boundary conditions. (a): Local jamming. (b): Global jamming. (c): Lane formation. (d): Disorder.

In this section (Figures 8, 9, and 10(a)), each simulation is performed for $M = 30$ times with different distributions of agents in the waiting areas, then the jamming probability P_{jam} is calculated as

$$P_{\text{jam}} = S_{\text{jam}}/M, \tag{11}$$

where S_{jam} is the number of simulations leading to a jamming state.

To further distinguish between the states of lane formation and disorder, the quantity Φ defined in [32] is introduced as

$$\Phi = \frac{1}{N}\sum_{i=1}^{N}\phi_i, \tag{12}$$

with

$$\phi_i = \frac{(N_i^{\text{same}} - N_i^{\text{diff}})^2}{(N_i^{\text{same}} + N_i^{\text{diff}})^2} \in [0, 1], \tag{13}$$

where N is the total number of agents in the corridor, N_i^{same} is the set of all agents initially in the same waiting area as agent i and currently moving in i's lane, and N_i^{diff} is the set of all agents initially in a different waiting area to agent i and currently moving in i's lane. The expressions of N_i^{same} and N_i^{diff} are

$$N_i^{\text{same}} = \Big\{ j, |y_j - y_i| < 3r/2 \text{ and } \vec{e}_i^{\,0} \cdot \vec{e}_j^{\,0} > 0 \Big\}, \tag{14}$$

$$N_i^{\text{diff}} = \Big\{ j, |y_j - y_i| < 3r/2 \text{ and } \vec{e}_i^{\,0} \cdot \vec{e}_j^{\,0} < 0 \Big\}, \tag{15}$$

where y_i is the vertical position of agent i.

Φ is an indicator of how pronounced lanes are formed in a simulation. Knowing that an order parameter is only measured at steady states, Φ is used here to compare models with respect to their performance of describing the transient state of lane formation. The values of Φ in the four simulations in Figure 7 are 0.66 (local jamming), 0.18 (global jamming), 1.00 (lane formation), and 0.31 (disorder), respectively. Nevertheless, there is no specific boundary to clearly distinguish between the states of lane formation and disorder.

4.2. Jamming transition

To study the jamming transition in bidirectional flow, simulations are performed with the AVM, the CSM, and the GCVM, respectively. The parameters of models are shown in Table 1. For each model, simulations are performed with different numbers of agents ranging from 20 to 200 (10 to 100 in each waiting area). The global density of agents in the corridor, ρ_{global}, is defined as the number of agents divided by the area of the whole corridor (including the waiting area). The relationship between P_{jam} and ρ_{global} for different models is shown in Figure 8. With an increase in ρ_{global}, a transition from moving states ($P_{\text{jam}} = 0$) to jamming states ($P_{\text{jam}} = 1$) is observed in the simulation of all three models. However, with the AVM, the transition occurs at a higher value of ρ_{global} compared to the other two models, which indicates the model's ability to reproduce lane formation even at higher density values.

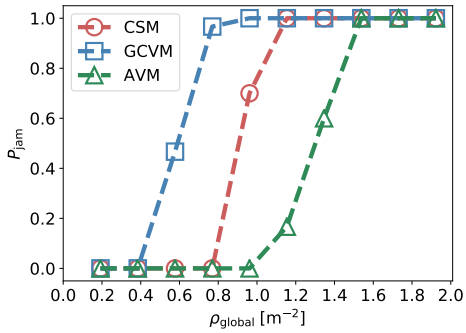

Figure 8: The relationship between P_{jam} and ρ_{global} for different models.

4.3. Parametric study

Parameters k and D are used to calibrate the strength and range of the impact from neighbors to the direction of movement in all three models (the CSM, the GCVM, and the AVM). Although the definitions vary slightly between the three models, higher values of k and larger D always led to agents being more stimulated to deviate from their desired directions. In this section, the effect of k and D on the jamming probability P_{jam} is studied for each of the three models.

For each model, simulations are performed with different values of k (1, 2, 3, 4, 5, and 6) and different values of D (0.01, 0.02, 0.05, 0.10, 0.20 m). To ensure simulations with jamming and moving states, the global density of agents ρ_{global} is set close to the critical density between the moving state and the jamming state (see Figure 8). The number of agents is 100 ($\rho_{\text{global}} \approx 0.96\,\text{m}^{-2}$) for the simulations using the CSM, 60 ($\rho_{\text{global}} \approx 0.58\,\text{m}^{-2}$) for the simulations using the GCVM, and 140 ($\rho_{\text{global}} \approx 1.35\,\text{m}^{-2}$) for the simulations using the AVM. Other parameters of the three models are given in Table 1.

The jamming probability of the simulation using the CSM and the GCVM is shown in Figures 9(a) and 9(b), respectively. The reason of the non-monotonic trend in Figure 9(b) when $D = 0.2\,\text{m}$ is that excessive influence from neighbors will cause agents to be more dispersed in the vertical direction of the corridor. When two groups of agents meet, more dispersed distribution leads to the formation of rows that exceed the maximum number of rows limited by the width of the corridor and ultimately results in the occurrence of jamming. Except for this non-monotonic trend, the value of P_{jam} in the simulation using the CSM and the GCVM decreases with increasing k and D, which means that the jamming probability decreases with increasing impact from neighbors on the direction of movement. However, the value of P_{jam} in the simulation using the AVM shows a different trend (see Figure 9(c)). When the value of D is small (0.01, 0.02, and 0.05 m), the value of P_{jam} changes slightly. With a larger value of D (0.1 m), the value of P_{jam} increases with increasing k. Note that when the value of D is large enough (0.2 m), the value of P_{jam} is close to 1 and the effect of

k is marginal again. Generally, in the AVM, with increasing impact from neighbors on the direction of movement, the jamming probability increases.

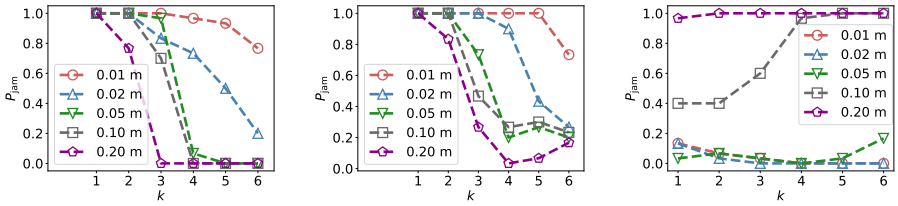

Figure 9: The relationship between P_{jam} and k for different values of D. The mean value of D can be read in the legend. (a): CSM. (b): GCVM. (c): AVM.

On the basis of all combinations of k and D in Figure 9, the set of parameters that leads to the minimal P_{jam} is identified for each model and shown in Table 2.

	CSM	GCVM	AVM
k	6	4	6
D [m]	0.2	0.2	0.01

Table 2: The set of k and D that leads to the minimal P_{jam} in Figure 9.

4.4. Lane formation

The values of k and D from Table 2, together with other parameter values from Table 1, are used for a comparative study of lane formation in the three models. For each model, simulations are performed with different numbers of agents from 20 to 300 (ρ_{global} from 0.19 to 2.8 m^{-2}). The relationship between P_{jam} and ρ_{global} for different models is shown in Figure 10(a). Compared to Figure 8, the jamming probability P_{jam} is significantly reduced in the simulation using the CSM and the AVM by adopting the optimal values of k and D. The GCVM, however, does not show any improvement.

Furthermore, to gain a better insights into the lane formation phenomenon, the average value of Φ in the last 10 s of each simulation is calculated. First, simulations are classified as "jamming" or "moving" according to their states. Then, the mean value and standard deviation of Φ in the simulations with the moving state are calculated for each model and each density. The variations in Φ with respect to the global densities are shown in Figure 10(b). For all the three models, when $\rho_{\text{global}} < 1.0\,\text{m}^{-2}$, the values of Φ in the moving states are always close to 1, which indicates that, in this case, lanes are always formed. When $\rho_{\text{global}} > 1.0\,\text{m}^{-2}$, for the moving states, the value of Φ is unavailable in the GCVM, and the values in the AVM are significantly higher than in the CSM. This indicates that, although both are in the moving states, the AVM reproduces lane formation much better.

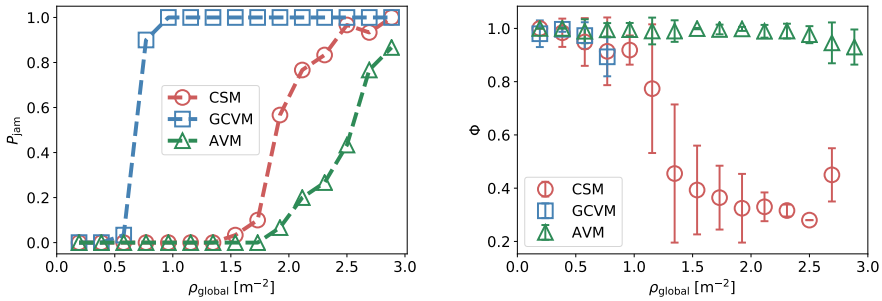

(a) (b)

Figure 10: Using the values of k and D from Table 2. (a): The relationship between P_{jam} and ρ for different models. (b): The mean value and standard deviation of Φ in the simulations with the moving state, for each model and each density.

The quantity Φ is a reliable indicator of the formation of lanes in a simulation. Since it changes in time, an artificial threshold of 0.8 for Φ is introduced to describe how fast lanes are developed. The time when the value of Φ first exceeds the threshold is denoted by t^{lane}. The mean value and standard deviation of t^{lane} in simulations with the moving state are calculated for each model and each density. See Figure 11(a). For all three models, the mean value of t^{lane} increases with increasing ρ_{global}, which is to be expected. Moreover, lanes form much faster in the simulation using the AVM than with the other models.

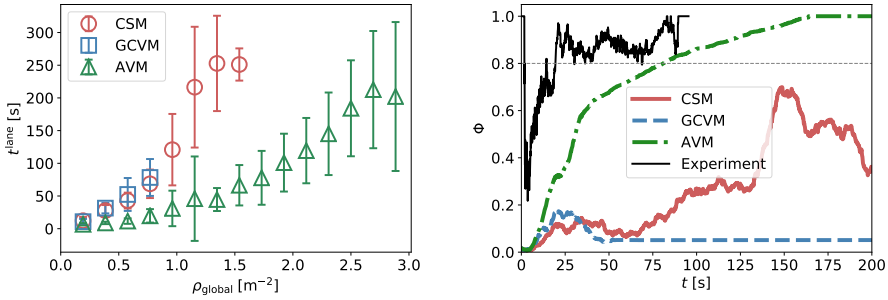

(a) (b)

Figure 11: (a) The mean value and standard deviation of t^{lane} in the simulations with the moving state, for each model and each density. (b):The relationship between the value of Φ and the simulation time t of three simulations using different models (ρ_{global}=1.92 m^{-2}) and an experiment [31].

Three single simulations using different models are further compared with bidirectional flow experiment [31]. Figure 11(b) shows the time series of Φ in the first 200 s. Here, Φ

continues to increase to 1 and then remains stable in the simulation using the AVM, while it keeps fluctuating below 0.7 for the CSM. For the GCVM, the quantity Φ is stable at a low value, indicating a lack of any lane formation. The possible reason for the difference between the AVM and the CSM here is that the moving state of the AVM can be attributed to the strategy of following, while the moving state of the CSM is due to agents pushing each other aside. This behavior is also reflected in the snapshots of the three simulations at different times, shown in Figure 12. The experiment compared in Figure 11(b) is performed in a 4 m corridor under open boundary conditions and it records the trajectories of pedestrians in the 10 m length measurement area. The steady density of pedestrians in the measurement area is around $2\,\mathrm{m}^{-2}$. The value Φ for pedestrians in the measurement area is calculated and the lane formation occurs even earlier in the experiment than in the simulation. It could not be excluded that, in the experiment, the formation of lanes starts even outside of the measurement area. Thus, the comparability of experiments and simulations is limited. However, a comparison of the time series of Φ, in particular, the increase in Φ over time, provides a rough estimate whether the time in which the system switches from an unordered state without lanes to an ordered state with lanes has the same order of magnitude.

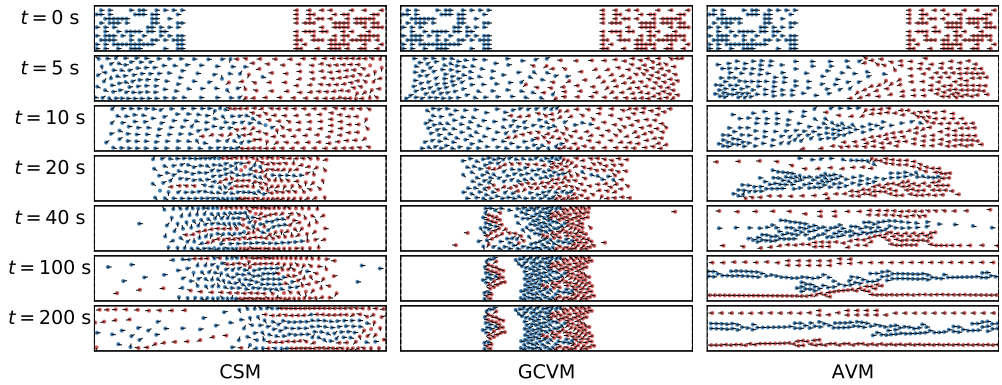

Figure 12: The snapshot of the simulations using the CSM, the GCVM, and the AVM (from left to right). From top to bottom: $t = 0$, 5, 10, 20, 40, 100, and 200 s.

5. Validation of the AVM using the fundamental diagram

After the AVM was compared to two other models and showed its ability to produce lane formation reasonably, the model was then validated with respect to the fundamental diagram. For this purpose, the fundamental diagram (FD) obtained from bidirectional flow experiments in a 3.6 m corridor [15] and a 4.0 m corridor [31] was used to calibrate the parameters of the AVM. Bidirectional flow simulations with open boundary conditions were performed in a corridor shown in Figure 6. The same number of agents were placed at the left and the right side of the corridor. The number of agents is varied in different simulations to realize different local densities in the corridor. Agents in the left waiting area move toward

the right, and vice versa. The simulation ends when all agents leave the corridor. The calibration was performed manually. First, simulations were performed with different sets of parameters, and the resulting fundamental diagrams were compared with the experimental data. According to this comparison, the parameters were adjusted repeatedly until the simulated fundamental diagram fits the experimental data. The final set of parameters is listed in Table 3.

Flow types	v^0 [m s^{-1}]	r [m]	k	D [m]	T [s]	τ [s]	t^a [s]
Bidirectional	$N \sim (1.55, 0.18^2)$	0.18	6	0.01	0.6	0.3	0.75
Unidirectional					0.5		

Table 3: Validated parameters of the AVM.

The FD obtained by simulations and experiments are compared in Figure 13. The speed v, the local density ρ_{local}, and the specific flow $J_s = \rho_{\text{local}} \cdot v$ in both the simulation and the experiment are measured from trajectories of pedestrians or agents using the same method. The measurement method is proposed in [31], where the local density is measured using the Voronoi method and the measured speed is the projection of the real speed in the horizontal direction. The FD obtained from the simulation is consistent with the FD obtained from the experiment.

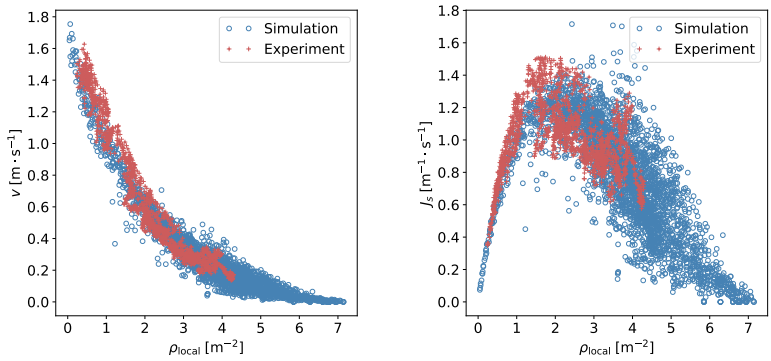

(a) (b)

Figure 13: The fundamental diagram of bidirectional flow from the experiment and the simulation. (a) Density-velocity. (b) Density-specific flow.

As well as the quantitative comparison of the FD, the process of lane formation in the simulation is qualitatively compared to the experiment (see Figure 14). The trajectory snapshots of a simulation and a bidirectional flow experiment in a 4 m wide corridor are compared. Note that the trajectories of the experiment are superimposed by the swaying of the head movement due to the bipedal movement in steps, which is not covered by the

model. Moreover, the course of lane formation in the simulation is similar in time to the experiment.

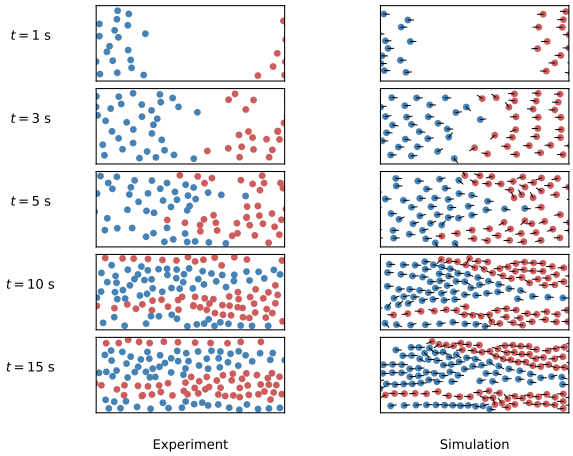

Figure 14: The trajectory snapshots of an experiment (left) and a simulation (right). Top to bottom: $t =$ 1, 3, 5, 10, and 15 s.

The first 50 s trajectories of agents in the simulation and pedestrians in the experiment are shown in Figure 15. Four lanes can be observed in both the experiment and the simulation.

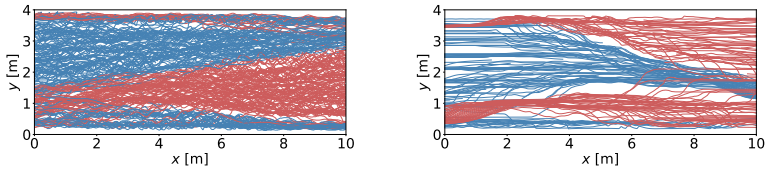

Figure 15: The trajectories of pedestrians (agents) in the first 50 s. (a) Experiment. (b) Simulation.

The fundamental diagram of the unidirectional flow was then reproduced with the calibrated parameters listed in Table 3. The value of T is lower from unidirectional flow than bidirectional flow, which means pedestrians keep a larger distance with the person in front in bidirectional flow than in unidirectional flow. It is assumed to be caused by pedestrians move more cautiously in the bidirectional flow. The FD of uni- and bidirectional flow obtained by simulations with the AVM are shown in Figure 16(a). The specific flow reaches a peak with increasing local density ρ_{local} in the unidirectional flow simulation, where a plateau is formed in the bidirectional flow simulation. The difference is in line with the observation

in the experiment [15]. See Figure 16(b). A similar result was also reproduced by using an improved cellular automata model in [33]. Note that the experimental data for higher densities than $4.5\,\mathrm{m}^{-2}$ cannot be reached. Data from simulations and experiments show different scatter. The larger scatter at the congested regime indicates that real pedestrians steer more smoothly at high densities than the agents modeled by the AVM. One possible reason for this discrepancy is that the agents in the model always jostle to move further and are apparently unaware of the strategy of simply standing still.

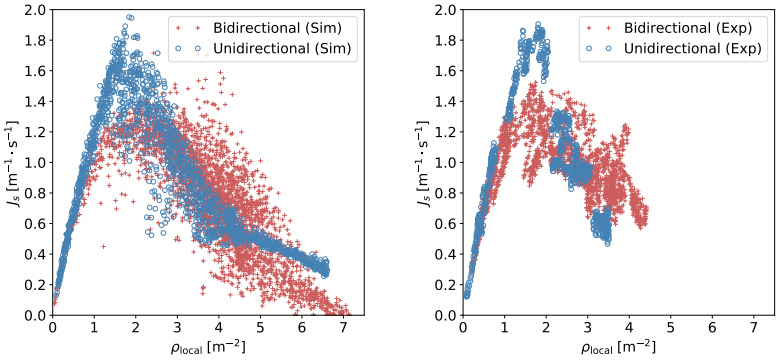

(a) (b)

Figure 16: The fundamental diagram of uni- and bidirectional flow. (a) The relation between the local density and the specific flow in the simulation. (b) The relation between the local density and the specific flow in the experiment.

6. Conclusion

A new velocity model is proposed to take into consideration anticipation of pedestrians. For this, the process of anticipation is divided into three parts: perception of the actual situation, prediction of a future situation and selection of a strategy leading to an action.

First, the AVM is compared to the two other velocity-based models (the generalized collision-free velocity model (GCVM), and the collision-free speed model (CSM)) in binary interaction scenarios. Even in these simplified situations, the simulated trajectories of agents show that the AVM can reproduce the movement of pedestrians more realistically than the other two models.

In a second step, these models are compared in the bidirectional flow scenario with periodic boundary conditions. Simulations are classified as jamming state or moving state, according to the number of static, or blocked, agents in the simulation. Compared to the other two models, the critical density between the moving states and jamming states is shifted to higher values using the AVM. This indicates that the AVM prevents imminent collisions better than the other models.

The influence of the parameters describing the effect from neighbors in the three models is studied in bidirectional flow scenarios. Only for the AVM does an increase in the impact from neighbors in the direction of movement lead to an increase in the jamming probability. The opposite occurs when the CSM and the GCVM are used. The bidirectional flow simulation with periodic boundary conditions is then performed using the set of parameters that leads to the minimum jamming probability. The jamming probability is significantly reduced in the simulation using the CSM and the AVM by adopting the new parameters but there is little change in the simulation using the GCVM.

After this, the quantity Φ, describing the degree of order given by lanes, is adopted to analyze the formation of lanes quantitatively. In line with experimental results of high-density situations, the AVM leads to the formation of lanes much faster than the CSM. One possible reason for this difference here is that the moving state of the AVM can be attributed to the strategy of following, while the moving state of the CSM could be associated with agents pushing each other aside.

Finally, the AVM is validated using the fundamental diagram (FD). After calibration based on the bidirectional FD, the FD for unidirectional flow is correctly reproduced by simulation using the AVM. The difference between the FD of uni- and bidirectional flow is also well reproduced. Moreover, the course of lane formation in time and the shape of the formed lanes in the simulations with the AVM are similar to those in the experiments.

Additional analyses using the AVM in the bidirectional flow simulation with periodic boundary conditions are conducted. In Appendix A, the decisive factors leading to improved performance in the simulation using the AVM are studied. The result shows that the prediction of the future situation and the strategy of following are both significant for reducing the jamming probability, and there is an optimal prediction time to realize the minimum jamming probability. In Appendix B, simulations are performed in corridors with different widths. When the corridor is wider than 2 m, the effect of the corridor width on the jamming probability is insignificant. In addition, the heterogeneity of agents' free speed is studied in Appendix C, where the jamming probability decreases with increasing heterogeneity of the free speed of agents.

Acknowledgments

The authors are grateful to the HGF for providing funding within the knowledge transfer project under Grant No. WT-0105. Qiancheng Xu wishes to express his thanks for the funding support received from the China Scholarship Council (Grant No. 201706060186). We would also like to thank Antoine Tordeux for his very useful comments and consultations.

Appendix A. Decisive factors in the anticipation velocity model

Using the AVM reduces the jamming probability and favors the formation of lanes in bidirectional flow simulations. The possible causes for the improvement are the prediction time t^{a}, and the dynamic $\alpha_{i,j}$ reflecting pedestrians' preference to follow others moving in the same direction. To identify the decisive factor of this improvement, simulations are

performed in periodic boundary conditions with dynamic $\alpha_{i,j}$ and constant $\alpha_{i,j}$ ($\alpha_{i,j} = k$), respectively. For each case, different values of t^{a} (0, 0.2, 0.5, 1.0, 1.5, and 2 s) are adopted. The simulation scenario is the corridor shown in Figure 6. The free speeds of agents are normally distributed $N \sim (1.55, 0.18^2)$ m s^{-1}. The number of agents in each simulation is 140 ($\rho \approx 1.35\,\mathrm{m}^{-2}$). This corresponds to the global density where the transition from moving states ($P_{\mathrm{jam}} = 0$) to jamming states ($P_{\mathrm{jam}} = 1$) occurs in the simulation using the AVM. The other parameters of the AVM are shown in Table 1.

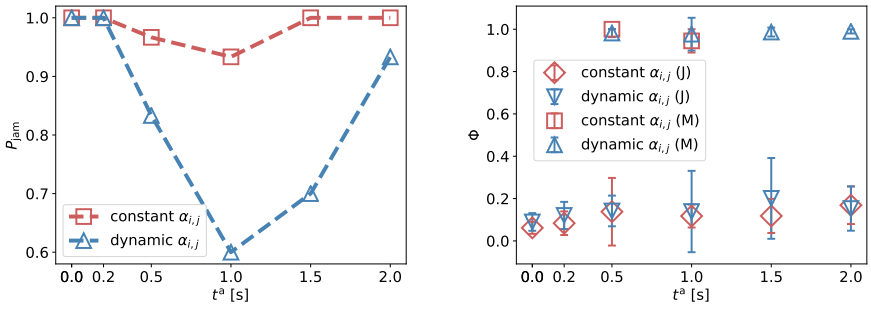

Figure A.17: (a): The relationship between the jamming probability P_{jam} and the prediction time t^{a} for dynamic and constant $\alpha_{i,j}$. (b): Mean value and standard deviation of Φ in the simulation with jamming (J) and moving (M) states for each value of t^{a} and each $\alpha_{i,j}$ (dynamic and constant).

The relationship between the jamming probability P_{jam} and the prediction time t^{a} for dynamic and constant $\alpha_{i,j}$ is shown in Figure 17(a). The same tendency of P_{jam} is observed in the simulation with dynamic and constant $\alpha_{i,j}$. As t^{a} increases, P_{jam} decreases until t^{a} reaches a specific value, then it increases. Moreover, the effect of the prediction time t^{a} on the jamming probability P_{jam} is more significant in the simulation with dynamic $\alpha_{i,j}$ than with constant $\alpha_{i,j}$.

The mean value and standard deviation of Φ in the simulation with jamming and moving states are calculated for each t^{a} and each $\alpha_{i,j}$ (dynamic and constant). See Figure 17(b). The values of Φ are close to 1 in the moving state and less than 0.3 in the jamming state. Neither the prediction time t^{a} nor the coefficient $\alpha_{i,j}$ affects the formation of lanes in the simulation with the moving state.

In conclusion, the prediction time t^{a} and the dynamic $\alpha_{i,j}$ both contribute to reducing the jamming probability in the bidirectional flow simulation. Moreover, a longer prediction time does not mean a lower jamming probability. An appropriate prediction time t^{a} can reduce the jamming probability. A similar conclusion also drawn from [11] is that there is an optimal strength of anticipation to realize the smoothest counterflow.

Appendix B. Width of the corridor

A transition from moving states ($P_{\text{jam}} = 0$) to jamming states ($P_{\text{jam}} = 1$) occurs with an increase of ρ_{global} (the global density of agents) in the bidirectional flow simulations. In this appendix, the effect of the corridor width on this transition is studied. Six corridors with different widths (1, 2, 3, 4, 5, and 6 m) are simulated. Apart from the width, these corridors are identical to the corridor shown in Figure 6. For each corridor, simulations are performed in periodic boundary conditions with different values of ρ_{global} (0.31, 0.62, 0.92, 1,23, 1.54, or 1.85 m^{-2}). The simulation is performed with the AVM using the parameters in Table 1. The free speeds of agents are normally distributed $N \sim (1.55, 0.18^2)$ $\text{m}\,\text{s}^{-1}$.

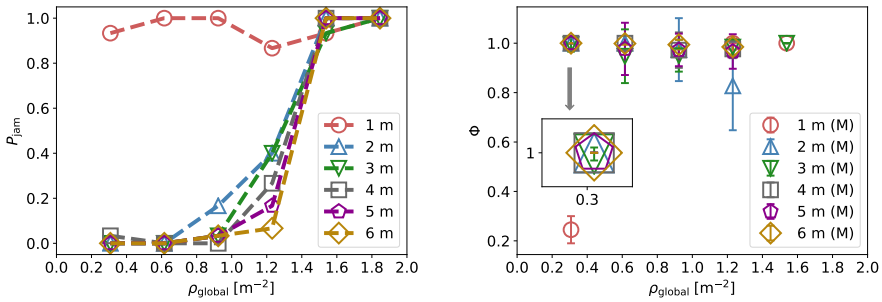

(a) (b)

Figure B.18: The numbers in the legend give the width of the corridor. (a): Relationship between the jamming probability P_{jam} and the global density ρ_{global} for corridors with different widths. (b): Mean value and standard deviation of Φ in the simulation with the moving state (M), for each corridor and each global density ρ_{global}.

The relationship between the jamming probability P_{jam} and the global density ρ_{global} for corridors with different widths is shown in Figure 18(a). The transition from moving states to jamming states is observed in the simulation with all corridors except for the corridor of 1 m width. When the width of the corridor is 1 m, the value of P_{jam} is close to 1 even if the global density is very low. One possible reason for this is that the effect of walls prevents agents from using the full width of the corridor.

The mean value and standard deviation of Φ in the simulation with the moving state are calculated for each corridor and each value of ρ_{global}. See Figure 18(b). When the width of the corridor is 1 m and $\rho_{\text{global}} = 0.31\,\text{m}^{-2}$, the value of Φ is lower than in other situations. In addition to this, there is no significant difference between the value of Φ in other simulations with the moving state, which is always close to 1.

Appendix C. Heterogeneity of the free speed of the agents

To analyze the influence of the heterogeneity of agents, the free speed is chosen according to a normal distribution. A larger standard deviation of the distribution corresponds to a

higher heterogeneity in the free speed of agents. In other sections, the normal distribution $N \sim (1.55, 0.18^2)$ m s^{-1} obtained from the experiment in [15] is used. In this subsection, normal distributions with the same mean value (1.55 m s^{-1}) but different standard deviations (0, 0.09, 0.18, 0.36, or 0.54 m s^{-1}), which is denoted by σ, are adopted in this analysis. To avoid negative values, the lower limit of the free speed is set as 0.1 m s^{-1}. Simulations are performed with periodic boundary conditions in the corridor shown in Figure 6. The number of agents is 140 in each simulation ($\rho \approx 1.35\,\mathrm{m}^{-2}$). It corresponds to the global density, where the transition from moving states ($P_{\mathrm{jam}} = 0$) to jamming states ($P_{\mathrm{jam}} = 1$) occurs in the simulation using the AVM. Other parameters of AVM are shown in Table 1.

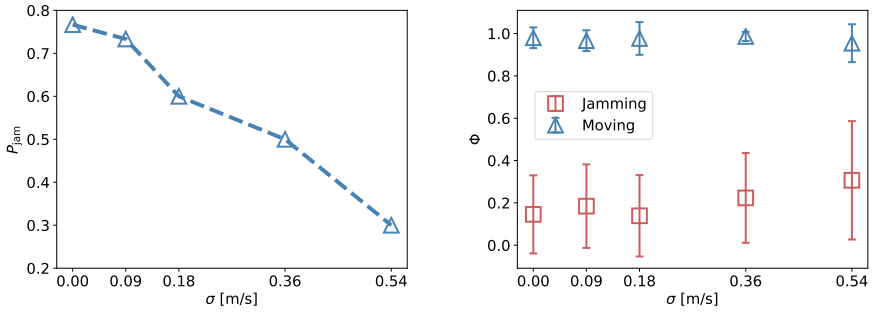

(a) (b)

Figure C.19: (a): The relationship between the jamming probability P_{jam} and the standard deviation σ. (b): The mean value and standard deviation of Φ in the simulation with jamming and moving states, for each value of σ.

The relationship between the jamming probability P_{jam} and the standard deviation σ is shown in Figure 19(a). The value of P_{jam} decreases as σ increases. The mean value and standard deviation of Φ in the simulation with jamming and moving states are calculated for each value of σ. See Figure 19(b). The value of Φ in the moving state is higher than in the jamming state. Moreover, there is no significant difference between the value of Φ in the simulation with the moving state, which is always all close to 1. In conclusion, with increasing heterogeneity of the free speed of agents, the jamming probability decreases, but the formation of lanes in the simulation with the moving state is not affected.

References

[1] K. Yamori, Going with the flow: Micro–macro dynamics in the macrobehavioral patterns of pedestrian crowds., Psychological review 105 (3) (1998) 530.

[2] D. Helbing, P. Molnár, I. J. Farkas, K. Bolay, Self-organizing pedestrian movement, Environment and planning B: planning and design 28 (3) (2001) 361–383.

[3] S. Hoogendoorn, W. Daamen, Self-organization in pedestrian flow, in: Traffic and Granular Flow'03, Springer, 2005, pp. 373–382.

[4] C. Feliciani, H. Murakami, K. Nishinari, A universal function for capacity of bidirectional pedestrian streams: Filling the gaps in the literature, PloS one 13 (12) (2018) e0208496.
[5] M. Boltes, J. Zhang, A. Tordeux, A. Schadschneider, A. Seyfried, Empirical results of pedestrian and evacuation dynamics, Encyclopedia of complexity and systems science (2018) 1–29.
[6] J. Adrian, M. Amos, M. Baratchi, M. Beermann, N. Bode, M. Boltes, A. Corbetta, G. Dezecache, J. Drury, Z. Fu, et al., A glossary for research on human crowd dynamics, Collective Dynamics 4 (A19) (2019) 1–13.
[7] J. Dzubiella, G. Hoffmann, H. Löwen, Lane formation in colloidal mixtures driven by an external field, Physical Review E 65 (2) (2002) 021402.
[8] M. E. Leunissen, C. G. Christova, A.-P. Hynninen, C. P. Royall, A. I. Campbell, A. Imhof, M. Dijkstra, R. Van Roij, A. Van Blaaderen, Ionic colloidal crystals of oppositely charged particles, Nature 437 (7056) (2005) 235–240.
[9] K. Sütterlin, A. Wysocki, A. Ivlev, C. Räth, H. Thomas, M. Rubin-Zuzic, W. Goedheer, V. Fortov, A. Lipaev, V. Molotkov, et al., Dynamics of lane formation in driven binary complex plasmas, Physical review letters 102 (8) (2009) 085003.
[10] D. Helbing, P. Molnar, Social force model for pedestrian dynamics, Physical review E 51 (5) (1995) 4282.
[11] Y. Suma, D. Yanagisawa, K. Nishinari, Anticipation effect in pedestrian dynamics: Modeling and experiments, Physica A: Statistical Mechanics and its Applications 391 (1-2) (2012) 248–263.
[12] H. Murakami, C. Feliciani, K. Nishinari, Lévy walk process in self-organization of pedestrian crowds, Journal of the Royal Society Interface 16 (153) (2019) 20180939.
[13] H. Murakami, C. Feliciani, Y. Nishiyama, K. Nishinari, Mutual anticipation can contribute to self-organization in human crowds, Science Advances 7 (12) (2021).
[14] M. Isobe, T. Adachi, T. Nagatani, Experiment and simulation of pedestrian counter flow, Physica A: Statistical Mechanics and its Applications 336 (3-4) (2004) 638–650.
[15] J. Zhang, W. Klingsch, A. Schadschneider, A. Seyfried, Ordering in bidirectional pedestrian flows and its influence on the fundamental diagram, Journal of Statistical Mechanics: Theory and Experiment 2012 (02) (2012) P02002.
[16] M. Moussaid, E. G. Guillot, M. Moreau, J. Fehrenbach, O. Chabiron, S. Lemercier, J. Pettré, C. Appert-Rolland, P. Degond, G. Theraulaz, Traffic instabilities in self-organized pedestrian crowds, PLoS Comput Biol 8 (3) (2012) e1002442.
[17] C. Feliciani, K. Nishinari, Empirical analysis of the lane formation process in bidirectional pedestrian flow, Physical Review E 94 (3) (2016) 032304.
[18] S. Nowak, A. Schadschneider, Quantitative analysis of pedestrian counterflow in a cellular automaton model, Physical review E 85 (6) (2012) 066128.
[19] M. Rex, H. Löwen, Lane formation in oppositely charged colloids driven by an electric field: Chaining and two-dimensional crystallization, Physical review E 75 (5) (2007) 051402.
[20] F. Zanlungo, T. Ikeda, T. Kanda, Social force model with explicit collision prediction, EPL (Europhysics Letters) 93 (6) (2011) 68005.
[21] I. Karamouzas, B. Skinner, S. J. Guy, Universal power law governing pedestrian interactions, Physical review letters 113 (23) (2014) 238701.
[22] U. Weidmann, Transporttechnik der fußgänger: transporttechnische eigenschaften des fußgängerverkehrs, literaturauswertung, IVT Schriftenreihe 90 (1993).
[23] R. Bailo, J. A. Carrillo, P. Degond, Pedestrian models based on rational behaviour, in: Crowd Dynamics, Volume 1, Springer, 2018, pp. 259–292.
[24] M. J. Seitz, N. W. Bode, G. Köster, How cognitive heuristics can explain social interactions in spatial movement, Journal of the Royal Society Interface 13 (121) (2016) 20160439.
[25] M. Muramatsu, T. Irie, T. Nagatani, Jamming transition in pedestrian counter flow, Physica A: Statistical Mechanics and its Applications 267 (3-4) (1999) 487–498.
[26] F. Weifeng, Y. Lizhong, F. Weicheng, Simulation of bi-direction pedestrian movement using a cellular automata model, Physica A: Statistical Mechanics and its Applications 321 (3-4) (2003) 633–640.

[27] D. Helbing, L. Buzna, A. Johansson, T. Werner, Self-organized pedestrian crowd dynamics: Experiments, simulations, and design solutions, Transportation science 39 (1) (2005) 1–24.
[28] T. Kretz, A. Grünebohm, M. Kaufman, F. Mazur, M. Schreckenberg, Experimental study of pedestrian counterflow in a corridor, Journal of Statistical Mechanics: Theory and Experiment 2006 (10) (2006) P10001.
[29] A. Tordeux, M. Chraibi, A. Seyfried, Collision-free speed model for pedestrian dynamics, in: Traffic and Granular Flow'15, Springer, 2016, pp. 225–232.
[30] Q. Xu, M. Chraibi, A. Tordeux, J. Zhang, Generalized collision-free velocity model for pedestrian dynamics, Physica A: Statistical Mechanics and its Applications 535 (2019) 122521.
[31] S. Cao, A. Seyfried, J. Zhang, S. Holl, W. Song, Fundamental diagrams for multidirectional pedestrian flows, Journal of Statistical Mechanics: Theory and Experiment 2017 (3) (2017) 033404.
[32] C. von Krüchten, Development of a cognitive and decision-based model for pedestrian dynamics, Ph.D. thesis, Universitäts-und Stadtbibliothek Köln (2019).
[33] C. Feliciani, K. Nishinari, An improved cellular automata model to simulate the behavior of high density crowd and validation by experimental data, Physica A: Statistical Mechanics and its Applications 451 (2016) 135–148.

Publication IV

Info: Xu Q, Chraibi M. On the effectiveness of the measures in supermarkets for reducing contact among customers during COVID-19 period. Sustainability, 2020, 12(22): 9385.

Note: The model used in this publication is the collision-free speed model (CSM), but it also involves the effect of walls and the elliptical agents, which are defined in the generalized collision-free velocity model (GCVM). Therefore, the model used in the publication is directly called the GCVM for convenience.

On the Effectiveness of the Measures in Supermarkets for Reducing Contact among Customers during COVID-19 Period

Qiancheng Xu[a,*], Mohcine Chraibi[a]

[a]*Institute for Advanced Simulation, Forschungszentrum Jülich, 52425 Jülich, Germany*

Abstract

The spread of the COVID-19 virus had a huge impact on human life on the global scale. Many control measures devoted to decrease contact among people have been adopted to slow down the transmission of the disease. A series of measures have been taken in supermarkets, which include restricting the number of customers, keeping social distance, and entering with a shopping cart. In this work, we investigate with numerical simulations the effectiveness of these measures in reducing the contact among customers. Several scenarios with different control measures are designed for numerical analysis. The movements of customers in a supermarket are simulated by a microscopic model for pedestrian dynamics. Moreover, an index based on the distance between customers is defined to measure the degree of contact and therefore evaluate it quantitatively. The effect of these measures on the average contact degree of each customer is explored, and the spatial distribution of the contact among customers in the supermarket is shown in a qualitative way. Simulation results show that except shopping cart measure, the other two measures are effective in reducing contact among customers.

Keywords: COVID-19 virus disease, control measures, supermarket, numerical simulation, microscopic model, contact

1. Introduction

The so-called Coronavirus (COVID-19) was first identified in December 2019 in Wuhan, Hubei, China and has became an infectious disease worldwide [1]. As of 29 June 2020, there have been more than 10 million confirmed cases of COVID-19, including nearly 500,000 deaths, as reported by the World Health Organization (WHO) [2]. The disease spreads primarily from person to person through small droplets produced by coughing, sneezing, or speaking of an infected person [3]. Therefore, as there is still no known vaccine against the virus, reducing close contact situations among people is one of the recommended measures to

*corresponding author

Email addresses: q.xu@fz-juelich.de (Qiancheng Xu), m.chraibi@fz-juelich.de (Mohcine Chraibi)

prevent infection [4]. Other measures taken by many countries to avoid or even prohibit situations leading to close contact among people, including travel restrictions, closing schools, and canceling large gatherings. The effectiveness of these control measures are investigated in some works [5, 6, 7].

The pandemic and these control measures also have a huge impact on pedestrian dynamics at different scales, e.g., touristic urban areas [8, 9] and university buildings [10, 11]. In this work, we focus on supermarkets, which are kept open during the outbreak. In order to keep the safety of customers, a series of measures have been adopted. These measures include setting a limitation on the number of customers in the supermarket, asking customers to keep a certain distance with each other (a minimum of 1.5 m), and requiring customers to enter the supermarket with a shopping cart, while wearing a face mask.

In this paper, we investigate the extent to which these measures are effective in reducing the contact among customers with the help of numerical simulations. Many simulations have been performed to predict the influence of this pandemic on the example of supermarket visitors, and to investigate the best measures to slow down its spread.

Existing models for COVID-19 transmission dynamics operate on different levels, which can be described as macroscopic and microscopic. On the macroscopic level, the investigated population is divided into different groups of individuals sharing the same status, and the interactions between groups are described by systems of differential equations. The most popular model in this category is the SEIR model (Susceptible–Exposed–Infected–Recovered). Many significant works about COVID-19 are based on this model and its extensions [12, 13, 14, 15, 16]. Macroscopic models are computationally cheap and can intuitively reflect the changing trend of groups of population with different infectious statuses. It can be used to predict the spread of the disease, and estimate the effectiveness of control measures in regions with large population, e.g., a city.

As opposed to macroscopic models, which divide population into several groups, microscopic models treat each person as an individual with different properties. The status of each people in the simulation is different, which can be healthy, infected or other. Microscopic models for COVID-19 are usually composed of a model for pedestrian dynamics and a model for disease transmission dynamics. The movement and interaction of individuals are simulated by a model for pedestrian dynamics, and the status transitions of individuals are simulated by a disease transmission model [17, 18, 19, 20]. Although microscopic models are computationally more expensive than macroscopic models, they can map more details in person level, therefore it is suitable to simulate the spread of virus in confined spaces during a short time period.

A supermarket is a relatively small scenario that can have a high population mobility. Therefore, in this work we use a microscopic model to investigate different scenarios in a supermarket and evaluate the effectiveness of measures taken in these scenarios. In the following, we focus on the contact among customers instead of the virus transmission among customers, as reducing contact is important to slow down the transmission of COVID-19. By measuring the contact degree, we can study the effectiveness of various measures more directly.

To simulate the movement of customers in the supermarket, the generalized collision-

free velocity model (GCVM) for pedestrian dynamics is adopted [21]. First, we define a distance-based index to quantify the degree of contact among customers. Second, according to the different measures taken by the supermarket, corresponding simulation scenarios are designed and executed. Finally, the values of the contact index obtained from different scenarios are analyzed and compared to evaluate the effectiveness of these measures. This work is organized as follows. In Section 2.1, we briefly introduce the GCVM adopted in this work and give the definition of the index to quantify the contact among pedestrians. Section 2.2 presents the supermarket scenarios designed for the simulations and describes how customers move in the supermarket. Section 3 gives simulation results obtained in the scenarios with different control measures and the corresponding analysis. Finally, in Section 4 we finish with a discussion.

2. Research methods

2.1. How to quantify contact among pedestrians

The generalized collision-free velocity model for pedestrian dynamics is used in this work to simulate the movement of customers in the supermarket. It is composed of a direction sub-model and a speed sub-model, and can be described as

$$\dot{X}_i(X_i, X_j, \dots) = \vec{e}_i(X_i, X_j, \dots) \cdot V_i(X_i, X_j, \dots), \tag{1}$$

where X_i, $\vec{e}_i$, and V_i are the position, moving direction, and moving speed, respectively.

The direction sub-model calculates the moving direction $\vec{e}_i$ for pedestrian i as

$$\vec{e}_i = u \cdot \left(\vec{e}_i^{\,0} + \sum_{j \in N_i} k \cdot \exp\left(\frac{-s_{i,j}}{D}\right) \cdot \vec{e}_{i,j} + \vec{w}_i \right), \tag{2}$$

where u is a normalization constant such that $\|\vec{e}_i\| = 1$. The new direction is decided by three different components. The first component is the $\vec{e}_i^{\,0}$, which is an unit vector representing the desired moving direction of the pedestrian i. The second component is the effect from other pedestrians belonging to N_i, which is the set that contains all the neighbors who affect the moving direction of pedestrian i. The magnitude of the effect from these neighbors is a function of $s_{i,j}$, which is the distance between the edges of pedestrian i and j along the line connecting their positions. Coefficients $k > 0$ and $D > 0$ are used to calibrate the function accordingly. The direction of the effect from pedestrian j to i is denoted by $\vec{e}_{i,j}$, which is a unit vector point from the position of pedestrian j to pedestrian i. The definitions of $s_{i,j}$ and $\vec{e}_{i,j}$ are shown in Figure 1. The last part is $\vec{w}_i$, which is the effect from walls and obstacles in the building.

The speed sub-model calculates the moving speed V_i for pedestrians i as

$$V_i = \min\left\{ V_i^0, \max\left\{0, \frac{s_i}{T}\right\}\right\}, \tag{3}$$

where V_i^0 is the desired moving speed of pedestrian i, s_i is the collision-free moving spacing of pedestrian i in the moving direction $\vec{e}_i$, and coefficient $T > 0$ is used to adjust the speed

according to the gap between two pedestrians. A more detailed definition of the model can be found in [21].

The distance among pedestrians changes with time while they are moving in space. We assume that small distances lead to a bigger contact index. Therefore, the index $C_i(t)$, representing the contact degree of pedestrian i with its neighbors at time t, is defined as

$$C_i(t) = \sum_{j \in N_i} \exp\big(-d_{i,j}(t)\big), \tag{4}$$

where $d_{i,j}$ is the distance between the position of pedestrians i and j, see Figure 1.

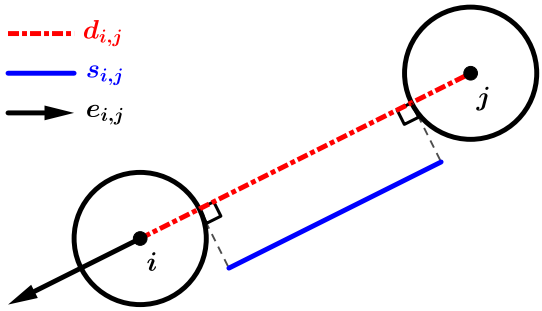

Figure 1: The definition of $s_{i,j}$, $d_{i,j}$ and $\vec{e}_{i,j}$. $s_{i,j}$ is the distance between the edges of pedestrian i and j along the line connecting their positions, $d_{i,j}$ is the distance between the position of pedestrians i and j, and $\vec{e}_{i,j}$ is a unit vector point from the position of pedestrian j to pedestrian i.

2.2. Simulation of shopping behavior in the supermarket

A fictive supermarket scenario, as shown in Figure 2, is built based on a real supermarket nearby the city Jülich in Germany to simulate several scenarios. It represents the typical structure of a medium-sized supermarket in Germany. The supermarket is 34 m long and 18 m wide. It is composed of three different areas: a checkout, a shopping, and an outside area.

The checkout area includes three counters 5 m × 1 m (in black) and three corridors (in gray), while the shopping area includes 10 goods shelves. The sizes of the far left two shelves are 6 m × 2 m and the sizes of other shelves are 10 m × 2 m. Except the area in front of the checkout area, the widths of the walking paths are 2 m. The entrance is located in the upper left corner of the supermarket (green dashed segments). The exits from the shopping area to the checkout area and the exits from checkout area to outside are all marked with red dash segments.

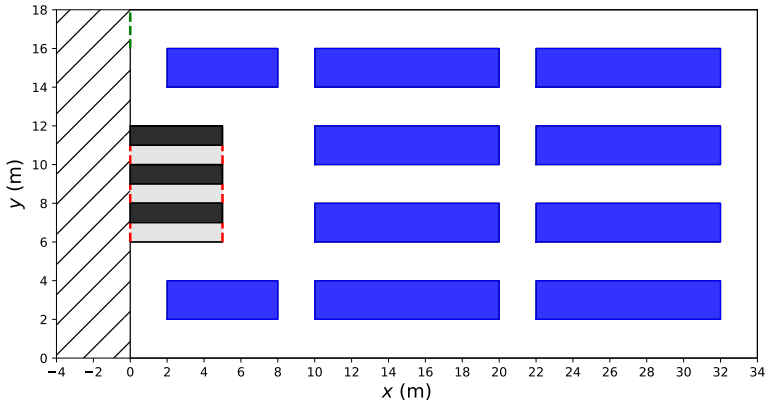

Figure 2: The geometrical structure of the supermarket used in the simulations, the outside area of the supermarket is filled with hatch lines.

We perform the simulations with a total of M customers. Hereby, P persons are generated outside the supermarket every minute until all the M customers are generated. The generated customers enter the supermarket from the entrance and move in the shopping area. Each customer is assigned a random goal within the supermarket after entering the supermarket. After reaching the goal, the customer is assigned another random goal until the time spent in the shopping area is longer than t_i^{shop}, the shopping time for customers.

As introduced before, there are three counters in the checkout area, which means customers have three choices after finishing the shopping. We assume customers prefer to check out at the counter with the fewest customers. Customers who choose the same counter check out one by one in the order of entering the corridor. The time spent for checking out t_i^{check} is proportional to the shopping time and is defined as

$$t_i^{\text{check}} = \alpha \cdot t_i^{\text{shop}}, \tag{5}$$

where $\alpha < 1$ is a parameter. Finally, after checking out, the customers leave the supermarket.

Besides the basic movement of customers, the behavior of customers is influenced by the measures adopted by the supermarket. Therefore, these measures are considered into the basic movement model. We introduce three main measures commonly used in supermarkets nowadays.

The first measure is setting a limitation for the maximal number of customers in the supermarket. This is realized by introducing a new parameter $L_{\max}$ in our model, which is the max allowable number of customers in the supermarket at the same time. Customers can only enter the supermarket when the number of persons inside the supermarket does not exceed the threshold $L_{\max}$. Otherwise, customers have to wait outside.

The second measure is asking customers to keep social distance to each other. From daily observations in supermarkets, the social distance rule is well maintained in the checkout area,

but cannot be maintained in a strict manner in the shopping area. Therefore, compared with simulations without the social distance rule, a larger value of D in Eq. 2 is adopted to enforce larger distances among pedestrians.

Besides, to simulate the queuing of customers, a modified speed sub-model as following is used when customers are in the checkout area.

$$V_i = \min\left\{V_i^0, \max\left\{0, \frac{d_i - d_i^{\text{wait}}}{T}\right\}\right\}. \tag{6}$$

In the modified speed sub-model, d_i is the distance between positions of customer i and the nearest front customer. d_i^{wait} is the distance that customer i wants to keep with the nearest front customer. The expression of d_i^{wait} is

$$d_i^{\text{wait}} = \max\left\{d_{\text{rule}}, \beta \cdot t_i^{\text{shop}}\right\}, \tag{7}$$

where d_{rule} is the social distance adopted and β is a parameter.

When there is no social distance rule, the distance between the customers in the checkout area is decided by the shopping time, as we assume that longer shopping times correspond to more space for putting purchased good on the conveyor belt. When the social distance measure is taken, customers maintain at least d_{rule} distances with each other even when they purchase few items in the market.

The last measure is requiring customers to enter the supermarket with a shopping cart. In our simulations, customers are represented by circles with a radius r. Considering that shopping carts increase the space occupied by each customer in the supermarket, a bigger ellipse is used to represent the customers with shopping carts. The length of the semi-major axis in the moving direction is a, and the length of semi-minor axis is b.

3. Simulation results

To explore if the measures taken by the supermarkets are efficient in reducing the contact among customers, the simulations are implemented in the geometry shown in Figure 2 with four different scenarios. For all cases, we use the following parameter values in Table 1. We assumed reasonable values for the desired moving speeds and the shopping times of customers, which are normally distributed for heterogeneity. The mean and standard deviation of the desired moving speeds refer to the free walking speed of pedestrians [22, 23]. The other values in Table 1 are kept constant to guarantee the justification of the comparisons between different scenarios. The differences among the settings of these four scenarios are shown in Table 2.

Parameters	Values
k	8
T (s)	1
α	0.1
β (m/s)	0.003
M (person)	100
P (person/minute)	10
V_i^0 (m/s)	$N \sim (1.34, 0.26^2)$
t_i^{shop} (s)	$N \sim (300, 50^2)$

Table 1: The same parameters in all four scenarios. k (Eq. 2) is the parameter to calibrate the strength of the impact from other pedestrians, T (Eq. 3 and Eq. 6) is the parameter to calibrate the speed according to the gap between two pedestrians, α (Eq. 5) is the parameter to calibrate the checkout time according to the shopping time, β (Eq. 7) is the parameter to calibrate the distance between customers in checkout area according to the shopping time, M is the total number of customers generated in the simulation, P is the number of customers generated every minute, V_i^0 (Eq. 3 and Eq. 6) is the desired moving speed of customers, and t_i^{shop} is the shopping time of customers.

Scenario ID	$L_{\max}$ (Person)	d_{rule} (m)	D (m)	Need Shopping Cart
1	50	0	0.1	No
2	30	0	0.1	No
3	30	1.5	0.3	No
4	30	1.5	0.3	Yes

Table 2: The setting of four scenarios in this work. $L_{\max}$ is the max allowable number of customers in the supermarket at the same time, d_{rule} is the social distance, and D (Eq. 2) is the parameter to calibrate the scale of the impact from other pedestrians.

The snapshots of each scenario are shown in Figure 3. The customers are represented by circles with $r = 0.2$ m in scenarios 1, 2, and 3, where customers can enter the supermarket without a shopping cart. In scenario 4, customers enter the supermarket with shopping carts, therefore they are represented by ellipses with semi-axes $a = 0.4\,\text{m}$ and $b = 0.25\,\text{m}$. Customers inside the supermarket are in green whereas customers outside are in red.

Supermarkets take measures to reduce the contact among customers, but these measures may result in a decrease in the service efficiency. Two quantities are chosen to study the trade-off between the efficiency of the supermarket and the effectiveness of the measures. The first one is t^{sim}, which is the time spent by all the M customers in the supermarket. t^{sim} reflects the efficiency of the supermarket. It can be represented by

$$t^{\text{sim}} = t^{\text{last}} - t^{\text{first}}, \tag{8}$$

where t^{first} is the time when the first customer enters the supermarket, and t^{last} is the time when the last customer leaves the supermarket. The second one is the average contact degree

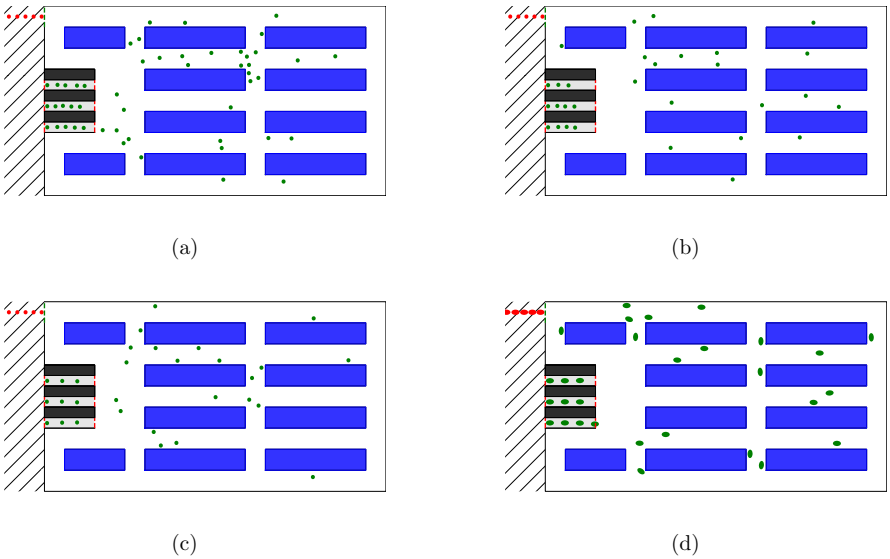

Figure 3: The snapshots of four scenarios, customers inside the supermarket are in green whereas customers outside are in red. (a): Scenario 1. (b): Scenario 2. (c): Scenario 3. (d): Scenario 4.

of all the M customers, which is defined as

$$\bar{C} = \frac{1}{M} \cdot \int_{t^{\text{first}}}^{t^{\text{last}}} \sum_{i=1}^{M} C_i(t) dt. \tag{9}$$

If customer i is outside the supermarket, C_i is equal to zero. A reasonable measure should reduce $\bar{C}$ as much as possible without increasing t^{sim} significantly.

The simulations of this work are performed using JuPedSim [24], which is an open framework for simulating and analyzing the dynamics of pedestrians. The simulations are executed on a standard computer (Inter(R) Core(TM) CPU of 2.50 GHZ) with Euler scheme using a time step $\Delta t = 0.05\,\text{s}$. The update of the customers is parallel in each time-step. We run simulations in each scenario for 30 times. Then, we calculated the mean value and standard deviation of t^{sim} and $\bar{C}$, which are shown in Figure 4.

Hypothesis testing is implemented before comparing the results of different scenarios. The null hypothesis is set as there is no significant difference between the results of two compared scenarios. The Shapiro–Wilks test is performed first to test the normality of the differences between the results of two scenarios. Since all the differences satisfy the condition of normality (p_1 is greater than 0.05), we can perform the Paired t-test for all the comparisons. The null hypothesis is accepted when p_2 is greater than 0.05. The results of Shapiro–Wilks test and Paired t-test are shown in Table 3.

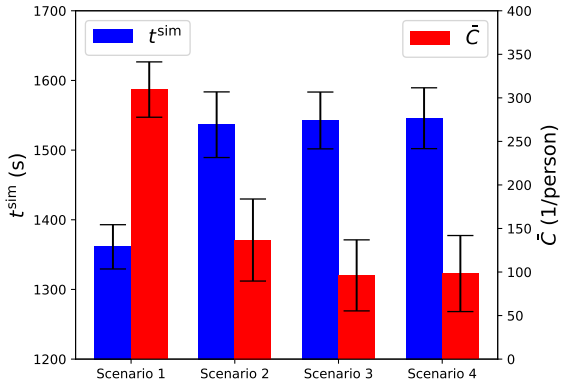

Figure 4: The comparison of t^{sim} (time spend by all customers) and $\bar{C}$ (average contact degree of all customers) for four scenarios, the error bars show the standard deviation.

		Mean	Standard Deviation	Shapiro–Wilks Test		Paired t-Test	
				W	p_1	t	p_2
t_{sim}	$S1$–$S2$	−175.3000	26.8790	0.9798	0.8200	−35.1211	0.0000
	$S2$–$S3$	−6.1125	16.1472	0.9666	0.4497	−2.0385	0.0507
	$S3$–$S4$	−3.2083	18.0953	0.9709	0.5639	−0.9548	0.3476
$\bar{C}$	$S1$–$S2$	172.7929	11.7533	0.9828	0.8938	79.1711	0.0000
	$S2$–$S3$	40.5942	5.8819	0.9755	0.6980	37.1660	0.0000
	$S3$–$S4$	−2.1007	7.5094	0.9426	0.1070	−1.5065	0.1428

Table 3: The result of Shapiro–Wilks test and Paired t-test. ($S1$ means the result from scenario 1.)

From scenario 1 to scenario 4, the protective measures adopted by the supermarket become stricter. Comparing scenario 1 and scenario 2, scenario 2 has smaller L_{max} than scenario 1. The values of p_2 for t_{sim} and $\bar{C}$ are both less than 0.05, showing a significant difference between the results of these two scenarios. From scenario 1 to scenario 2, the mean value of $\bar{C}$ decreases roughly 56%, and the mean value of t^{sim} increases roughly 13%. In conclusion, restricting the number of customers in the supermarket is an effective measure to reduce the contact among customers with a slightly reduced efficiency of the supermarket.

Scenario 2 and scenario 3 have the same $L_{\max}$, but the social distance rule is adopted in scenario 3. Since the value of p_2 for t_{sim} is greater than 0.05, we can say there is no significant difference between t_{sim} of these two scenarios. For $\bar{C}$, the value of p_2 is less than 0.05. The mean value of $\bar{C}$ decreases nearly 29% from scenario 2 to scenario 3. Therefore, social distance rule is also effective to reduce the contact, and hardly affect the efficiency of the supermarket.

In scenario 4, the shopping cart is required for entering the supermarket. Compared with scenario 3, the values of p_2 for t_{sim} and $\bar{C}$ are both greater than 0.05. Therefore, it seems

that the shopping cart rule has limited effect with respect to reducing the contact, although this rule can reduce the workload of counting customers, since the supermarket can limit the number of people in the supermarket by placing a shopping cart with a quantity of $L_{\max}$.

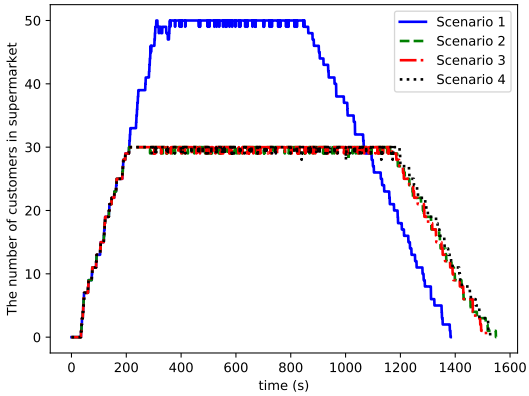

Figure 5: The steady states of the four scenarios.

In addition to the two quantities, the spatial distribution of the contact among customers in the supermarket is investigated. The steady state of each scenario is identified first, which is defined as the status that the number of customers in the supermarket reaches $L_{\max}$. For each scenario, one run is picked out to show the steady states. The steady states of these four scenarios correspond to the flat regions of four lines in Figure 5. The steady areas of scenarios 2, 3, and 4 are almost overlapped, as the value of $L_{\max}$ are the same. The vertical axis represents the number of customers in the supermarket. The oscillation of the steady state is caused by the time gap between customers entering and leaving the supermarket. The start time and the end time of the steady state is defined as t^{start} and t^{end}, respectively.

The geometry of the supermarket is divided into regular grids of size $0.2\,\text{m} \times 0.2\,\text{m}$, and an index C^{grid} is calculated for each grid according to

$$C^{\text{grid}} = \frac{\int_{t^{\text{start}}}^{t^{\text{end}}} \sum_{i \in G} C_i(t) dt}{\int_{t^{\text{start}}}^{t^{\text{end}}} \sum_{i \in G} dt}, \tag{10}$$

where G is the set containing all the customers in the grid. We calculate the mean value of C^{grid} in each grid with the 30 times simulations of each scenario. The distributions of C^{grid} in the supermarket for four scenarios are shown in Figure 6.

A qualitative observation shows that the distribution of C^{grid} changes with the measures taken by the supermarket. The same conclusions as before can be obtained, for instance, restricting the number of customers and social distance rule are useful to reduce the contact among customers, and the shopping cart rule is not effective.

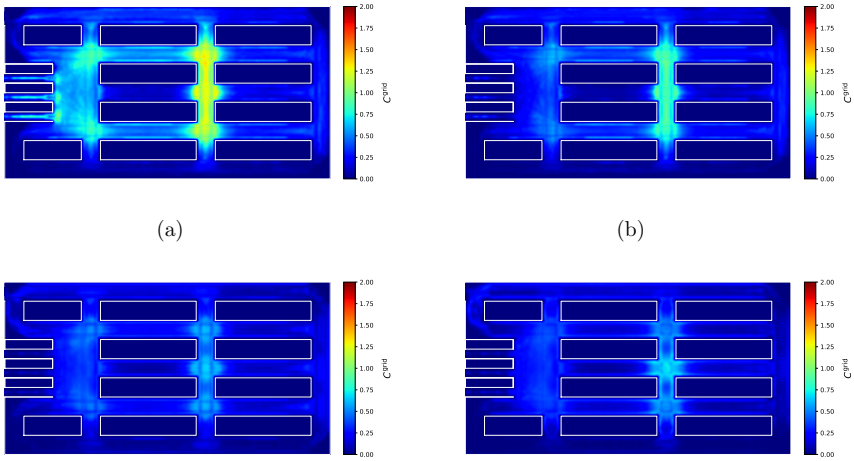

(a) (b)

(c) (d)

Figure 6: The distributions of C^{grid} in the supermarket for four scenarios. (a) Scenario 1. (b) Scenario 2. (c) Scenario 3. (d) Scenario 4.

The four profiles in Figure 6 also show that the values of C^{grid} differ depending on different parts of the supermarket. Therefore, in Figure 7(a) four areas in the supermarket are specified, and the average values of C^{grid} in these areas are calculated. The grids which are located in the obstacles (e.g., counters and goods shelves) are ignored in the calculation, as the values of C^{grid} in the obstacle areas are always equal to zero. The mean values and standard deviations of 30 times simulations for four scenarios are compared in Figure 7(b).

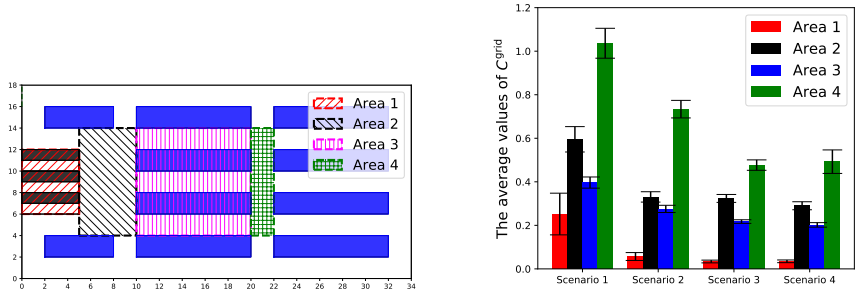

(a) (b)

Figure 7: The average values of C^{grid} in specified areas. (a) The locations of these areas. (b) The comparison of average values; the error bars show the standard deviation.

The same hypothesis testing is implemented for following comparisons. Paired t-test is performed when the difference between two scenarios satisfy the condition of normality. Otherwise, Wilcoxon signed-rank test is used. The testing results are shown in Table 4.

The common point of these four scenarios is the average values of C^{grid} in Area 2 and Area 4 are higher than in Area 1 and Area 3. The reason is that crossing structures are exist in Area 2 and Area 4. Customers in these crossing areas can move in more directions, thus increasing the likelihood of congestion, especially when the number of customers in the supermarket is high.

More information can be obtained by combining Figure 7 and Table 4. Restricting the number of customers decreases the value of C^{grid} in all four areas. The social distance rule also reduces the contact of customers in Area 1, Area 3 and Area 4, but has no effect in Area 2. As for the shopping cart rule, it has a little influence in Area 2 and Area 3, and no effect in Area 1 and Area 4.

		Mean	Standard Deviation	Shapiro–Wilks Test		Paired t-Test (Wilcoxon)	
				W	p_1	t (W)	p_2
Area 1	$S1$–$S2$	0.1952	0.0907	0.6739	0.0000	0.0000	0.0000
	$S2$–$S3$	0.0229	0.0135	0.9247	0.0355	0.0000	0.0000
	$S3$–$S4$	−0.0009	0.0052	0.9837	0.9140	−0.8889	0.3814
Area 2	$S1$–$S2$	0.2646	0.0663	0.9414	0.0994	21.5000	0.0000
	$S2$–$S3$	0.0070	0.0285	0.9705	0.5527	1.3228	0.1962
	$S3$–$S4$	0.0336	0.0257	0.9638	0.3851	7.0483	0.0000
Area 3	$S1$–$S2$	0.1210	0.0316	0.9822	0.8799	20.5898	0.0000
	$S2$–$S3$	0.0582	0.0167	0.9939	0.9996	18.7725	0.0000
	$S3$–$S4$	0.0153	0.0133	0.9488	0.1566	6.1786	0.0000
Area 4	$S1$–$S2$	0.3027	0.0774	0.9711	0.5688	21.0676	0.0000
	$S2$–$S3$	0.2570	0.0520	0.9908	0.9946	26.6224	0.0000
	$S3$–$S4$	−0.0157	0.0587	0.9714	0.5795	−1.4439	0.1595

Table 4: The testing result of comparisons for different areas in the supermarket. ($S1$ means the result from scenario 1.)

4. Conclusions

Supermarkets are closely related to people's daily life. During the COVID-19 period, a series of measures are adopted in supermarkets to slow down the propagation of the disease. The effectiveness of these measures are investigated in this paper. The contact degree among customers is treated as the standard for comparing different measures. Simulations of several scenarios corresponding to different measures taken by supermarkets are performed.

We run simulations in each scenario for 30 times and implement hypothesis testing. Although the supermarket scenarios used in this work is simplified and the behavior of customers in our simulations are based on several assumptions, the following results can be obtained by comparing the accumulation of the time spent by all the customers in the supermarket and the average contact degree of these costumers. The limitation on the number of customers in the supermarket slightly reduces the efficiency of the supermarket, but significantly reduces the contact among customers. The social distance rule is also

effective at reducing the contact among customers. However, the shopping cart rule has little effect in reducing the contact among customers.

Moreover, the spatial distribution of the contact between customers in the supermarket shows that the contact in the areas with crossing structure is obviously higher than in other areas. Therefore, reducing the crossing area in the supermarket may be an effective measure to reduce the contact among customers.

In summary, supermarkets should continue to limit the number of customers and require customers to maintain a minimum social distance. Besides, supermarkets can change the layout to reduce the crossing area.

The work in this paper only focus on the contact among people using on a velocity-based model, but has potential to be extended to an epidemiology model by combining the knowledge and data about the spread COVID-19 into the movement model.

The results of this work may change with the structure of the fictive supermarket scenario and the behavior of customers in simulations, but nonetheless we believe that the framework presented in this study can evaluate the effectiveness of control measures in indoors scenarios.

Future research will focus on the dependence of our results on the structure of scenarios (like the width of walking paths, the number of counters in the checkout area) and behavior of customers (i.e., the shopping time t^{shop} and the desired moving speed V_i^0). Besides, the validation of both movement and behavioral models in this work will be proceed.

Acknowledgments

Qiancheng Xu thanks the funding support from the China Scholarship Council (Grant NO.201706060186).

References

[1] World Health Organization, WHO timeline - COVID-19, https://www.who.int/news-room/detail/27-04-2020-who-timeline---covid-19.

[2] World Health Organization, WHO coronavirus disease (COVID-19) dashboard, https://covid19.who.int/.

[3] World Health Organization, Q&A on coronaviruses (COVID-19), https://www.who.int/emergencies/diseases/novel-coronavirus-2019/question-and-answers-hub/q-a-detail/q-a-coronaviruses.

[4] World Health Organization, Novel coronavirus (2019-ncov) advice for the public, https://web.archive.org/web/20200126025750/https://www.who.int/emergencies/diseases/novel-coronavirus-2019/advice-for-public.

[5] K. Prem, Y. Liu, T. W. Russell, A. J. Kucharski, R. M. Eggo, N. Davies, S. Flasche, S. Clifford, C. A. Pearson, J. D. Munday, et al., The effect of control strategies to reduce social mixing on outcomes of the covid-19 epidemic in wuhan, china: a modelling study, The Lancet Public Health (2020).

[6] M. U. Kraemer, C.-H. Yang, B. Gutierrez, C.-H. Wu, B. Klein, D. M. Pigott, L. Du Plessis, N. R. Faria, R. Li, W. P. Hanage, et al., The effect of human mobility and control measures on the covid-19 epidemic in china, Science 368 (6490) (2020) 493–497.

[7] H. Tian, Y. Liu, Y. Li, C.-H. Wu, B. Chen, M. U. Kraemer, B. Li, J. Cai, B. Xu, Q. Yang, et al., An investigation of transmission control measures during the first 50 days of the covid-19 epidemic in china, Science 368 (6491) (2020) 638–642.

[8] M. D'Orazio, G. Bernardini, E. Quagliarini, Sustainable and resilient strategies for touristic cities against covid-19: an agent-based approach, arXiv preprint arXiv:2005.12547 (2020).
[9] R. Szczepanek, Analysis of pedestrian activity before and during covid-19 lockdown, using webcam time-lapse from cracow and machine learning, PeerJ 8 (2020) e10132.
[10] E. Ronchi, R. Lovreglio, Exposed: An occupant exposure model for confined spaces to retrofit crowd models during a pandemic, arXiv preprint arXiv:2005.04007 (2020).
[11] M. D'Orazio, G. Bernardini, E. Quagliarini, A probabilistic model to evaluate the effectiveness of main solutions to covid-19 spreading in university buildings according to proximity and time-based consolidated criteria (2020).
[12] A. J. Kucharski, T. W. Russell, C. Diamond, Y. Liu, J. Edmunds, S. Funk, R. M. Eggo, F. Sun, M. Jit, J. D. Munday, et al., Early dynamics of transmission and control of covid-19: a mathematical modelling study, The lancet infectious diseases (2020).
[13] D. W. Berger, K. F. Herkenhoff, S. Mongey, An seir infectious disease model with testing and conditional quarantine, Tech. rep., National Bureau of Economic Research (2020).
[14] M. V. Barbarossa, J. Fuhrmann, J. H. Meinke, S. Krieg, H. V. Varma, N. Castelletti, T. Lippert, The impact of current and future control measures on the spread of covid-19 in germany, medRxiv (2020).
[15] C. Hou, J. Chen, Y. Zhou, L. Hua, J. Yuan, S. He, Y. Guo, S. Zhang, Q. Jia, C. Zhao, et al., The effectiveness of quarantine of wuhan city against the corona virus disease 2019 (covid-19): A well-mixed seir model analysis, Journal of medical virology (2020).
[16] K. Iwata, C. Miyakoshi, A simulation on potential secondary spread of novel coronavirus in an exported country using a stochastic epidemic seir model, Journal of clinical medicine 9 (4) (2020) 944.
[17] Z. Fang, Z. Huang, X. Li, J. Zhang, W. Lv, L. Zhuang, X. Xu, N. Huang, How many infections of covid-19 there will be in the" diamond princess"-predicted by a virus transmission model based on the simulation of crowd flow, arXiv preprint arXiv:2002.10616 (2020).
[18] M. D'Orazio, G. Bernardini, E. Quagliarini, How to restart? an agent-based simulation model towards the definition of strategies for covid-19" second phase" in public buildings, arXiv preprint arXiv:2004.12927 (2020).
[19] D. Kai, G.-P. Goldstein, A. Morgunov, V. Nangalia, A. Rotkirch, Universal masking is urgent in the covid-19 pandemic: Seir and agent based models, empirical validation, policy recommendations, arXiv preprint arXiv:2004.13553 (2020).
[20] Y. Xiao, M. Yang, Z. Zhu, H. Yang, L. Zhang, S. Ghader, Modeling indoor-level non-pharmaceutical interventions during the covid-19 pandemic: a pedestrian dynamics-based microscopic simulation approach, arXiv preprint arXiv:2006.10666 (2020).
[21] Q. Xu, M. Chraibi, A. Tordeux, J. Zhang, Generalized collision-free velocity model for pedestrian dynamics, Physica A: Statistical Mechanics and its Applications 535 (2019) 122521.
[22] E. Bosina, U. Weidmann, Estimating pedestrian speed using aggregated literature data, Physica A: Statistical Mechanics and its Applications 468 (2017) 1–29.
[23] S. Buchmueller, U. Weidmann, Parameters of pedestrians, pedestrian traffic and walking facilities, IVT Schriftenreihe 132 (2006).
[24] A. U. K. Wagoum, M. Chraibi, J. Zhang, G. Lämmel, Jupedsim: an open framework for simulating and analyzing the dynamics of pedestrians, in: 3rd Conference of Transportation Research Group of India, 2015.

Schriften des Forschungszentrums Jülich
IAS Series

Band / Volume 37
Analysis of I/O Requirements of Scientific Applications
S. El Sayed Mohamed (2018), XV, 199 pp
ISBN: 978-3-95806-344-0
URN: urn:nbn:de:0001-2018071801

Band / Volume 38
Wayfinding and Perception Abilities for Pedestrian Simulations
E. Andresen (2018), 4, x, 162 pp
ISBN: 978-3-95806-375-4
URN: urn:nbn:de:0001-2018121810

Band / Volume 39
Real-Time Simulation and Prognosis of Smoke Propagation in Compartments Using a GPU
A. Küsters (2018), xvii, 162, LIX pp
ISBN: 978-3-95806-379-2
URN: urn:nbn:de:0001-2018121902

Band / Volume 40
Extreme Data Workshop 2018
Forschungszentrum Jülich, 18-19 September 2018
Proceedings
M. Schultz, D. Pleiter, P. Bauer (Eds.) (2019), 64 pp
ISBN: 978-3-95806-392-1
URN: urn:nbn:de:0001-2019032102

Band / Volume 41
A lattice QCD study of nucleon structure with physical quark masses
N. Hasan (2020), xiii, 157 pp
ISBN: 978-3-95806-456-0
URN: urn:nbn:de:0001-2020012307

Band / Volume 42
Mikroskopische Fundamentaldiagramme der Fußgängerdynamik – Empirische Untersuchung von Experimenten eindimensionaler Bewegung sowie quantitative Beschreibung von Stau-Charakteristika
V. Ziemer (2020), XVIII, 155 pp
ISBN: 978-3-95806-470-6
URN: urn:nbn:de:0001-2020051000

Band / Volume 43
Algorithms for massively parallel generic *hp*-adaptive finite element methods
M. Fehling (2020), vii, 78 pp
ISBN: 978-3-95806-486-7
URN: urn:nbn:de:0001-2020071402

Schriften des Forschungszentrums Jülich
IAS Series

Band / Volume 44
The method of fundamental solutions for computing interior transmission eigenvalues
L. Pieronek (2020), 115 pp
ISBN: 978-3-95806-504-8

Band / Volume 45
Supercomputer simulations of transmon quantum computers
D. Willsch (2020), IX, 237 pp
ISBN: 978-3-95806-505-5

Band / Volume 46
The Influence of Individual Characteristics on Crowd Dynamics
P. Geoerg (2021), xiv, 212 pp
ISBN: 978-3-95806-561-1

Band / Volume 47
Structural plasticity as a connectivity generation and optimization algorithm in neural networks
S. Diaz Pier (2021), 167 pp
ISBN: 978-3-95806-577-2

Band / Volume 48
Porting applications to a Modular Supercomputer
Experiences from the DEEP-EST project
A. Kreuzer, E. Suarez, N. Eicker, Th. Lippert (Eds.) (2021), 209 pp
ISBN: 978-3-95806-590-1

Band / Volume 49
Operational Navigation of Agents and Self-organization Phenomena in Velocity-based Models for Pedestrian Dynamics
Q. Xu (2022), xii, 112 pp
ISBN: 978-3-95806-620-5

Weitere ***Schriften des Verlags im Forschungszentrum Jülich*** unter
http://wwwzb1.fz-juelich.de/verlagextern1/index.asp

IAS Series
Band / Volume 49
ISBN 978-3-95806-620-5

Mitglied der Helmholtz-Gemeinschaft

JÜLICH
Forschungszentrum